EFFECTS OF THE GENERAL ANESTHETIC ISOFLURANE ON VOLTAGE-GATED SODIUM CHANNELS AND THE PRESYNAPTIC ACTION POTENTIAL

A Dissertation

Presented to the Faculty of the Weill Cornell Graduate School

of Medical Sciences

in Partial Fulfillment of the Requirements for the Degree of

Doctor of Philosophy

by

Kerry Purtell

August 2015

EFFECTS OF THE GENERAL ANESTHETIC ISOFLURANE ON VOLTAGE-GATED SODIUM CHANNELS AND THE PRESYNAPTIC ACTION POTENTIAL

Kerry Purtell, Ph.D.

Cornell University, 2015

The molecular mechanisms of general anesthetic action are poorly understood, especially in regard to widely used inhaled anesthetic agents. Optimization of anesthetic drug design and clinical use requires detailed understanding of the roles of specific targets involved in the therapeutic actions (unconsciousness, amnesia, immobility) and undesirable effects (cardiovascular and respiratory depression, neurotoxicity) of various anesthetics. Voltage-gated sodium channels (Na_v) have been implicated as targets for anesthetic inhibition of neurotransmitter release, but block of Na_v by general anesthetics was previously considered too modest at clinical concentrations to be pharmacologically relevant. However, studies in whole animals show that block of Na_v by the prototypical inhaled anesthetic agent isoflurane is necessary for producing immobility and determining anesthetic potency.

This dissertation addresses the electrophysiological effects of isoflurane on Na_v and the presynaptic action potential in primary cultures of rat hippocampal neurons. At

concentrations equivalent to those used in the clinic, isoflurane, and not the nonanesthetic molecule F6, significantly decreased spontaneous activity of hippocampal neurons and also reduced peak amplitude and upstroke velocity of the action potential. Peak current of endogenous Na_v was inhibited ~10% by clinical concentrations of isoflurane, similar to previous reports. However, we found that the magnitude of Na_v block depended on the state of the channel and increased at higher stimulation frequencies. Using heterologously expressed rat $Na_v1.2$, a widely expressed neuronal isoform, we show that isoflurane stabilizes the fast-inactivated state of the channel. We propose that by stabilizing Na_v in the inactivated state, isoflurane leads to accumulation of inactivated channels and inhibition of I_{Na} during trains of high frequency stimuli as would be experienced by a burst-firing neuron. This work shows that activity-dependent block contributes significantly to overall block of Na_v, and supports a role for Na_v inhibition in the presynaptic action of general anesthetic ethers such as isoflurane.

Dedicated to my parents,

Mary and Gerry

For putting my education

before anything else

ACKNOWLEDGMENTS

First of all I would like to thank my advisor, Hugh C. Hemmings Jr. for giving me the means and the opportunity to carry out this work, for sharing his expertise and for always providing guidance and constructive criticism with a calm reassurance and a great sense of humor. I would also like to thank Charles Inturrisi and Steven Gross for taking the time to evaluate this thesis and for providing encouragement and intellectual contributions during its preparation. Also, thank you to Francis Lee and Roberto Levi for serving on my thesis committee and providing support and guidance.

I would like to give a very special and sincere thank you to Lorraine Gudas for encouraging me to pursue this degree, for leading a wonderful research department and for teaching me how to do cell culture. I would like to thank my former advisor, Geoffrey Abbott whose brilliance and enthusiasm allowed me to experience the thrill of scientific discovery and my undergraduate advisor, Hugh Foley for identifying and encouraging my strengths and for teaching me to cherish the learning process.

A special thanks to my teachers and collaborators: Karl Herold, Kevin Gingrich, Torsten Roepke, Nancy Carrasco, Jeffrey Young, Peter Goldstein, David Christini, Trine Krogh-Madsen, Crina Nimigean, and David Posson for sharing their wisdom and expertise. Your generosity has made this a truly exceptional experience.

I would like to thank Karl for training me in the Hemmings lab and Joel and Rheanna for guiding my reseach. I would also like to thank all the members of the

Hemmings lab: Christina, Zhenyu, Julia, Masato, Dan, Jimcy, Kenny, and Lacey and the members of the Abbott lab and the A3 lab space: Francis, Will, Sushila, Liz, Kemar, Stephanie, Dia, and Vikram for many fun times and for being dear friends.

Thank you to my friends Sweta, Christina, Hadiya, and Madiha for their love and support and to my roomates: Shruti, Mrinalini and Anerudh for making a home for me in Irvine, CA. Thank you to my brother for being my best friend since day 1 and for making me a good person. Thank you to my brother- and sister-in-law, Alex and Cristina Hernandez, and finally, thank you to my husband Chris for making every day pretty frakking great.

TABLE OF CONTENTS

APPENDIX

LIST OF FIGURES

ABBREVIATIONS

A	ampere
AMPA	α-amino-3-hydroxy-5-methyl-4-isoxazolepropionic acid
AP	action potential
APV	(2R)-amino-5-phosphonovaleric acid
Ca^{2+}	calcium ion
Ca_v	voltage-gated calcium channel
CNS	central nervous system
CNQX	6-cyano-7-nitroquinoxaline-2,3-dione
DRG	dorsal root ganglion
E_{ion}	equilibrium potential
EDTA	ethylene diamine tetraacetic acid
EGTA	ethylene glycol tetraacetic acid
EPSP	excitatory postsynaptic potential
F6	1,2-dichlorohexafluorocyclobutane
G	conductance
GABA	γ-aminobutyric acid
Gly	glycine
I	current
K^+	potassium ion
K_v	voltage-gated potassium channel
K2P	2-pore K^+ channel
LGIC	ligand-gated ion channel
min	minute
Na^+	sodium ion
nAChR	nicotinic acetylcholine receptor

Na_v	voltage-gated sodium channel
NMDA	N-Methyl-D-aspartate
PKA	protein kinase A
PKC	protein kinase C
s	second
SD	standard deviation
TEA	tetraethylammonium
TTX	tetrodotoxin
V	volt
VA	volatile anesthetic
V_h	holding potential
Vm	membrane voltage

CHAPTER ONE

INTRODUCTION

General anesthesia is the reversible, pharmacological state of amnesia, unconsciousness, and immobility that can be induced by a remarkable variety of inhaled and intravenous agents (Franks, 2006; Rudolph and Antkowiak, 2004; Urban, 2008). Despite widespread use and the invaluable role anesthetics play in modern medicine, the exact mechanism of action remains incompletely understood especially for the volatile anesthetics (VAs) (Campagna et al., 2003; Franks and Lieb, 1994; Hemmings, 2009; Solt and Forman, 2007). The first successful public demonstration of anesthesia during surgery was performed in 1846 at Massachusetts General Hospital by William T. G. Morton. Using a colorless gas, Morton sedated a patient while a surgeon removed a tumor from his neck. With some persuading, Morton later revealed the gas was ether, the medicinal properties of which had been known for centuries, and that had already been used during surgery by Dr. Crawford W. Long and colleagues in Georgia (Chivukula et al., 2014; Hudson et al., 2013). However, Morton's public demonstration is largely credited with bringing general anesthesia into widespread clinical practice and marking the dawn of modern surgery.

In the mid-20th century fluorine chemistry led to the discovery of modern day VAs - fluorinated methyl ethyl ethers: enflurane, isoflurane, sevoflurane and desflurane that are less flammable than ether and have a better therapeutic index (Hudson et al., 2013; Terrell, 2008). Since the 1980's, major advancements have been made towards the discovery of how these drugs work as the field has moved away from nonspecific lipid-based mechanisms of action to protein-target based mechanisms (Franks and Lieb, 1984).

The molecular pharmacology of the anesthetic state involves multiple target proteins, prominently including ligand-gated and voltage-gated ion channels (Eger et al., 2008; Franks and Lieb, 1994; Hemmings et al., 2005c; Krasowski and Harrison, 1999). Research into understanding the mechanism of action of general anesthetics can lead to advances in both clinical practice and the field of neuroscience, since understanding how anesthetics work will tell us a good deal about consciousness itself (Arhem et al., 2003; Perouansky and Pearce, 2011). Elucidation of the mechanisms that produce the desired behavioral state (amnesia, unconsciousness and immobility) as well as those that cause undesirable side effects (cardiovascular and respiratory depression, neurotoxicity) will guide the development of safer drugs and lead to improved clinical outcomes (Grasshoff et al., 2006; Hemmings et al., 2005c; Solt and Forman, 2007). Furthermore, research into understanding the neuroprotective effects of general anesthetics can also indentify protein targets to protect against damage induced by ischemia, stroke, and neurodegenerative disease (Li and Zuo, 2009; Sun et

al., 2015; Yin et al., 2012; Zhao and Zuo, 2004) and could guide the selection of anesthetics to optimize neurologic outcomes (Schifilliti et al., 2010).

Bioelectricity and neuronal communication in the central nervous system

Drugs that produce anesthesia interfere with the electrical and chemical signalling between neurons, which are the principal cells of the central nervous system (CNS) (Figure 1). Neurons have a cell body, called the soma, out from which extends large filipodial-like protrusions called dendrites that receive incoming chemical stimuli and convert it into electrical signals. The space between two communicating neurons is called the synapse, and information is sent primarily from the 'presynaptic neuron' to the 'postsynaptic neuron'.

The cell membrane is composed of a lipid bilayer that, due to its hydrophobicity, is impermeable to charged molecules and separates the ionic milieu of the cytosol from the extracellular space. The Na^+/K^+ pump exchanges Na^+ and K^+ against their concentration gradients and maintains a relatively high $[K^+]$ inside the cell and relatively high $[Na^+]$ outside. When the neuron is at rest, the inside of the membrane is negative with respect to the outside, producing a voltage of ~ -60 mV. The action potential (AP) is an electrical signal that transmits information in the neuron and is produced through the coordinated opening and closing of voltage-gated proteins that span the cell membrane and form hydrophilic channels that selectively

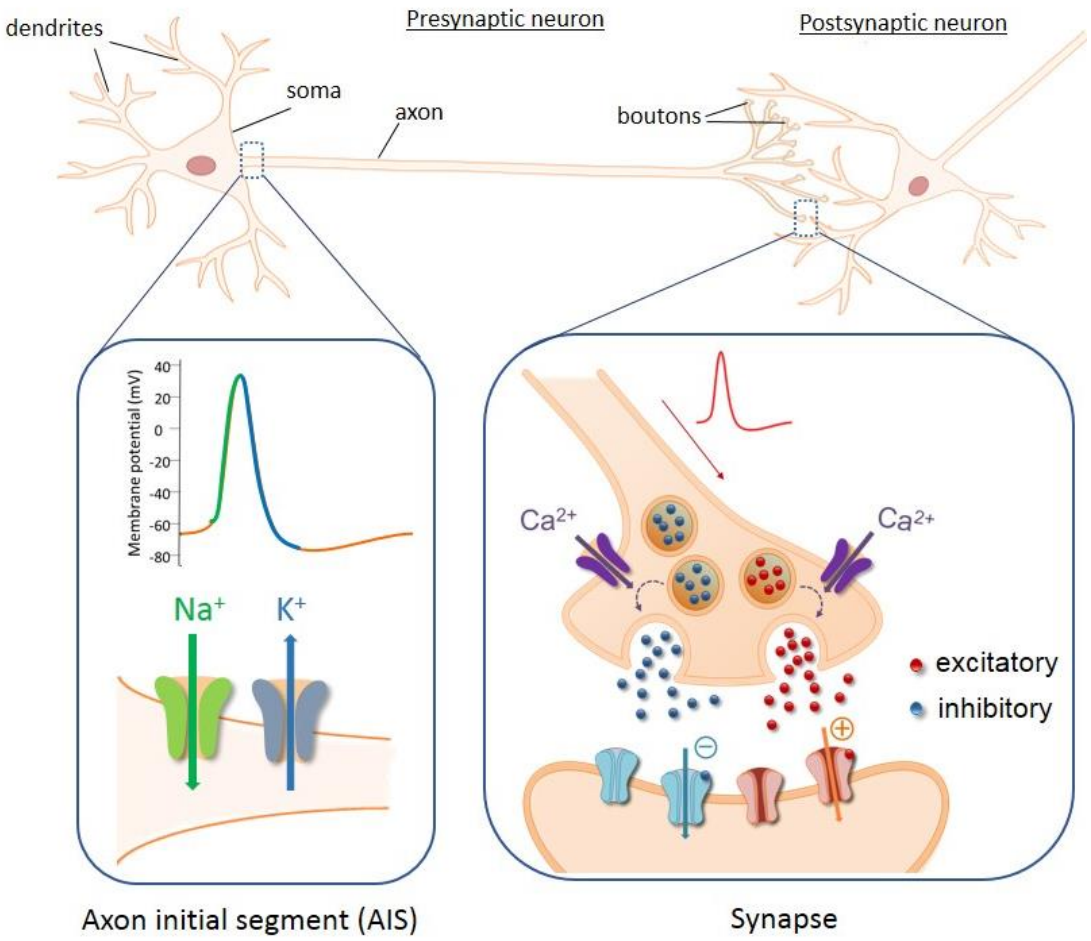

FIGURE 1. Electrical and chemical signalling in the neuron. Cartoon of a presynaptic neuron synapsing onto the dendrites of a postsynaptic neuron. Expanded view of the AIS shows a neuronal action potential (AP) with contributions from voltage-gated Na^+ and K^+ channels indicated in green and blue, respectively. Arrows indicate direction of current flow through the channels. Expanded view of the synapse shows the incoming AP and Ca^{2+} entry causing synaptic vesicles to fuse to the presynaptic membrane. Excitatory neurotransmitters (red) open cation channels (red, +) and inhibitory neurotransmitters (blue) open anion channels (turquoise, −)

pass Na^+ or K^+ current (Armstrong and Bezanilla, 1973; Hille, 1967; Hodgkin and Huxley, 1952; Nakamura et al., 1965) (Figure 1). When the channel for a particular

ion is open, the current (I_{ion}) is driven by an electrochemical gradient due to the ion concentration inside and outside of the cell, and the membrane voltage (Vm). The equilibrium potential (E_{ion}) is the Vm where the concentration gradient and the electrical driving force balance each other and there is no net current flow. Alternatively, the further Vm is from E_{ion}, the greater the electrical driving force for that ion.

Voltage-gated Na^+ channels (Na_v) are closed at hyperpolarized potentials and the equilibrium potential for Na^+, E_{Na}=+60 mV. Therefore, when Na_v open at ~−30 mV, Na^+ current (I_{Na}) flows into the cell and rapidly depolarizes the membrane, creating the upstroke of the AP. Na_v inactivate within milliseconds after opening, halting the upstroke of the AP (Aldrich et al., 1983; Armstrong and Bezanilla, 1977; Cota and Armstrong, 1989) and the now depolarized Vm creates the driving force for K^+ (E_K=~−90 mV), to move out of the cell and repolarize the membrane. Upon membrane repolarization, Na_v recover from inactivation and return to the resting state.

The AP propagates down the axon, which is a long thin process that extends from the soma (Boiko et al., 2003; Carras et al., 1992; Stuart et al., 1997) to varicosities that emerge *en passant* or at the axon terminals called boutons. Boutons contain lipid-bound vesicles packed with neurotransmitter molecules that are released into the synapse during exocytosis. The depolarization of the membrane during the AP opens voltage-gated Ca^{2+} channels (Ca_v), which pass Ca^{2+} into the cell where it binds machinery that facilitates fusion of synaptic vesicles with the plasma membrane,

which results in release of neurotransmitters into the synapse. The boutons of the presynaptic neuron are apposed to neurotransmitter receptors on dendrites or the soma of the postsynaptic neuron across the synapse. These receptors are 'ligand-gated' ion channels (LGICs) and can be excitatory, such as AMPA and NMDA receptors that open cation channels and cause membrane depolarization, or inhibitory, such as $GABA_A$ and glycine receptors that open Cl^- channels and cause the membrane to hyperpolarize (Figure 1). Glutamate is the major excitatory neurotransmitter in the CNS and GABA is the major inhibitory neurotransmitter. Neurons are often referred to by the neurotransmitters they release or by the actions of those neurotransmitters (e.g. GABAergic/inhibitory neurons or glutamatergic/excitatory neurons).

Pharmacology of general anesthetics

General anesthetics induce a reversible, drug-induced loss of consciousness with a unique pharmacology. The use of general anesthesia requires immediate onset and reversibility of the drug effect as opposed to more conventional therapeutics that can take days or weeks to reach full effect. General anesthetics also have a very narrow therapeutic index; concentrations that cause toxic or lethal side effects are only 2 – 4 times that used for anesthesia. However, dose-response curves for anesthetics are very steep, meaning only slight changes in drug concentration exert large effects on physiological response (Hemmings et al., 2005b). This is important because it allows

the anesthesiologist to keep the administered dose close to the EC_{50}, which avoids toxic side effects and allows for quick reversibility of the anesthetic state.

Some of the most widely used general anesthetics are inhaled or gaseous agents. This class of drugs include halogenated ethers that are referred to as 'volatile' anesthetics (VAs), which reflects their tendency to vaporize at room temperature and standard pressure. VAs are small lipophilic molecules that can easily pass through cell membranes and into the blood stream from the lung where they quickly reach the well-perfused CNS. Potency of inhaled anesthetics is measured as the exhaled concentration at steady-state, and is referred to as minimum alveolar concentration (MAC), which is the concentration at which 50% of patients do not respond to a surgical incision (Eger et al., 1965). MAC, determined using immobility as the endpoint, translates to aqueous concentrations in the hundreds of micromolar to millimolar range for commonly used volatile anesthetics (Franks and Lieb, 1994). However, the concentrations of drug needed for half maximal effect of amnesia and unconsciousness are a fraction of MAC, which indicates that these behavioral endpoints are mediated by distinct neural circuits and/or target proteins.

VAs are minimally metabolized by cytochrome P450 enzymes in the liver (Kharasch and Thummel, 1993; Spracklin et al., 1996); the extent to which these anesthetics are metabolized determines their level of hepatic and renal toxicity (Hudson et al., 2013). VAs with high rates of metabolism, such as halothane that is 40-60% metabolized, have a high risk of 'halothane hepatitis', which has subsequently

reduced its use in the clinic (Cohen, 1978; Safari et al., 2014). Isoflurane is used widely in part because of its very low (<0.1%) rate of metabolism and sevoflurane is also considered relatively non-toxic because it is poorly metabolized (Pihlainen and Ojanperä, 1998; Safari et al., 2014).

Mechanisms of general anesthetic action

Until the late 20th century, the structural diversity of general anesthetics cultivated the idea of a common, nonspecific mechanism of action (Franks, 2006; Hemmings et al., 2005c; Kopp Lugli et al., 2009). The Meyer-Overton correlation describes a direct correlation between anesthetic potency and lipid solubility (Meyer, 1899; Overton, 1901; Perouansky, 2012). This led to lipid-based theories of anesthetic action that implied that anesthetics act by dissolving into the lipid bilayer and disrupting the cell membrane. Lipid-based theories dominated the field for the majority of the 20th century but, following the introduction of the fluorinated methyl ethyl ethers in the 1960s, failed to explain the differences in potency *in vivo* between enantiomers of inhaled anesthetics such as isoflurane that have a chiral carbon (Dickinson et al., 1994; Koblin et al., 1981; Lysko et al., 1994). Also, the discovery of lipophilic halogenated hydrocarbons that lack anesthetic potency and therefore disobey the Meyer-Overton correlation proved incongruous to lipid-based theories of anesthetic action (Koblin et al., 1994; Perouansky, 2008).

In the 1980's Franks and Lieb redirected the focus from nonspecific lipid-based theories to identifying specific protein targets of general anesthetics (Franks and Lieb, 1978; Franks and Lieb, 1982). Using purified firefly luciferase, they demonstrated that anesthetics bind the protein in the absence of lipid and displace luciferin, the endogenous ligand (Franks and Lieb, 1984). Today many targets have been identified, mostly voltage- and ligand-gated ion channels. Targets for general anesthetics have to show a reversible response to clinical concentrations of drug, stereoselectivity *in vitro* matching that *in vivo*, and a lack of response to nonanesthetic agents (Franks and Lieb, 1994; Hemmings et al., 2005c).

It is now widely accepted that the behavioral endpoints of general anesthesia arise from different areas and circuits within the CNS. For a protein to be considered a plausible target, it must be expressed in the area of the CNS that gives rise to the relevant behavioral endpoint (Hemmings et al., 2005c). Immobility arises from anesthetic effects in the spinal cord (Sonner et al., 2003). This was discovered through experiments in rats that showed isoflurane retains the ability to depress motor reflexes in response to noxious stimuli even when the brain is disconnected from the spine (Rampil, 1994; Rampil et al., 1993). Amnesia arises from the regions in the forebrain important for learning and memory such as the hippocampus and cerebral cortex (Caraiscos et al., 2004; Rau et al., 2011; Wang and Orser, 2011). The neuronal correlates of unconsciousness are less clear and are generally thought to include areas of the cortex, thalamus and brainstem (Alkire et al., 2000; Rudolph and Antkowiak,

2004) and may involve hypothalamic sleep-promoting pathways as well (Han et al., 2014; Zecharia et al., 2009).

General anesthetics enhance inhibitory postsynaptic currents, depress excitatory postsynaptic currents and depress exocytosis of excitatory neurotransmitters (Hemmings, 2009). A number of ion channels, mostly postsynaptic LGICs, have been identified as targets for general anesthetics, but no one target is sufficient to explain the behavioural state induced by any given anesthetic. $GABA_A$ receptors ($GABA_AR$) are LGICs found mainly in the brain that pass inhibitory Cl^- current. These channels have emerged as important anesthetic targets since they are potentiated by a wide variety of general anesthetics and account for a majority of the effects of the widely used intravenous anesthetic propofol (Krasowski and Harrison, 1999). While $GABA_AR$ plays more of a role in the mechanism of action of propofol than VAs (Kungys et al., 2009; Sonner et al., 2007; Wakasugi et al., 1999), the amnestic effects of isoflurane are attributed to enhancement of $GABA_AR$ since forebrain-specific knock-down of essential $GABA_AR$ subunits prevent the amnestic effects of isoflurane in mice (Rau et al., 2009; Rau et al., 2011). Extrasynaptic $GABA_ARs$ in the thalamus and hippocampus, which produce tonic inhibitory postsynaptic currents, are especially sensitive to VAs (Caraiscos et al., 2004; Jia et al., 2008) and play a role in isoflurane-induced amnesia and sedation (Orser, 2006; Wang and Orser, 2011; Zurek et al., 2012). Effects on $GABA_ARs$ cannot however, explain immobility produced by VAs (Kim et al., 2007; Werner et al., 2011).

VAs have a number of other targets that they modulate at clinically relevant concentrations (Figure 2). Glycine receptors (GlyR) are inhibitory postsynaptic LGICs found mainly in the spinal cord that are potentiated by VAs and contribute to their immobilizing effects (Zhang et al., 2003). VAs also inhibit excitatory postsynaptic currents by blocking NMDA (Nishikawa and MacIver, 2000; Wakasugi et al., 1999), AMPA (de Sousa et al., 2000) and nicotinic acetylcholine receptors (nAChRs) (Hudson et al., 2013). Postsynaptic effects of VAs also include potentiation of outward K^+ current through 2-pore K^+ leak channels (K2P) which hyperpolarizes the membrane (Sirois et al., 2000; Westphalen et al., 2007; Winegar et al., 1996) and desensitizes the neuron to excitatory input (Berg-Johnsen and Langmoen, 1990).

VAs also have presynaptic effects, which cause a reduction in excitatory neurotransmitter release (Maclver et al., 1996; Perouansky et al., 1995; Schlame and Hemmings, 1995). Direct evidence shows that isoflurane inhibits exocytosis (Hemmings et al., 2005a; Winegar and MacIver, 2006) and this inhibition is selective for glutamatergic over GABAergic terminals (Westphalen and Hemmings, 2006). Presynaptic effects indicate actions on the voltage-gated Na^+, K^+, and Ca^{2+} channels that underly the AP and exocytosis. However, experiments on myelinated mammalian nerve fibers previously showed that AP propogation is not affected by clinical concentrations of VAs (Larrabee and Posternak, 1952). This led to the idea that VAs have no effect on voltage-gated ion channels. However, more recent studies show conduction along unmyelinated nerve fibers are sensitive to clinical concentrations of VAs (Berg-Johnsen and Langmoen, 1986; Mikulec et al., 1998). Moreover, isoflurane

inhibits the presynaptic AP in glutamatergic nerve terminals (Ouyang and Hemmings, 2005; Wu et al., 2004). Isoflurane inhibits low-voltage activated T-type Ca^{2+} channels that underlie burst firing in thalamocortical neurons (Orestes et al., 2009) as well as presynaptic high-voltage activated L- and R-type channels in the hippocampus and thalamus (El Beheiry et al., 2007; Joksovic et al., 2009). There is also some, albeit conflicting evidence that VAs inhibit N- and P/Q type channels in heterologous expression systems (Orestes and Todorovic, 2010).

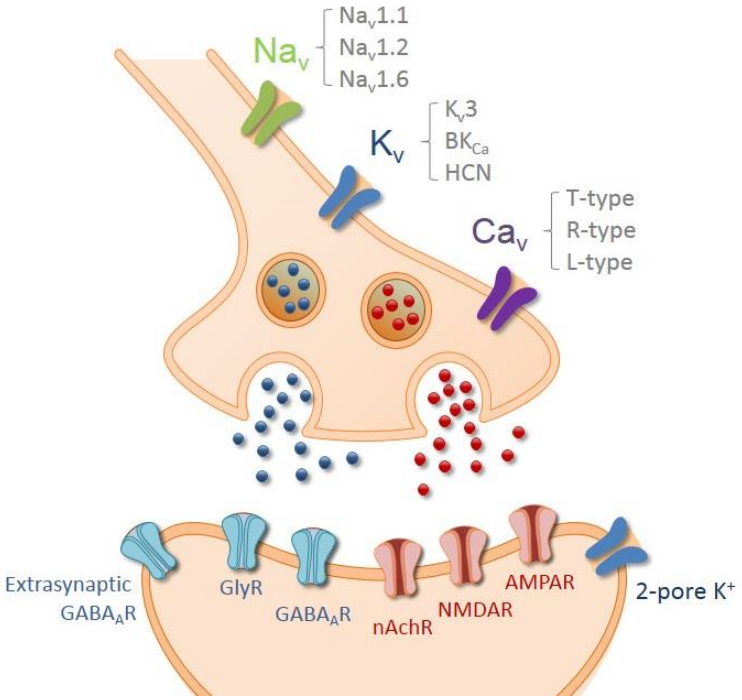

FIGURE 2. Putative targets of volatile anesthetics. Diagram of protein targets at the synapse. VAs inhibit presynaptic Na_v, K_v and Ca_v subtypes (indicated in gray). VAs inhibit excitatory postsynaptic receptors (shown in red) and enhance inhibitory postsynaptic and extrasynaptic receptors (turquoise) and postsynaptic 2-pore K^+ leak channels (blue).

Voltage-gated sodium channels as targets for general inhaled anesthetics

Voltage-gated sodium channels (Na_v) are essential components of all excitable cells in that they underlie the depolarization of the membrane during the AP. Na_v are

large macromolecular complexes embedded in the cell membrane that selectively allow Na^+ to pass through. The pore forming α-subunit of Na_v contains 4 domains with 6 transmembrane domains each (S1-S6). Na_v are closed at hyperpolarized membrane potentials and open when positively charged residues in the S4 transmembrane segment move outward in response to membrane depolarization and open the channel (Catterall, 2002; Cestèle et al., 2006) (Figure 3). Channels rapidly enter an inactivated state after opening and are unavailable for opening upon membrane depolarization. Na_v have rapid gating kinetics and cycle through these states within a matter of milliseconds.

There are nine mammalian isoforms of Na_v that share significant sequence homology and have similar gating kinetics (Goldin et al., 2000; Mechaly et al., 2005). However, distinct expression patterns of the different subtypes points to a specialization of subtype function (Goldin, 2001; Gordon et al., 1987). $Na_v1.1$, $Na_v1.2$ and $Na_v1.6$ are found in the adult mammalian brain (Beckh et al., 1989) with $Na_v1.7$ $Na_v1.8$ and $Na_v1.9$ mainly found in the periphery (Goldin, 2001). $Na_v1.4$ and $Na_v1.5$ are found in skeletal and heart muscle, respectively, with $Na_v1.5$ also expressed in the entorihnal cortex where it maintains distinctive 'cardiac Na_v-like' properties (White et al., 1993). $Na_v1.5$, along with $Na_v1.8$ and $Na_v1.9$, are relatively resistant to the puffer fish toxin tetrodotoxin (TTX) which blocks all major CNS isoforms in the nanomolar range (Goldin, 2001). The pore-forming 'α-subunit' of Na_v is transcribed from a single gene that undergoes alternative splicing and also assembles with auxillary β-subunits and scaffolding proteins that modulate channel activity and surface expression to add

to the diversity of possible Na_v complexes (Goldin, 2001; Isom, 2001). Na_v are also highly regulated by phosphorylation *in vivo* which mediates expression, localization and channel activity (Baek et al., 2011; Berendt et al., 2010).

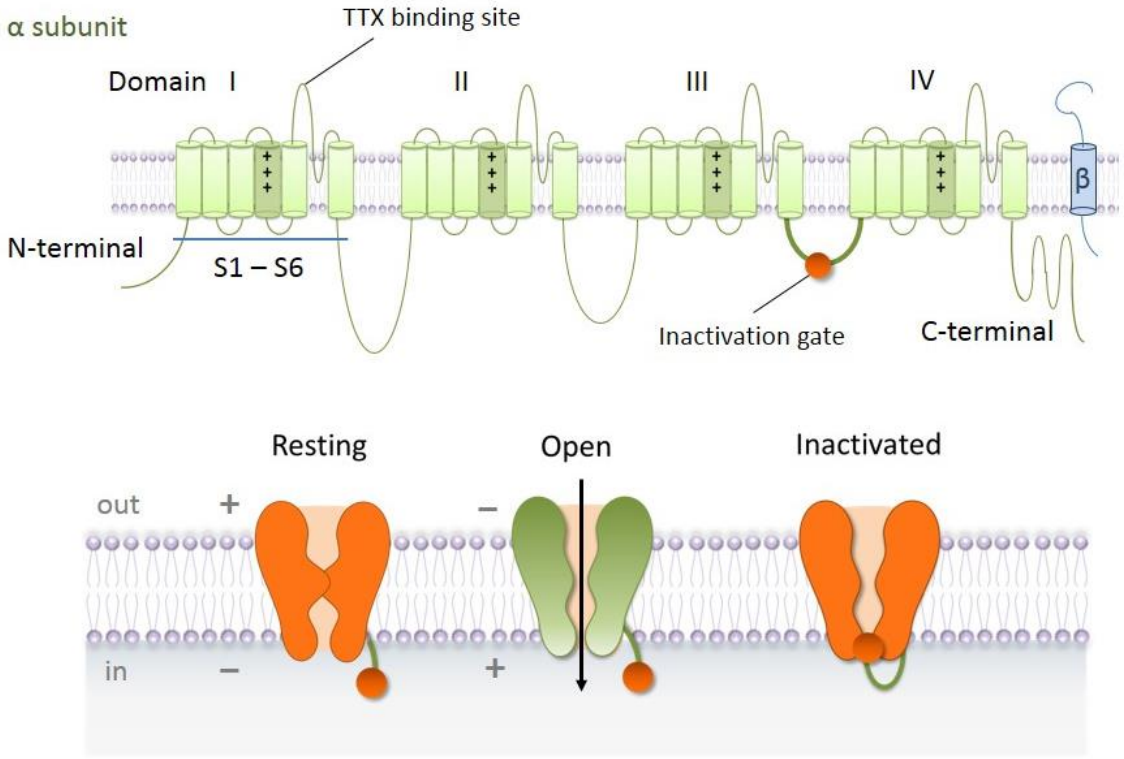

FIGURE 3. Voltage-gated sodium channel topology and conformational states. *Top,* Topology of the Na_v α-subunit containing 4 domains each with 6 transmembrane segments (S1-S6). Positively charged residues in S4 are indicated with '+'. The loop between S5-S6 of domain I contains the TTX binding site and the loop between domains III and IV is the inactivation gate. The single-transmembrane spanning β subunit is shown in blue. *Bottom,* Conformation states of Na_v: 'Resting', 'Open', and 'Inactivated'. Membrane voltage indicated by +/−.

The subcellular distribution and cell-type specific expression profiles highlight the various cellular functions of Na_v. A high concentration of Na_v in the AIS is

necessary for AP generation (Colbert and Johnston, 1996). In the AIS of excitatory neurons that mainly express $Na_v1.2$ and $Na_v1.6$, $Na_v1.2$ is concentrated proximal to the cell body and $Na_v1.6$ is more concentrated distally (Boiko et al., 2003). Due to the more hyperpolarized activation voltage of $Na_v1.6$ (Rush et al., 2005) and its distance from the soma (Kress et al., 2010), the AP is generated in the distal region of the AIS and propagates down the length of the axon. APs also backpropogate into the soma and the dendrites since $Na_v1.2$ is activated only after the AP is generated (Hu et al., 2009). The backpropogation of APs into dendrites regulates incoming stimuli (Jung et al., 1997; Kole and Stuart, 2012). $Na_v1.1$ makes up only 10% of brain Na_v (Gordon *et al.* 1987). There is evidence that $Na_v1.1$ is specifically expressed in GABAergic neurons where it is found in the AIS and nodes of Ranvier (Lorincz and Nusser, 2008). This poses an interesting question of whether the greater anesthetic sensitivity of glutamate release compared to GABA could be due to differences in Na_v subtype expression.

In unmyelinated central axons there is a high density of Na_v in presynaptic terminals suggesting that the AP is actively regenerated in boutons rather than passively transmitted (Engel and Jonas, 2005). $Na_v1.2$ is the predominant isoform in unmyelinated axons in the CNS (Boiko et al., 2001) and has been detected on the presynaptic membrane of hippocampal neurons using immunoelectron microscopy (Lorincz and Nusser, 2010). $Na_v1.6$ is the predominant isoform in myelinated axons and has been shown to be both pre- and postsynaptic in cortical neurons (Boiko et al., 2001; Caldwell et al., 2000). The subcellular distribution of Na_v may play a key role in

understanding anesthetic sensitivity and cell-type specific effects of anesthetics. Different Na_v subtypes may be expressed in the axon as opposed to the bouton for example, and the relative sensitivity of Na_v subtypes to general anesthetics may determine effects on neurotransmitter release.

A role for Na_v in the modulation of neurotransmission by general anesthetics is supported by evidence that presynaptic blockade of Na^+ current (I_{Na}) contributes to suppression of the release of multiple neurotransmitters by VAs (Hemmings et al., 2005a; Westphalen and Hemmings, 2003; Wu et al., 2004). Isoflurane blocks multiple subtypes of Na_v (Herold et al., 2009; Ouyang and Hemmings, 2007; Rehberg et al., 1996; Shiraishi and Harris, 2004), and reduces AP amplitude in rat hippocampal neurons (Berg-Johnsen and Langmoen, 1990), isolated rat neurohypophysial terminals (Ouyang and Hemmings, 2005) and rat Calyx of Held (Wu et al., 2004).

Intrathecal delivery of the highly specific Na_v inhibitor tetrodotoxin (TTX) in adult rats enhances isoflurane potency in producing immobilization, a primarily spinal cord-mediated effect, whereas the Na_v activator veratridine reduces isoflurane potency and antagonizes the effect of TTX (Zhang et al., 2010). Futhermore, altered concentrations of Na^+ in the spinal cord, but not in the brain, have been shown to affect MAC, arguing that a protein regulated by the Na^+ gradient is a target for isoflurane in the spinal cord (Laster et al., 2007).

Drugs that block Na_v are often state-dependent, that is they have a greater affinity for one state of the channel, be it open, closed, inactivated (Figure 3), or some

other intermediate state (Fozzard et al., 2005; Ragsdale et al., 1994). This is the case for local anesthetics that preferentially bind open or inactivated Na_v with greater potency (~30 μM) than Na_v in the resting state (~300 μM) (Nau and Wang, 2004; Wang et al., 2004). This phenomenon makes the potency of the drug dependent on the activity of the channel and the voltage of the membrane. Isoflurane alters the voltage-dependence of $Na_v1.2$ gating *in vitro* (Ouyang et al., 2003; Rehberg et al., 1996; Shiraishi and Harris, 2004), which indicates block of Na_v by isoflurane is state-dependent.

This dissertation focuses on the mechanism of action of the widely used inhaled anesthetic isoflurane as it pertains to Na_v. We measure the effects of clinical concentrations of isoflurane on neuronal excitability in cultures of neonatal rat hippocampal neurons. Hippocampal neurons form extensive synaptic connections after 7 DIV and allow us to study the effects of isoflurane on spontaneous AP firing as well as intrinsic membrane excitability. Dissociated hippocampal neurons also retain electrophysiological properties *in vitro* similar to those seen in slice recordings (Kay and Wong, 1986). We further investigate the effects of isoflurane on Na_v in a heterologous system expressing recombinant $rNa_v1.2$, the most abundant Na_v isoform in unmyelinated axons of central neurons (Boiko et al., 2001). We use this system to measure changes in Na_v voltage-dependance and gating kinetics in the presence of isoflurane. We find that isoflurane at clinical concentrations has significant effects on Na_v and neuronal excitability and we discuss these findings in the context of modern theories of anesthetic action.

CHAPTER TWO

MATERIALS AND METHODS

Materials

Isoflurane was obtained from Abbott Laboratories (North Chicago, IL). TTX was purchased from Sankyo Kasei (Tokyo, Japan). Amphotericin B, tetraethylammonium chloride (TEACl), and other chemical reagents were purchased from Sigma-Aldrich (St. Louis, MO). E16 – E18 pregnant Sprague-Dawley rats were purchased from Charles River Laboratories (Wilmington, MA).

Anesthetic solutions

External bath solutions were saturated with isoflurane (12-12.5 mM; Abbott Laboratories, North Chicago, IL) and diluted to final concentrations of 0.45-0.5 mM in gas-tight glass syringes. Isoflurane solutions were perfused using a pressure driven microperfusion system (ALA BPS-8; ALA Scientific, Westbury, NY) positioned 100-150 µm away from the cell. Concentrations of isoflurane sampled at the perfusion pipette tip were measured using a Shimadzu GC-2010 Plus gas chromatograph (Shimadzu, Tokyo, Japan) following extraction into octane (1:1 v/v), and reflected ~10% loss from the syringe to the bath (Herold et al., 2009).

Solutions of 1,2-dichlorohexafluorocyclobutane (F6) were prepared in the same manner with the saturated solution (0.25 mM) diluted to final concentrations of 0.025mM (2 MAC).

Primary rat hippocampal neuron cultures

Animal protocols were approved by the Institutional Animal Care and Use Committee of Weill Cornell Medical College. Postnatal Day 1 Sprague-Dawley rats (Charles River Laboratories) were decapitated and the hippocampus dissected out and chopped into pieces in ice cold HBSS + 20% FBS (GIBCO). Tissue was washed in HBSS and digested in 10mg/mL trypsin (Sigma-Aldrich) for 5 minutes at RT. Cells were dissociated by pipetting up and down in HBSS with 1mg ml^{-1} DNAse (Sigma-Aldrich). Cells were spun down in HBSS + 20% FBS, 1300 rpm for 10 min and plated cells 250,000 cells mL^{-1} on glass coverslips coated with poly-D-lysine and laminin (BD Biosciences, East Rutherford, NJ). The anti-mitotic cytosine arabinoside (Ara-C) was added to the media after 36 hours and cells were patched after 7-14 DIV.

Cell culture and Na_v transfection of ND7/23 cells

Neuroblastoma ND7/23 cells were plated on 12-mm glass coverslips and incubated in a humidified atmosphere at 37°C in 5% CO_2 in Dulbecco's modified Eagle's medium supplemented with 10% (v/v) fetal bovine serum, 2 mM L-glutamine, 100 U ml^{-1} penicillin and 100 μg ml^{-1} streptomycin (all reagents from Sigma-Aldrich unless specified).

Wild-type rat $Na_v1.2a$ (accession number NM_012647) was kindly provided by Prof. William Catterall (University of Washington, Seattle). TTX-resistance was engineered into $Na_v1.2a$ by site-directed mutagenesis (F385S) (Leffler et al., 2005) (referred to as $Na_v1.2_R$) to allow isolation from endogenous channels and expression in a neuronal background, which is crucial to measuring the effect of isoflurane on Na_v in heterologous expression systems (Herold et al., 2009). Cells were transiently transfected with $Na_v1.2_R$ and pEGFP-N1 (Clontech, Mountain View, CA) cDNA using Lipofectamine LTX (Invitrogen, Carlsbad, CA) to allow identification of transfected cells by eGFP fluoresence imaging. Experiments were performed in the presence of 250 nM tetrodotoxin (TTX; Sankyo Kasei, Tokyo, Japan) to block endogenous I_{Na}.

Electrophysiological recording of ND7/23 cells

Whole-cell patch-clamp experiments were performed at room temperature (23-24°C) using an Axopatch 200B amplifier (Axon Instruments, Burlingame, CA), digitized via a Digidata 1321A interface, and analysed using pClamp 10.2 software (Axon Instruments). Whole-cell currents were sampled at 50 kHz and low-pass filtered at 5 kHz. Whole-cell seal resistance was 2–8 GΩ prior to patch rupture. Pipette resistance was 1.5-2.5 MΩ when filled with internal solution containing (in mM): 120 CsF, 10 NaCl, 10 HEPES, 10 EGTA, 10 TEA-Cl, 1 $CaCl_2$, and 1 $MgCl_2$ and adjusted to pH 7.3 (with CsOH) and 310 mOsm kg^{-1} H_2O. External solution contained (in mM): 130 NaCl, 10 HEPES, 3.25 KCl, 2 $MgCl_2$, 2 $CaCl_2$, 20 TEA-Cl, 5 D-glucose, 0.00025

TTX and was adjusted to pH 7.4 with NaOH and 310 mOsm kg^{-1} H_2O with sucrose. The liquid–junction potential (~7.8 mV) was not corrected.

Only cells expressing 2-8 nA of peak current were analysed in order to minimise space clamp and series resistance errors. Capacitive transients were electronically cancelled and voltage error was minimised using 70-80% series resistance compensation. Series resistance was typically 2–4 MΩ and data were discarded if >10 MΩ. Experiments began 5 min after attaining whole-cell patch to allow equilibration of the pipette solution with the cytosol. Voltage protocols were applied from a holding potential (V_h) of −70 mV or −90 mV with 5 s intervals between sweeps. Protocols were applied in control solution and again after 5 min perfusion with isoflurane. Perfused cells showed stable responses (rundown <10%) for up to 5 min in control experiments (data not shown). Linear leak currents were subtracted using the P/4 method (Bezanilla and Armstrong, 1977).

Stimulation protocols

Current-voltage (I-V) relationships were determined by measuring the peak current at a series of 10-ms voltage commands ranging from -50 mV to +30 mV in 10-mV steps applied at 5-s intervals using a holding potential (V_h) of either -70 mV or -90 mV. Voltage steps were preceded by a 50-ms prepulse to -100 mV to relieve Na_v from inactivation. The relationship between conductance (G) and voltage was derived from the I-V relationship using the equation $G = I/(V-V_{rev})$, where *I* is the peak I_{Na} at a given voltage (V) and V_{rev} is the measured Na^+ reversal potential. Normalized conductance values (G/G_{max}) were fit to the Boltzmann equation $G/G_{max} = 1/[1 +$

exp($V_{1/2}$ - V/*k*)], where $V_{1/2}$ is the voltage at half-maximal activation and *k* is the slope factor. Steady-state inactivation was measured using a two-pulse protocol consisting of a 50-ms prepulse to voltages ranging from −100 mV to −20 mV in 10-mV increments followed by a 10-ms pulse to 0 mV. Normalized peak current (I_{Na}/I_{Na}max) was plotted against prepulse voltage and fitted with a Boltzmann function. Recovery from inactivation was measured at V_h of −70 or −90 mV by administering two 5-ms pulses to 0 mV separated by a recovery period of increasing durations from 1 – 100 ms. I_{Na} of the second pulse was divided by I_{Na} of the first pulse ($Pulse_2/Pulse_1$) and plotted against the time of the interpulse interval and fitted with a single exponential equation. The onset of inactivation was measured using a pulse to 0 mV for increasing durations of 0.7 to 50 ms, followed by a brief 2-ms return to V_h (−90 mV) before a test pulse to 0 mV for 5 ms. The ratio of I_{Na} for $Pulse_2/Pulse_1$ was plotted against the duration of the first pulse and fit with a mono-exponential function.

Activity-dependent block was quantified by administering 50-Hz trains of either 5- or 15-ms pulses to 0 mV for 200 ms from V_h of −70 or −90 mV. I_{Na} for each pulse was normalized to I_{Na} of Pulse 1 ($Pulse_n/Pulse_1$) and plotted against pulse number. Data were fitted to the mono-exponential function $Pulse_n/Pulse_1 = \exp(-\tau*n)+A_P$, where τ is the time constant, A_P is the plateau and n is stimulus number. To determine the kinetics of macroscopic inactivation, I_{Na} was elicited by a 5-ms pulse to 0 mV from a V_h of −70 mV. Current traces from paired control and isoflurane experiments were normalized to peak I_{Na} and the decay phases were fit with a bi-exponential equation.

Statistical analysis

Data were analysed using Prism v6.05 (Graph-Pad Software Inc., San Diego, CA) and SigmaPlot 6.0 (SPSS Science Software Inc., Chicago, IL). Conductance (G) values were derived from the I-V relationship using the equation $G = I/(V-V_{rev})$, where I is the peak I_{Na} at a given voltage (V) and V_{rev} is the measured Na^+ reversal potential. Voltages at half-maximal activation ($V_{½act}$) were obtained from fitting the data for each cell to a Boltzmann equation of the form $G/G_{max} = 1/[1 + \exp(V_{½act} - V/k)]$, where G/G_{max} is the normalized fractional conductance and k is the slope factor. The voltage at which fast inactivation is half-maximal ($V_{½}$) was measured by fitting normalized steady-state I_{Na} values to a Boltzmann function of the form $I_{Na}/I_{Na}max = 1/[1 + \exp(V_{½} - V/k)]$. Time course data were fitted to the mono-exponential function $Y = \exp(-\tau*n)+A_P$, where τ is the time constant, A_P is the plateau and n is stimulus number. To determine the kinetics of macroscopic inactivation, the decay phase of the current trace was fit with a bi-exponential equation of the form $A_1 \bullet \exp(-t/\tau_1) + A_2 \bullet \exp(-t/\tau_2) + B$, where A_n is the nth component amplitude, B is the plateau, t is time and τ_n are time constants.

Data are expressed as mean [standard deviation, SD], and were analyzed using two-tailed paired Student's *t*-test or ANOVA with post hoc testing as indicated, with statistical significance set as p=0.05.

CHAPTER THREE

RESULTS

Isoflurane reduces spontaneous activity of isolated hippocampal neurons

First we determined the effects of isoflurane on the spontaneous activity of hippocampal CA2/3 pyramidal neurons cultured for 10-14 DIV. We recorded from actively firing neurons with a 'pyramidal-like' morphology and RMP between −55 and −65 mV and measured responses to concentrations of isoflurane that produce anesthesia in rats [0.42 mM; equivalent to ~1.5 times MAC (minimum alveolar concentration)] (Taheri et al., 1991). We also applied the nonimmobilizer 1,2-dichlorohexafluorocyclobutane (F6), which is a small halogenated hydrocarbon that disobeys the Meyer-Overton correlation in that it lacks anesthetic potency at concentrations predicted by its lipophilicity (Perouansky, 2008).

Neurons fired spontaneously in culture for up to 15 min as APs were recorded passively using the whole-cell configuration in current-clamp mode. We recorded spontaneous activity in the absence or presence of F6 and isoflurane and measured the frequency of AP firing in the final minute of each 3 min perfusion. Isoflurane significantly reduced firing frequency by 87% compared to control (CTL=6.1±1.1 Hz, *vs.* ISO=0.8±0.4 Hz, n=4, $^{**}p$=0.003, one-way ANOVA and Tukey's post-hoc test)

whereas F6 had no effect (CTL=6.1±1.1 Hz, *vs*. F6=6.0±0.9 Hz, *n*=4, n.s.) (Figure 4). To test whether this effect of isoflurane was reversible, we washed with control buffer for 5 min following perfusion with isoflurane. Firing frequency was determined by counting the number of APs in the last minute of perfusion. Isoflurane significantly lowered firing frequency compared to control (CTL= 4.5±1.2 Hz *vs*. ISO= 0.8±0.4 Hz , *n*=5, mean±SD, ***p*=0.009), and this effect was reversible upon washout (ISO= 0.8±0.4 Hz, *vs*. WASH= 3.9±1.3 Hz, *n*=5, **p*=0.01; CTL= 4.5±1.2 Hz *vs*. WASH= 3.9±1.3 Hz , *n*=5, n.s., one-way ANOVA w/ Tukey's post hoc test) (Figure 5).

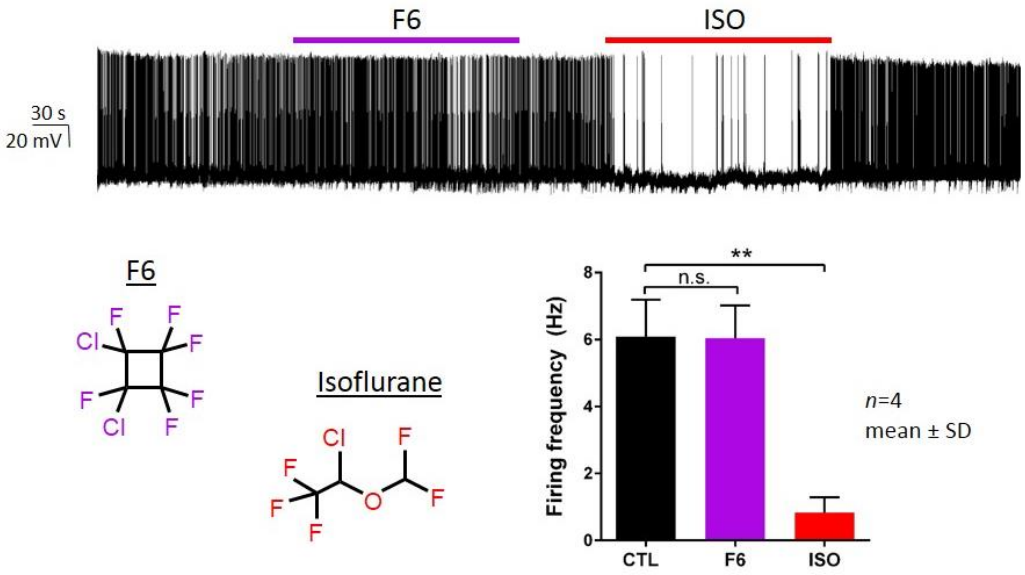

FIGURE 4. Isoflurane but not the nonimmobilizer F6 inhibits spontaneous activity of hippocampal neurons. *Top*, A spontaneously firing cultured rat hippocampal neuron superfused with 2 MAC 1,2-dichlorohexafluorocyclobutane (F6) for 3 min followed after 1 min by 1.5 MAC isoflurane for 3 min. *Lower left*, Structure of F6 and isoflurane. *Lower Right*, Average firing frequency (Hz) of 4 cells in control (6.1±1.1 Hz), during the last minute of F6 perfusion (6.0±0.9 Hz) and during the last minute of isoflurane perfusion (ISO, 0.8±0.4 Hz). Data are presented as mean±SD and tested with one-way repeated measures ANOVA and Tukey's post-hoc test.

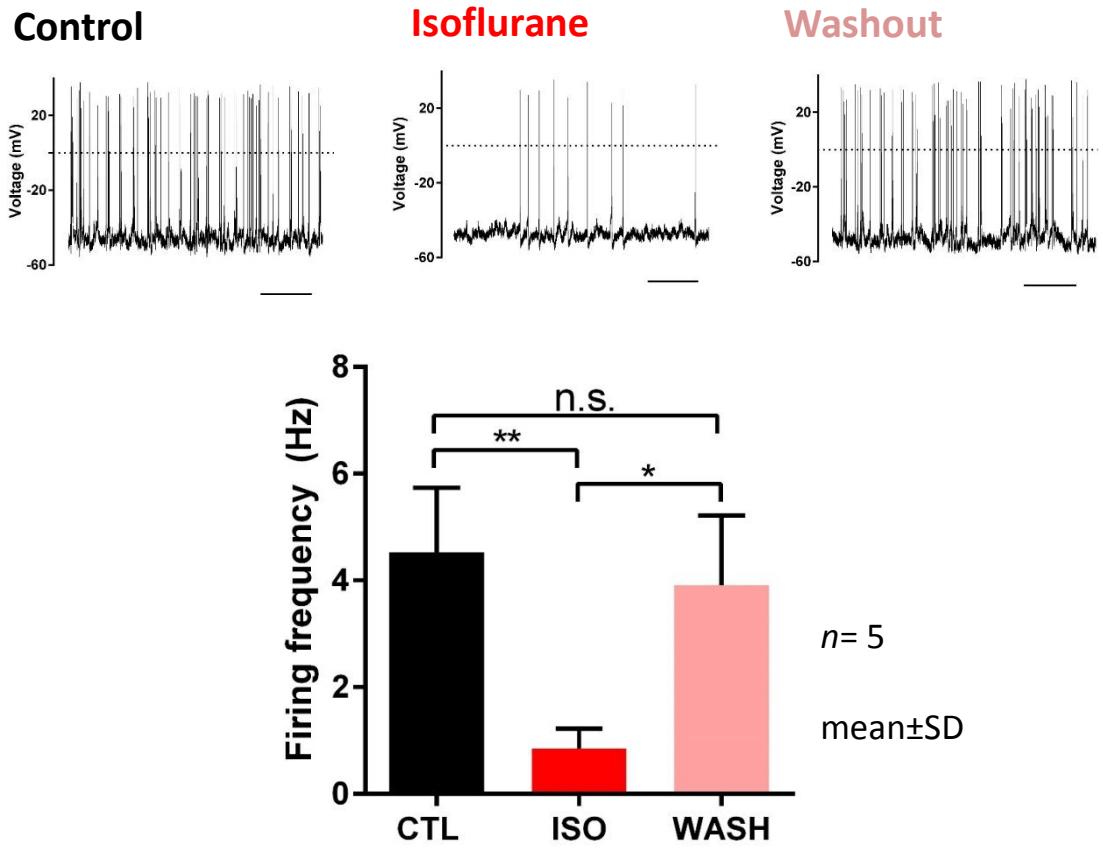

FIGURE 5. Isoflurane reversibly inhibits spontaneous firing activity in hippocampal neurons. *Top panels from left*, 10 s segment of action potential firing in control, in the presence of ~1.5 MAC isoflurane, and after 5 min washout of isoflurane. Dotted line denotes 0 mV, scale bar = 2 s. Average firing frequencies of 5 cells in all three conditions (CTL= 4.5±1.2 Hz, ISO= 0.8±0.4 Hz, WASH= 3.9±1.3 Hz). Data are presented as mean±SD and are compared using a one-way repeated measures ANOVA with Tukey's post-hoc test *p<0.05, **p<0.01

In approximately 1 out of every 5 neurons, firing activity was characterized by prominent waves of membrane depolarization that lasted a few seconds and were

crowned by bursts of APs (Figure 6). These cells were analyzed separately using the area under the raised membrane potential to estimate Ca^{2+} current and the crowning spikes as a measure of Na^+ and K^+ current (Huguenard, 1996). In control and isoflurane conditions, the area under the raised membrane potential was similar (CTL= 15±5 vs. ISO= 13±5 [AU], *n*=3, mean±SD, n.s. *p*=0.2, two-tailed, paired Student's *t*-test), but isoflurane significantly decreased the number of spikes per wave (CTL= 8.4±2.7 vs. ISO= 3.8±2.0, *n*=3, mean±SD, **p*=0.01, two-tailed, paired Student's *t*-test). Together these results indicate Na_v or K_v are more sensitive to isoflurane than Ca_v in these neurons.

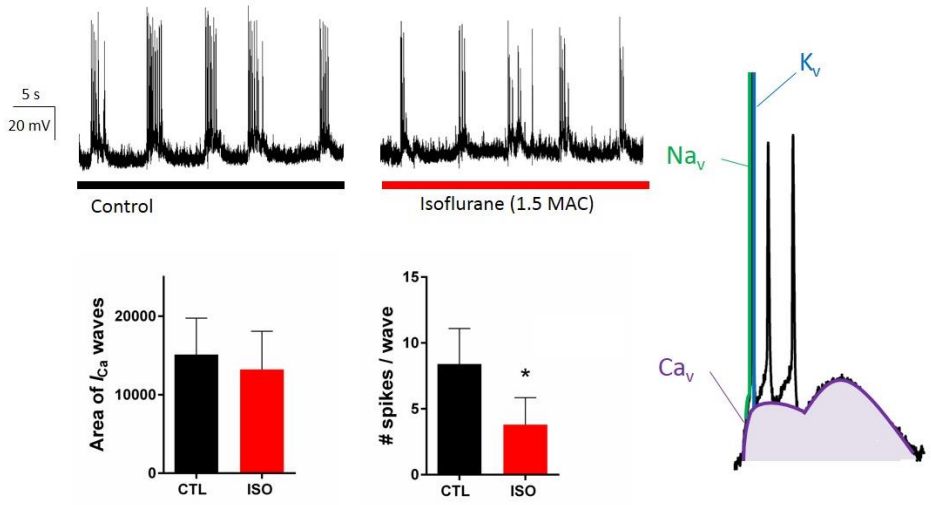

FIGURE 6. Isoflurane significantly decreases the number of spikes but does not affect the size of Ca^{2+} waves in hippocampal neurons. *Top*, 30 s traces of spontaneous activity in control and in the presence of isoflurane. *Right*, cartoon of ionic currents underlying this type of spontaneous activity. *Bottom left,* Area under the curve in control (15.1±4.6) and in the presence of isoflurane (13.2±4.8, *n*=3, mean±SD, n.s.). Average number of spikes per wave in a 1 min period for 3 different neurons in control (8.4±2.7 spikes $wave^{-1}$) and isoflurane (3.8±2.0 spikes $wave^{-1}$, mean±SD, **p*=0.01, two-tailed, paired Student's *t*-test).

We next looked more closely at the AP waveform since effects on Na_v or K_v alter the shape of the AP, which could consequently lead to altered Ca^{2+} influx and neurotransmitter release (Borst and Sakmann, 1999; Boudkkazi et al., 2011; Kole et al., 2007). We overlaid APs that were passively recorded in control and in the presence of ~1.5 MAC isoflurane. Control and isoflurane APs recorded from the same neuron were compared based on the resting membrane potential immediately preceding the AP, since this could strongly affect the shape of the AP (Gong *et al.* 2008). We compared APs initiated from the resting membrane potential (~−60 mV) as opposed to spikes elicited from on top of a depolarizing Ca^{2+} wave. Data collected from 5 neurons showed that ~1.5 MAC isoflurane significantly decreased AP amplitude ($CTL_{AP\ amplitude}$=92±6 mV *vs.* $ISO_{AP\ amplitude}$=67±13 mV, n=4, *p=0.03, two-tailed paired Student's *t*-test) (Figure 7). This effect could indicate a decrease in I_{Na}, accelerated Na_v inactivation or accelerated activation of repolarizing K_v currents. We next measured the velocity of the upstroke of the AP and the threshold for AP firing, two parameters that are determined largely by Na_v density and subtype expression (Bean, 2007; Hu et al., 2009). Isoflurane significantly decreased the velocity of the upstroke of the AP ($CTL_{AP\ velocity}$= 120±14 dV/dt, *vs.* $ISO_{AP\ velocity}$= 87±7 dV/dt, n=4, mean±SD, **p=0.009, two-tailed paired Student's *t*-test) and also shifted the threshold for AP firing in a depolarizing direction ($CTL_{AP\ threshold}$=−37±2 mV *vs.* $ISO_{AP\ threshold}$=−32±2 mV, n=5, mean±SD, **p=0.007, two-tailed paired Student's *t*-test) (Figure 7).

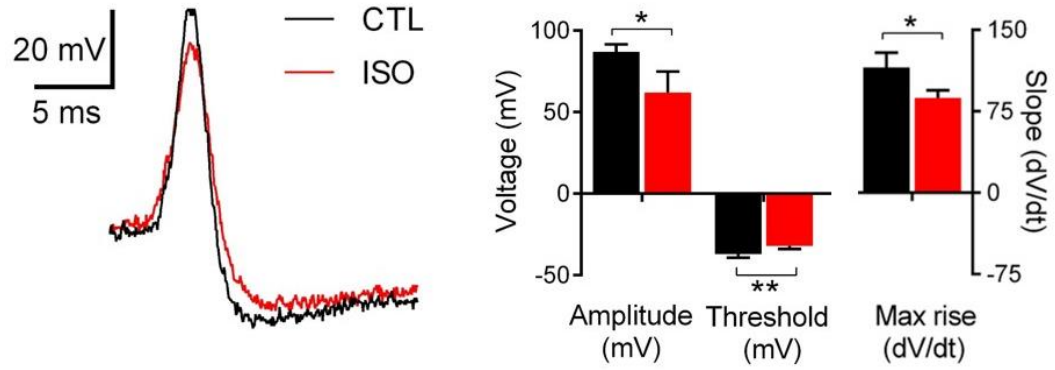

FIGURE 7. Effects of isoflurane on the presynaptic AP waveform in hippocampal neurons. *Left,* Representative APs recorded from the same cell in the absence (CTL) and presence of ~1.5 MAC isoflurane (ISO). *Right,* Parameters measured from paired APs in control or in the presence of isoflurane. Isoflurane reduced AP amplitude (CTL=92±6 mV vs. ISO=67±13 mV, **p*=0.03), raised the threshold for AP firing (CTL=−37±2 mV vs. ISO=−34±2 mV, ***p*=0.007) and decreased the maximum rate of rise (CTL=120±14 dV/dt, *vs.* ISO= 87±7 dV/dt, ***p*=0.04). Data are presented as mean±SD, *n*=4-5, *p* results from two-tailed paired Student's *t*-tests.

Isoflurane reduces intrinsic membrane excitability of hippocampal neurons.

When grown in culture, hippocampal neurons form extensive synaptic connections allowing for the generation of spontaneous activity. We determined whether the effects of isoflurane on Na_v–dependent AP parameters stemmed from block of Na_v or was a result of actions on postsynaptic LGICs that modulate incoming

excitatory and inhibitory stimuli. We did this by blocking synaptic input with a cocktail of neurotransmitter receptor inhibitors. We voltage-clamped the membrane at −60 mV and recorded postsynaptic activity in the presence of the inhibitors: 20 µM D-(-)-2-Amino-5-phosphonopentanoic acid (APV) to inhibit NMDA receptors (Davies and Watkins, 1982), 40 µM 6-Cyano-7-nitroquinoxaline-2,3-dione (CNQX) to inhibit AMPA receptors (Honore et al., 1988), 10 µM strychnine (Stry) to inhibit glycine receptors (White, 1985) and 100 µM picrotoxin (PTXN) to inhibit synaptic and extrasynaptic $GABA_A$ receptors (Alger and Nicoll, 1982). This cocktail blocked large depolarizing postsynaptic currents (Figure 8) and inhibited spontaneous firing activity.

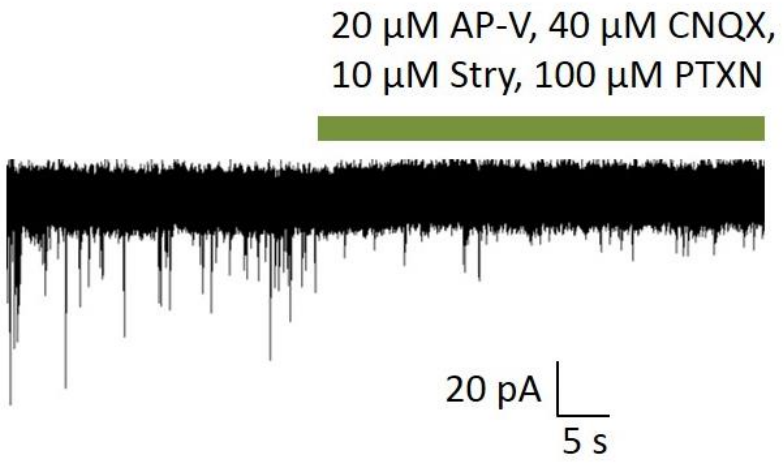

Figure 8. Inhibitors of synaptic ligand-gated channels and receptors block synaptic input. Voltage-clamp recording, V_h=−60 mV. Large depolarizing currents are blocked by addition of 20 µM AP-V (AMPAR), 40 µM CNQX (NMDAR), 10 µM Strychnine (Stry; GlyR) and 100 µM Picrotoxin (PTXN; $GABA_AR$).

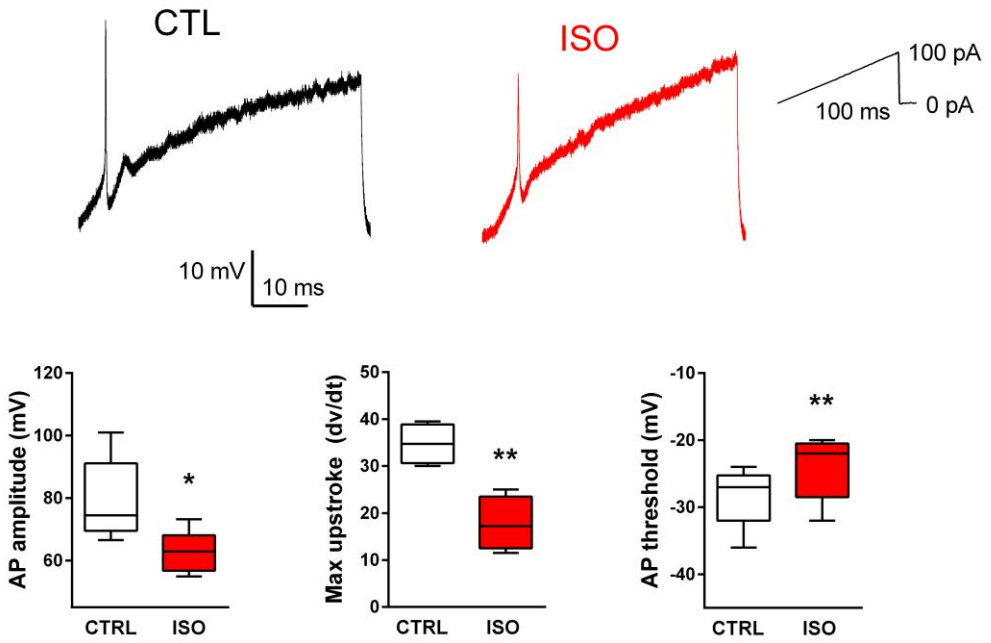

FIGURE 9. Isoflurane slows AP velocity, reduces AP amplitude and raises threshold of AP firing. *Top,* Representative traces of APs evoked in the absence (*left,* black) and presence (*right*, red) of ~1.5 MAC isoflurane using the protocol at the top *right* recorded in the presence of a cocktail of inhibitors of synaptic transmission (see Figure 8).

In the absence of spontaneous firing activity, we evoked APs with ramp current protocols that slowly increase the membrane potential by injecting steadily increasing amounts of depolarizing current. We used these protocols to determine the threshold for AP firing and measure the shape of APs evoked using electrical stimulation as opposed to synaptic input. Figure 9 shows exemplar traces of APs evoked using ramp current injections in control and in the presence of ~1.5 MAC

isoflurane. Isoflurane significantly decreased AP amplitude ($CTL_{AP\ amplitude}$=79±13 mV *vs.* $ISO_{AP\ amplitude}$=63±7 mV, *n*=5, **p*=0.02, two-tailed paired Student's *t*-test), decreased the velocity of the AP upstroke ($CTL_{AP\ velocity}$= 35±4 dV/dt, *vs.* $ISO_{AP\ velocity}$= 18±6 dV/dt, *n*=4, mean±SD, ***p*=0.009, two-tailed paired Student's *t*-test) and shifted the threshold for AP firing in a depolarizing direction ($CTL_{AP\ threshold}$=−28±5 mV *vs.* $ISO_{AP\ threshold}$=−24±4 mV, *n*=5, mean±SD, ***p*=0.004, two-tailed, paired Student's *t*-test). These results parallel the effects of isoflurane seen on spontaneous APs (Figure 7) yet the the amplitude and upstroke velocity of evoked APs are much smaller than spontaneous APs. This may be because excitatory input is blocked leaving the dendrites and soma hyperpolarized and able to act as a sink for the current generated by the AP. While this truncates the APs, the effect of isoflurane remains and further supports a role for block of presynaptic Na_v in hippocampal neurons.

Isoflurane blocks endogenous hippocampal Na_v at clinical concentrations

To directly measure isoflurane effects on Na_v, we recorded whole-cell I_{Na} from hippocampal neurons in the absence and presence of ~1.5 MAC isoflurane. We used a Cs^+-based internal pipet solution to eliminate outward K^+ currents. Whole-cell I_{Na} was recorded in the voltage-clamp configuration with the membrane potential clamped at −70 mV and depolarized to 0 mV for 5 ms to open Na_v. Na_v exhibited fast activation and inactivation kinetics on the millisecond time scale (Figure 10). Addition of ~1.5 MAC isoflurane reduced peak I_{Na} ~10%, similar to previous reports (CTL= −2.7±0.9

nA *vs.* ISO= −2.3±1.1 nA, *n*=6, mean ± SD, **p*=0.04, two-tailed paired Student's *t*-test).

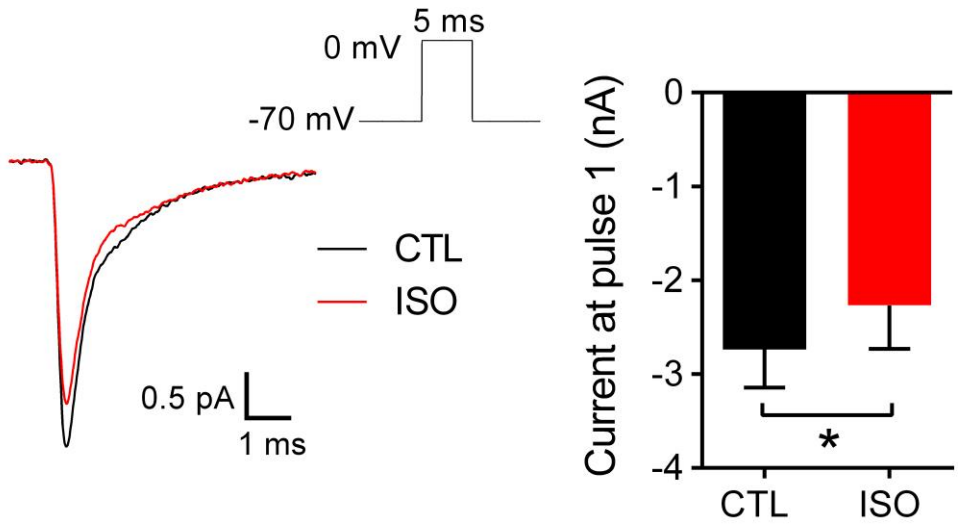

FIGURE 10. Isoflurane inhibits peak I_{Na} of endogenous neuronal Na_v. *Left*, Overlaid traces of whole-cell hippocampal neuron I_{Na} recorded at physiologic [Na^+] in control (CTL, *black*) or in the presence of ~1.5 MAC isoflurane (ISO, *red*) using a Cs^+-based internal solution. Inward current was elicited using the protocol at *top*. *Right*, Peak I_{Na} averaged from 6 neurons in control (CTL, −2.7±0.9 nA) and isoflurane (ISO, −2.3±1.1 nA). Data are presented as mean±SD, **p*=0.04, two-tailed paired Student's *t*-test.

Isoflurane blocks Na_v in a voltage-dependent manner (Ouyang et al., 2003; Shiraishi and Harris, 2004). We therefore investigated block of Na_v by isoflurane during repetitive high-frequency stimulation as would be seen in fast-firing neurons using trains of 10 5-ms depolarizing pulses at frequencies of 20 – 50 Hz from a holding potential of −70 mV (Figure 11A). In order to measure the activity-dependent block by isoflurane that develops over the course of the stimulus train in the absence

of tonic or resting block, peak I_{Na} at each pulse was plotted as a fraction of the peak I_{Na} of Pulse 1. The decrease in current between Pulse 1 and Pulse 10 in control conditions is due to accumulation of inactivated channels at high stimulation frequencies, which have insufficient time between stimuli to fully recover from inactivation at the hyperpolarized resting membrane potential. Inhibition of I_{Na} was increased at higher stimulation frequencies ($Pulse_{10}/Pulse_1$: 20 Hz=0.90±0.03, 50 Hz=0.64±0.02, mean±SD, *n*=5-6) (Figure 11B). Addition of ~1.5 MAC isoflurane further enhanced this inhibition at stimulation frequencies of 20 Hz ($CTL_{Pulse10/Pulse1}$= 0.90±0.03 *vs.* $ISO_{Pulse10/Pulse1}$= 0.85±0.03, *n*=6, mean±SD, ***p=0.0005, two-tailed paired Student's *t*-test) and 50 Hz ($CTL_{Pulse10/Pulse1}$= 0.64±0.02 *vs.* $ISO_{Pulse10/Pulse1}$= 0.54±0.03, *n*=5, mean±SD, **p=0.006, two-tailed paired Student's *t*-test) (Figure 11B).

We quantified the fraction of block at each pulse due to isoflurane and independent of inactivation to compare block by isoflurane at different stimulation frequencies. We divided the inhibition of current resulting from isoflurane block together with accumulation of inactivation ($Pulse_n/Pulse_1ISO$) by block due to inactivation alone ($Pulse_n/Pulse_1CTL$) for each pulse of the train (Figure 11C). The resultant fractional block due to isoflurane at the 10^{th} pulse of the train (1-[$Pulse_{10}/Pulse_1ISO/Pulse_{10}/Pulse_1CTL$]) was significantly greater at 50 Hz stimulation (−0.13±0.05, *n*=5) compared to 20 Hz (−0.03±0.03, *n*=6; mean±SD, *p=0.02, two-tailed unpaired Student's *t*-test). This analysis shows for the first time that additional block of Na_v develops during trains of depolarizing stimuli and the extent of this 'activity-dependent' block is increased at higher stimulation frequencies.

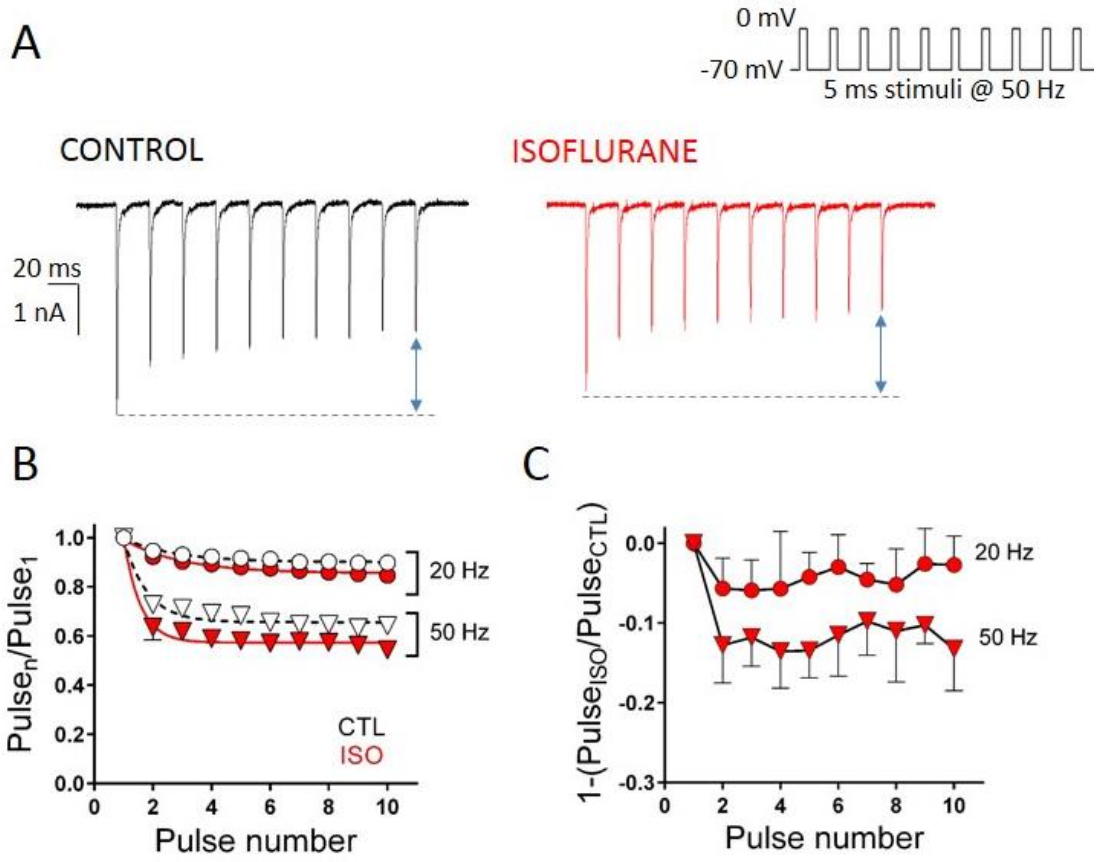

FIGURE 11. Block of hippocampal I_{Na} by isoflurane is increased at higher stimulation frequencies. *A*) Whole-cell I_{Na} recorded from hippocampal neurons in control (*left*) and in the presence of ~1.5 MAC isoflurane using the protocol in *inset*. Dotted lines denote peak I_{Na} of Pulse 1. Blue arrows indicate decease in current between Pulse 1 and Pulse 10. *B*) Fraction of peak current at each pulse normalized to Pulse 1 for control (*open symbols*) and isoflurane (*filled symbols*) stimulated at 20 Hz (*circles*) and 50 Hz (*triangles*). *C*) Fraction of block attributed to isoflurane [1-(Pulse$_{ISO}$/Pulse$_{CTL}$)] at each pulse for 20 Hz (*circles*) and 50 Hz (*triangles*) pulse trains. Data are presented as mean±SD, *n*=6.

Isoflurane inhibits $Na_v1.2_R$ in ND7/23 neuroblastoma cells

To further investigate the mechanism of action of activity-dependent block, we transiently transfected rat $Na_v1.2$ into a neuronal cell line and measured channel gating kinetics in the absence and presence of isoflurane. Na_v are exceptionally large proteins that express well in a neuronal expression system (Herold et al., 2009). We used ND7/23 cells which are a hybrid of mouse neuroblastoma and rat dorsal root ganglion (DRG) neurons to transiently express a TTX-resistant mutant of the neuronal isoform, $Na_v1.2$ (F385S) (Leffler et al., 2005), which we refer to as $Na_v1.2_R$. External saline solutions contained 250 nM TTX to block endogenous I_{Na} in the ND7/23 cells in order to isolate $Na_v1.2_R$ current. Figure 12 shows whole-cell I_{Na} from untransfected ND7/23 cells and cells transfected with $Na_v1.2_R$.

Figure 13 shows whole-cell $Na_v1.2_R$ currents recorded from ND7/23 cells in the absence and presence of ~1.5 MAC isoflurane. Current was evoked by a series of voltage steps from −50 to +50 mV and preceded by a 50-ms prepulse to −100 mV to relieve channels from inactivation. Isoflurane inhibited peak I_{Na} at test potentials of −10 to +40 mV [n=7, *p<0.05, two-way (voltage x drug) ANOVA with Sidak's multiple comparisons test], without altering the current-voltage (I-V) relationship; maximum I_{Na} for both control and isoflurane conditions occurred at pulses to 0 mV (Figure 13B).

To measure effects of isoflurane on the voltage-dependence of channel activation, we calculated conductance (G), which describes the open probability of the

population of channels at a given voltage by removing the effect of the electrical driving force from the peak current (see *Materials and Methods*). Normalized conductance (G/G_{MAX}) at each voltage step was fit with a Boltzmann function and changes in the voltage-dependence of activation were determined by comparing the mid-points of the curves. In the presence of isoflurane, there was no change in the voltage-dependence of activation ($V_{½act}$ control = −15.3±2.7 mV *vs.* $V_{½act}$ isoflurane = −15.4±2.0 mV, *n*=6, n.s.) indicating that voltage-dependent effects of isoflurane are not due to changes in channel activation (Figure 13C).

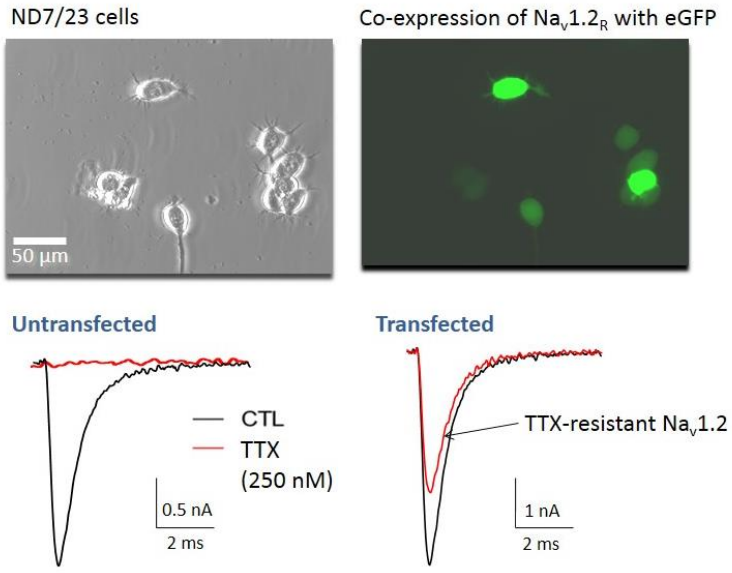

FIGURE 12. Expression of functional TTX-resistant $Na_v1.2$ ($Na_v1.2_R$) in ND7/23 neuroblastoma cells. *Top*, brightfield image (*left*) and fluorescent detection (*right*) of ND7/23 cells plated on glass coverslips and co-transfected $Na_v1.2_R$ and eGFP. Scale bar in *inset*. *Bottom*, ND7/23 whole-cell I_{Na} in control (*black*) and in the presence of 250 nM TTX (*red*) in an untransfected cell (*left*, scale bar = 0.5 nA) and a cell transfected with $Na_v1.2_R$ (*right*, scale bar = 1 nA).

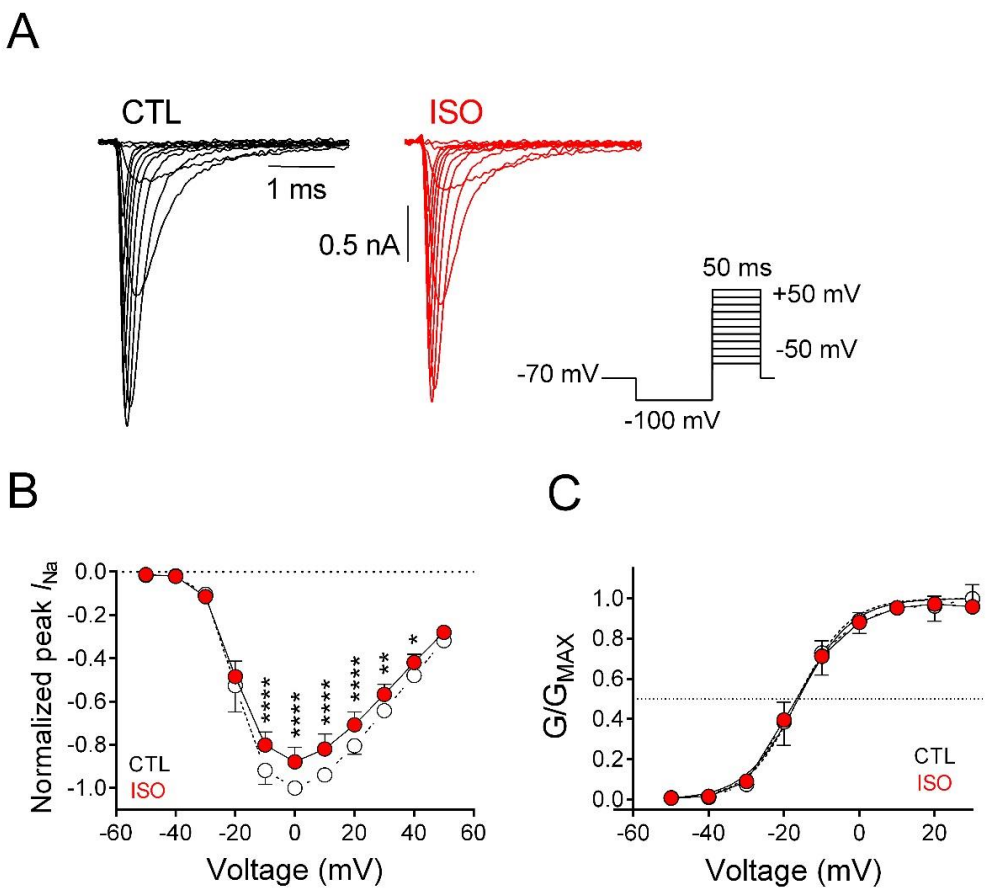

FIGURE 13. Effects of isoflurane on activation properties of $Na_v1.2_R$ in ND7/23 cells. A) Representative whole-cell $Na_v1.2_R$ current traces in the absence (*left*) or presence (*right*) of 1.5 MAC isoflurane using the protocol in *inset*. (B) Normalized peak current (I_{Na}) plotted against test potential in the absence (CTL) or presence (ISO) of isoflurane (mean±SD, n=7, *p<0.05, **p<0.01, ****p<0.0001 compared to respective control value by two-way ANOVA). C) Normalized conductance (G/G_{max}) values (mean±SD, n=7) plotted against the voltage command and fit with a Boltzmann function.

We next investigated the effect of isoflurane on the voltage-dependence of inactivation by eliciting currents by depolarization to 0 mV following a 50-ms prepulse to voltages ranging from −100 to −20 mV (Figure 14A). The current elicited

by the 0 mV step following a given prepulse voltage was normalized to the maximum current elicited at 0 mV following the most hyperpolarized potentials where inactivation is minimal. This fractional current (I_{Na}/I_{Na}max) reflects the degree of inactivation at each prepulse potential and is referred to as steady-state inactivation. When fit with a Boltzmann function, isoflurane shifted the voltage-dependence of steady-state inactivation in a hyperpolarizing direction ($V_{½}$ control = −56±2 mV *vs.* $V_{½}$ isoflurane = −59±2 mV, n=6, **p=0.008, two-tailed paired Student's t-test) (Figure 14B, C). These data suggest that steady-state levels of inactivated channels are greater in the presence of isoflurane compared to control. This results in a reduction of peak I_{Na} by increasing the fraction of inactivated channels at normal resting membrane potentials.

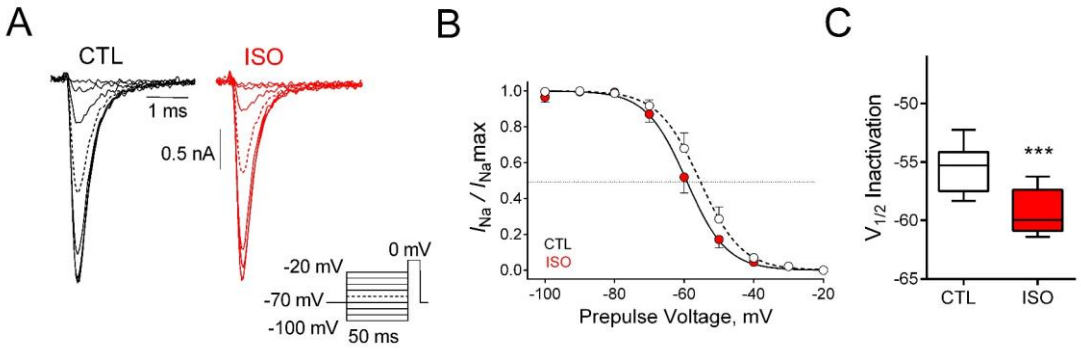

FIGURE 14. Effects of isoflurane on inactivation properties of $Na_v1.2_R$ in ND7/23 cells. *A*) Representative whole-cell $Na_v1.2_R$ current in the absence (*left*) and presence (*right*) of 1.5 MAC isoflurane using the protocol in *inset* (prepulse to −60 mV indicated with a dashed line). *B*) Steady-state fast inactivation for control (CTL) and isoflurane (ISO), where I_{Na} at 0 mV was normalized to the maximum I_{Na} for each condition (I_{Na}/I_{Na}max). Average values (n=6, mean±SD) plotted against the voltage command and fit with a Boltzmann function. Dotted line denotes 50% channel availability *C*) Average values for voltage at 50% inactivation for control (CTL) and isoflurane (ISO; n=6, ***p=0.002).

Activity-dependent block of $Na_v1.2_R$ by isoflurane

We predicted that this shift in voltage-dependence of inactivation would result in similar progressive inhibition of I_{Na} during high-frequency trains of stimuli as we saw in primary cultures of hippocampal neurons (see Figure 11). We tested this hypothesis using high-frequency trains of depolarizing stimuli to elicit I_{Na} in the absence of presence of ~1.5 MAC isoflurane (Figure 15A). We normalized I_{Na} at each pulse to the first pulse of the train ($Pulse_n/Pulse_1$) to remove any effect of tonic block by isoflurane (Figure 15B). For 5-ms pulses delivered at 50-Hz, from a V_h of −90 mV, isoflurane reduced the fraction of current at $Pulse_{10}$ ($Pulse_{10}/Pulse_1$) from 0.90±0.03 to 0.85±0.03 (*n*=6, ***p=0.0009). From a V_h of −70 mV, isoflurane reduced $Pulse_{10}/Pulse_1$ from 0.68±0.08 to 0.53±0.11 (*n*=5, ***p=0.0006) (Figure 15C).

Block was increased at the more depolarized V_h of −70 mV where steady-state levels of channel inactivation are greater than at −90 mV, implicating stabilization of the inactivated state as the mechanism of activity-dependent block. This mechanism supports our previous observation that with increased stimulation frequency channels have less time at hyperpolarized membrane potentials to return to the resting state and activity-dependent inhibition increases. To determine whether activity-dependent block increases with increased stimulation frequency, we compared data from 50- and 100-Hz pulse trains. Inhibition of I_{Na} was undetectable using 20-Hz pulse trains in our heterologous system, presumably because of differences in Na_v subunits or Na_v phosphorylation states compared to endogenous channels expressed in our neuronal

cultures. We applied trains of 5-ms pulses at 100 Hz from a V_h of −90 mV in control and in the presence of ~1.5 MAC isoflurane and compared these results to the 50 Hz pulse trains (Figure 15). Increasing the stimulation frequency from 50 to 100 Hz more than doubled the fractional block by isoflurane at Pulse 10 (50 Hz= 0.058±0.018 *vs.* 100 Hz, 0.137±0.034, *n*=6, ***p*=0.008) (Figure 16). These results provide additional support for stabilization of inactivation as the mechanism of activity-dependent block.

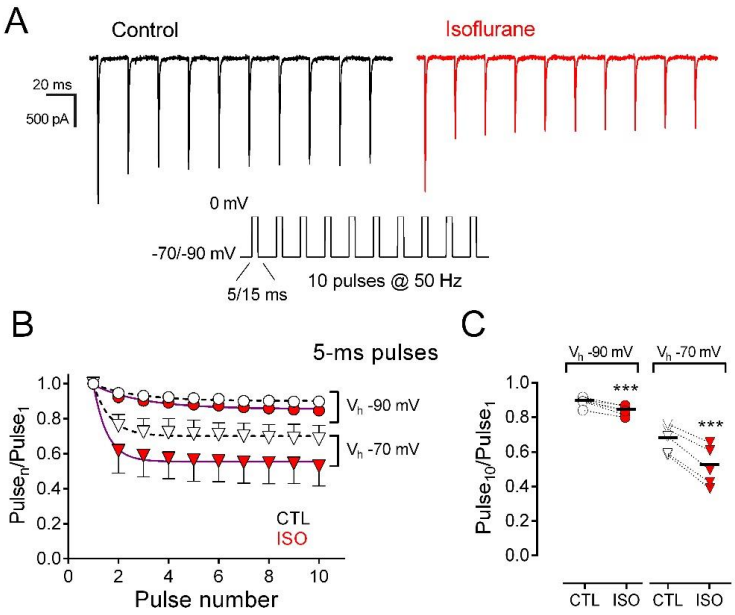

FIGURE 15. Activity-dependent block of $Na_v1.2_R$ expressed in ND7/23 cells. *A*) Representative current traces in response to a 50-Hz train of 5-ms depolarizing pulses to 0 mV from a V_h of −70 mV in the absence (*left*) or presence (*right*) of 1.5 MAC isoflurane (protocol in *inset*). *B*) Peak I_{Na} elicited by each pulse from a V_h of −70 mV (*triangles, n*=5) or −90 mV (*circles, n*=6) normalized to the first pulse of the train (Pulse$_n$/Pulse$_1$). Mean± SD data were fit to a mono-exponential function. *C*) Normalized I_{Na} at Pulse$_{10}$ for each cell in B. Dotted lines denote paired data. ****p*<0.001, by two-tailed, paired Student's *t*-test.

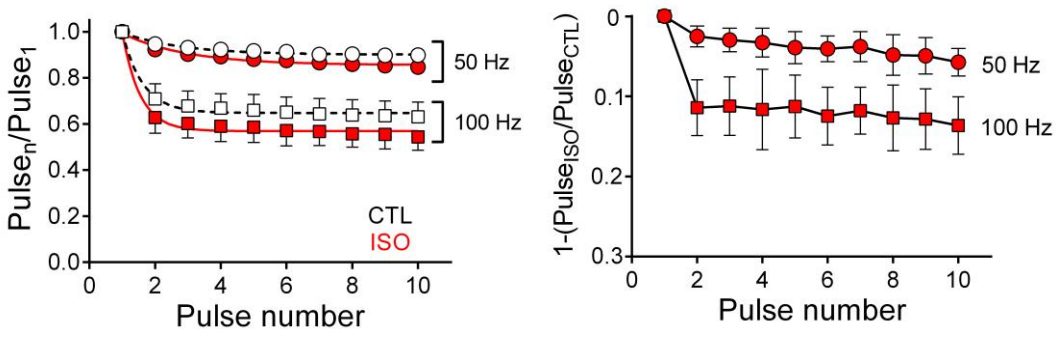

Figure 16. Fractional inhibition by isoflurane during 50-Hz or 100-Hz pulse trains. *Left panel,* normalized peak I_{Na} at each pulse of a 50-or 100-Hz pulse train in the absence (CTL) or presence of 1.5 MAC isoflurane (ISO*; n*=6). Trains consisted of 5-ms pulses to 0 mV from a holding potential of −90 mV. *Right panel*, fractional inhibition by isoflurane at each pulse of a 50- or 100-Hz pulse train (*n*=6). Data presented as mean±SD.

Isoflurane effects on Na_v gating kinetics

We constructed a simple gating model to test whether stabilization of inactivation can account for our experimental observations. Figure 17 shows a model of Na_v gating including 3 states: resting (R), open (O), and inactivated (I). We assigned rate constants to the forward transitions between these states and measured them using different voltage protocols in control and in the presence of isoflurane. If isoflurane stabilizes I, we expected to see either an increase in the rate of entry into I from O ($\uparrow k_{OI}$), a decrease in the rate of entry into R from I ($\downarrow k_{IR}$), or a combination of these two effects.

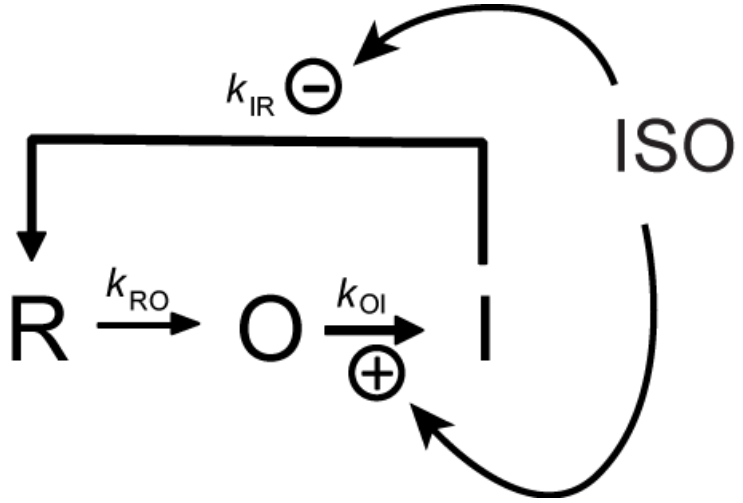

FIGURE 17. Gating model for isoflurane inhibition of $Na_V1.2_R$ involving stabilization of inactivation. A) Simple gating model of isoflurane inhibition involving resting (*R*), open (*O*) and inactivated (*I*) states. Transitions between states are indicated by arrows with associated rate constants. During activation, channels transition from *R* to *O* to *I*, and upon repolarization channels recover to availability by transitioning from *I* to *R*. Curved arrows identify transitions modulated by isoflurane (ISO), which enhances (+) transitions from *O* to *I* and slows (-) transitions from *I* to *R*, together representing *I* stabilization.

We tested this hypothesis by measuring the rate of recovery from inactivation to estimate k_{IR}. Peak I_{Na} was recorded in response to two 5-ms pulses to 0 mV where the duration between the two pulses was varied from 1-100 ms. Data are shown as a ratio of Pulse 2:Pulse 1 and plotted against the interpulse interval. Recovery time-courses were fit with a mono-exponential function in both control and in the presence of ~1.5 MAC isoflurane, indicating that channels predominantly entered a single 'fast'-inactivated state and not any other 'slow'-inactivated states. Isoflurane increased the time required for full channel recovery at a hyperpolarized V_h of −90 mV ($\tau_{control}$ =

3.1±0.6 ms *vs.* $\tau_{isoflurane}$ = 3.9 ±0.8 ms, *n*=6, **p*=0.04, two-tailed paired Student's *t*-test); this effect was enhanced at more physiological V_h (recovery at −70 mV, $\tau_{control}$ = 6.9 ±1.1 ms; $\tau_{isoflurane}$ = 9.0 ±1.9 ms, *n*=7, ***p*=0.004, two-tailed paired Student's *t*-test) (Figure 18B, C).

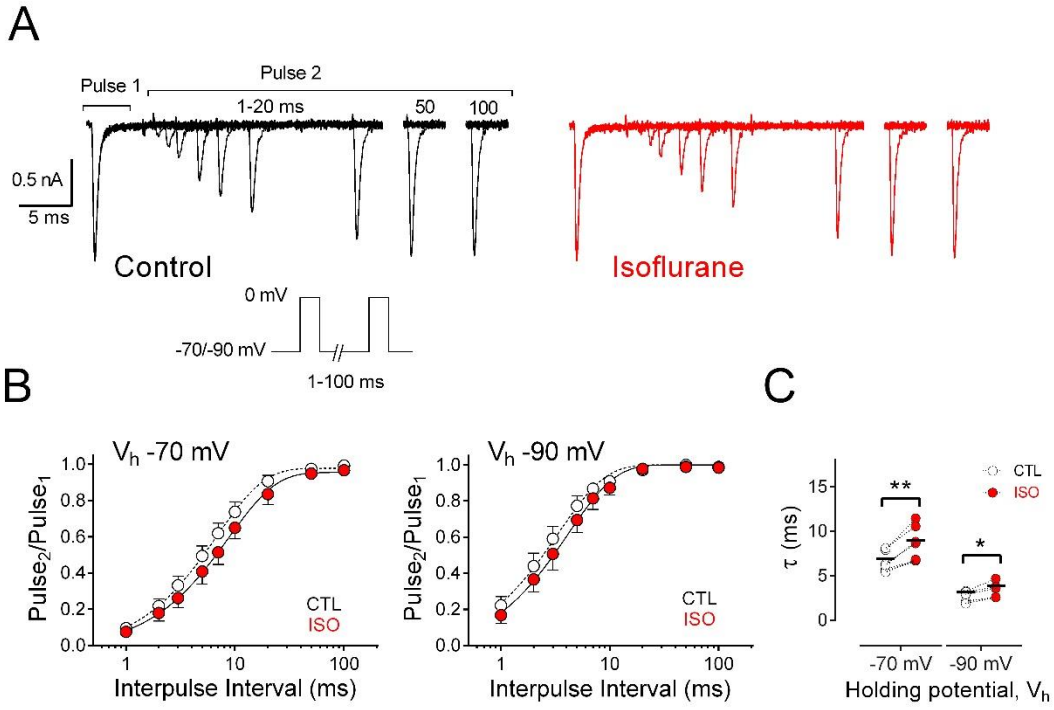

FIGURE 18. Effects of isoflurane on recovery of $Na_v1.2_R$ from fast inactivation. A) Families of whole-cell $Na_v1.2_R$ current traces recorded in the absence (*left*) or presence (*right*) of 1.5 MAC isoflurane and evoked from a V_h of −70 mV using a paired-pulse protocol where the duration between two 5-ms pulses to 0 mV was varied from 1-100 ms (protocol in *inset*). B) Normalized peak current ($Pulse_2/Pulse_1$) plotted against duration of the interpulse interval for control (CTL) and isoflurane (ISO) from a V_h of −70 mV (*n*=7) or −90 mV (*n*=6). Data are presented as mean±SD and fit with a mono-exponential function. C) Time constants (τ) determined from mono-exponential fits of data from individual cells in *B* (**p*<0.05, ***p*<0.005; by two-tailed, paired Student's *t*-test).

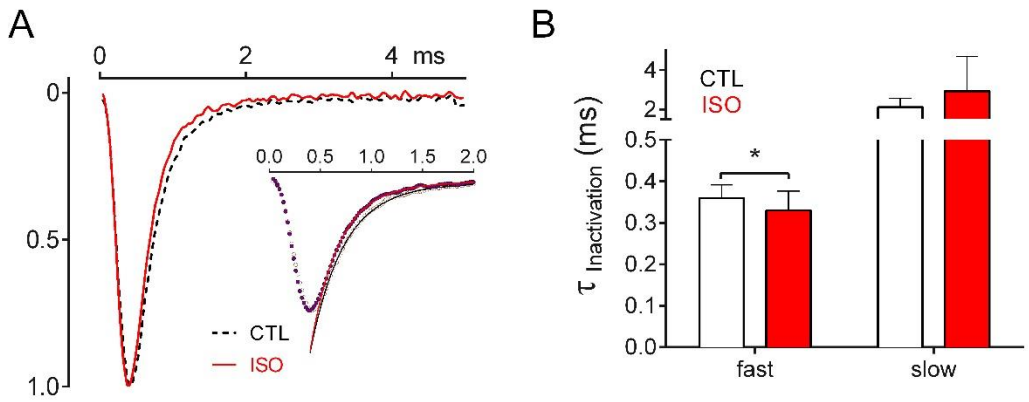

FIGURE 19. Isoflurane accelerates inactivation in $Na_v1.2_R$ expressed in ND7/23 cells. A) Representative responses to a 5-ms stimulus pulse to 0 mV from a V_h of −70 mV for control (CTL) or 1.5 MAC isoflurane (ISO) treated cells normalized to the peak of CTL. *Inset* shows a bi-exponential fit (*dashed line*) of the decay phase for CTL (*solid line)* and ISO (*red line*). B) Fast and slow τ derived from bi-exponential fitting of individual cells in the absence (CTL) or presence (ISO) of 1.5 MAC isoflurane. Bars represent mean±SD, n=6, *p<0.05, by two-tailed, paired Student's t-test.

We estimated the rate of entry into the inactivated state from the open state (k_{OI}) by measuring the rate of macroscopic I_{Na} decay during a single pulse to 0 mV from a holding potential of −70 mV. We normalized current traces in the presence of isoflurane to peak I_{Na} of paired control experiments (Figure 19A) and fit the decay phases using a double exponential function. The majority of the decay phase (~95%) could be described by the fast time constant (τ), again indicating that channels only enter the fast-inactivated state using this protocol. Isoflurane reduced the fast τ from 0.36±0.03 ms in control to 0.33±0.05 ms (n=5, *p=0.04, two-tailed paired Student's t-test), indicating k_{OI} is increased in the presence of isoflurane. Isoflurane had little effect on the slow time constant (2.11±0.99 for control *vs.* 2.93±1.67 for isoflurane,

n=5, n.s.) (Figure 19B). Together with a decrease in k_{IR}, the increase in k_{OI} suggests that isoflurane blocks Na_v by stabilizing channels in the fast-inactivated state and increasing the probability that channels will be inactivated and unavailable for opening upon membrane depolarization during high-frequency stimulation.

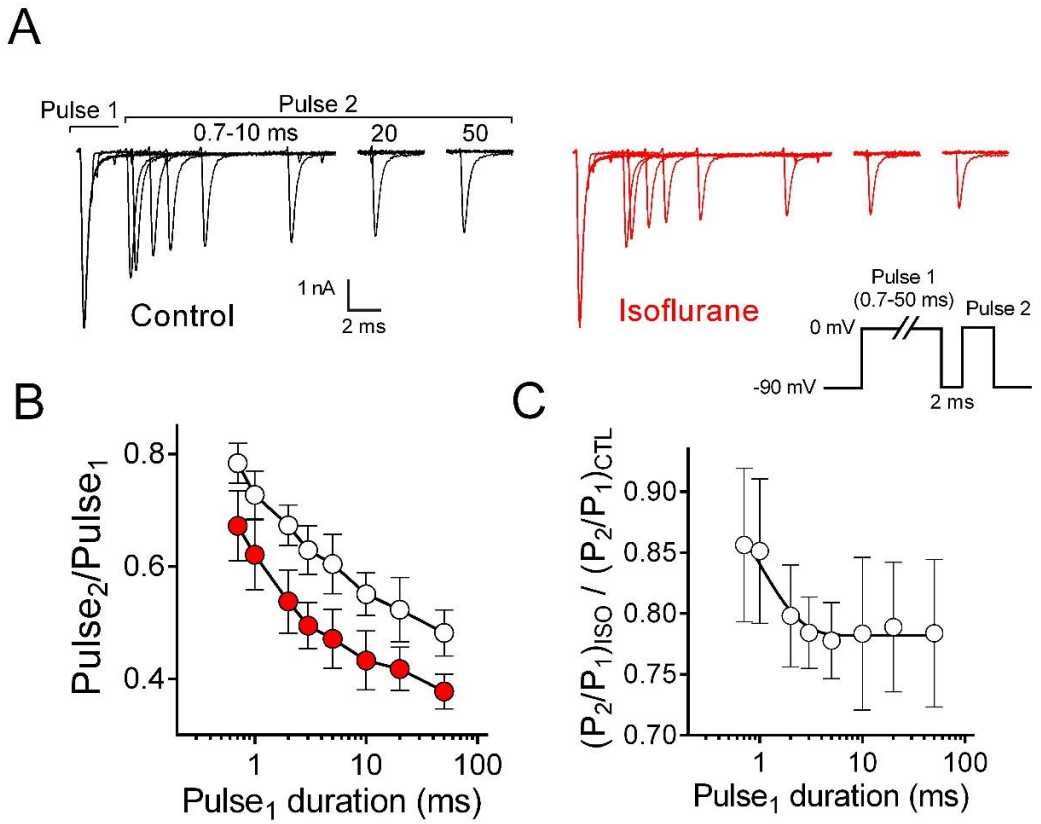

FIGURE 20. Onset of isoflurane inhibition matches the time course of inactivation. A) Representative current traces recorded in the absence (*left*) or presence (*right*) of 1.5 MAC isoflurane using a two-pulse protocol (*inset*) to investigate onset of isoflurane inhibition. From a V_h of −90 mV, cells were stimulated with two pulses to 0 mV with the duration of the first pulse varied from 0.7 – 50 ms. B) Peak I_{Na} of the test pulse ($Pulse_2$) normalized to that of the conditioning pulse ($Pulse_1$) to yield fractional I_{Na} ($Pulse_2/Pulse_1$). Mean±SD fractional I_{Na} (*n*=8) plotted versus $Pulse_1$ duration. C) Fractional I_{Na} (mean±SD, *n*=8) for ISO normalized to that of CTL to determine the onset of isoflurane inhibition fitted with a mono-exponential function

Onset of isoflurane inhibition matches the time-scale of fast-inactivation

We investigated the onset of isoflurane inhibition to compare the time course to that of fast-inactivation. We used a double-pulse protocol with the duration of the first pulse to 0 mV varied from 0.7−50 ms. We used a range of pulse durations that typically produce complete channel inactivation (>3 ms). Consequently, the protocol briefly (2 ms) returns to V_h to allow partial recovery of fast inactivated and inhibited channels (Figure 20A).

In control conditions, longer Pulse 1 durations reduced fractional I_{Na} (Pulse 2 normalized to Pulse 1), reflecting a growing population of inactivated channels that fail to fully recover between pulses. Isoflurane decreased fractional I_{Na} for all Pulse 1 durations relative to control (Figure 20B). To investigate the time course of inhibition onset, we normalized the isoflurane response to that of control (Figure 20C). The response reached an apparent plateau at around 10 ms and was well fit by a mono-exponential function with kinetics (τ=2.4±1.6 ms, A_P=0.76±0.04, n=8) comparable to fast inactivation. These findings further support involvement of Na_v fast inactivation in isoflurane action and the validity of our model that stabilization of fast-inactivation underlies activity-dependent block of Na_v by isoflurane.

CHAPTER FOUR

DISCUSSION

We have shown here for the first time that isoflurane reduces neuronal excitability and produces activity-dependent block of Na_v by stabilizing the fast-inactivated state of the channel. This work investigates a novel mechanism of Na_v block and supports a role for Na_v inhibition in the presynaptic effects of isoflurane. Using primary cultures of hippocampal neurons and recombinant rat $Na_v1.2_R$, we measured activity-dependent block of endogenous neuronal Na_v and further investigated the underlying kinetic mechanism in a reduced system. Activity-dependent block of Na_v contributed significantly to overall block during high-frequency stimulation and could have significant effects on fast-firing neuronal networks. Here we discuss the implications of these findings and how they can be interpreted in current theories of anesthetic action.

Effects of isoflurane on neuronal excitability

We show that concentrations of isoflurane equivalent to those used in the clinic reversibly inhibit AP firing of rat hippocampal neurons in culture. VAs have been shown to depress excitability of hippocampal neurons at much lower concentrations *in vitro* (Fujiwara 1988). However, since anesthetics perfuse readily through the CNS

and are only minimally metabolized, MAC is the assumed concentration of drug at the receptor and is the concentration that should be used to measure effects *in vitro,* especially since isoflurane has been shown to have bidirectional effects on cellular processes depending on drug concentration (Tachibana et al., 2007).

The effects of isoflurane on spontaneous firing in cultured hippocampal neurons are at least in part due to block of Na_v since isoflurane affected AP parameters largely determined by Na_v. The threshold for AP initiation is determined by the density of Na_v as well as the subtype of Na_v expressed in the AIS (Kole et al., 2008; Lorincz and Nusser, 2008; Platkiewicz and Brette, 2010). This could imply that isoflurane blocks all Na_v isoforms present in the AIS equally, thereby shifting the threshold for firing by reducing the effective density of Na_v, or could imply that isoflurane selectively blocks a particular Na_v subtype that activates at more negative voltages than the other subtypes present. In rat hippocampal neurons $Na_v1.2$ is highly expressed in the proximal region of the AIS while $Na_v1.6$ is concentrated in the more distal region where its more negative threshold for activation supports AP initiation in the distal AIS (Boiko et al., 2003; Hu et al., 2009; Lorincz and Nusser, 2010). We hypothesize that subtype-selective block by isoflurane results from $Na_v1.6$ being more sensitive than $Na_v1.2$, which would shift the threshold for AP firing towards the more depolarized threshold for $Na_v1.2$ activation. A previous study comparing effects of 1 MAC isoflurane on $Na_v1.2$ and $Na_v1.6$ currents shows that peak $Na_v1.6$ current (with and without β1) is relatively more sensitive to inhibition than $Na_v1.2$ (~36% vs. ~28% of peak I_{Na} at $V_{½}$), but the voltage-dependence of inactivation was shifted to similar

extents in the two isoforms (~10 mV) (Shiraishi and Harris, 2004). This work was done in *Xenopus* oocytes which are a notoriously poor system for studying channel behaior as the composition of the membrane can interfere with channel activity (Tammaro et al., 2008). However, it suggests that isoflurane might inhibit $Na_v1.6$ to a greater extent than $Na_v1.2$. Changes in $Na_v1.6$ current density, but not $Na_v1.2$ density, have been shown to affect the threshold for AP firing in a computational model (Platkiewicz and Brette, 2010). Interestingly, $Na_v1.6$ is also essential for maintaining temporal resolution of APs in response to incoming stimuli (Osorio et al., 2010). This may be relevant to systems-level theories of anesthesia that suggest unconsciousness arises through the uncoupling of signals within and between the thalamus and the cortex (Hudetz, 2012).

Computational models show that the threshold for AP firing can also be affected by the membrane potential and hyperpolarization of the K_v activation curve (Wester and Contreras, 2013). While evidence suggests that VAs modulate K_v at clinical concentrations (Bhattacharji et al., 2015; Friederich et al., 2001; Urban and Haydon, 1987), the majority of evidence shows that VAs inhibit K_v while one study suggests VAs enhance activation of K_v (Barber et al., 2011). The latter study was done using sevoflurane on a *Drosophila* homolog of mammalian K_v3 channels, and may reflect agent-specific or K_v subtype-specific effects, whereas the predominant K_v subtypes expressed in the AIS of hippocampal neurons are $K_v1.1$ and $K_v1.2$ (Lorincz and Nusser, 2008; Van Wart et al., 2007). Other candidate channels that could supply outward I_K to shift the threshold for AP firing are K2P channels, that are known

targets of VAs (Franks and Lieb, 1988)(Franks and Lieb, 1988). These channels affect resting membrane potential, but since they are not gated, the flow of current through them could presumably be controlled by maintaining a steady membrane potential by injecting current.

Our proposal that activity-dependent block affects overall excitability of the neuron is supported by evidence that the degree of Na_v inactivation modulates neuronal excitability and the threshold for AP firing in computational models (Wester and Contreras, 2013). Na_v inactivation can be modulated by phosphorylation by a number of protein kinases and phosphatases (Scheuer and Catterall, 2006). Regulation of Na_v by PKC has been shown to affect neuronal excitability (Carr et al., 2002), and there is evidence to suggest that PKC itself can be a target of VAs (Gomez et al., 2003; Hemmings and Adamo, 1994). This poses the question of whether Na_v-dependent anesthetic effects reflect modulation of the channel itself or indirect effects on PKC or other modulatory proteins. However, our analysis of the onset of isoflurane block of $Na_v1.2$ shows that drug effects are complete within 10 ms, which is on the time-scale of inactivation and indicates direct effects on this channel rather than modulation through second messengers. Our findings support the hypothesis that isoflurane inhibits neuronal excitability through direct actions on neuronal Na_v that enhance fast-inactivation.

Isoflurane effects on the presynaptic AP and neurotransmitter release

We show that clinical concentrations of isoflurane alter the shape of the AP, which can affect synaptic transmission and thereby neuronal activity by altering neurotransmitter release (Kole et al., 2007; Wu et al., 2004). Isoflurane has been shown to preferentially depress exocytosis of glutamate compared to GABA (Westphalen and Hemmings, 2003), which can result in relative increases in inhibitory GABAergic signalling that would depress firing of pyramidal neurons. VAs have also been shown to increase activity of inhibitory neurons by increasing activity of $GABA_A$ receptors(Nishikawa and MacIver, 2001) (Nishikawa and MacIver, 2001), which could result in an overall depression of activity in neuronal cultures. To minimize possible neurotransmitter receptor effects and direct effects on $GABA_A$ receptors or other major transmitter receptors, we measured APs evoked by electrical stimulation in pharmacologically isolated neurons. The amplitude of the AP is determined by coordinated opening of Na_v and K_v, so effects on either could underlie the reduction in amplitude caused by isoflurane. Additional evidence for effects on Na_v come from the decrease in the maximum velocity of the AP upstroke, which is determined by the number of open Na_v (Bean, 2007), and the rise in AP threshold, which is determined by the voltage-sensitivity and density of Na_v (Kole et al., 2008; Rush et al., 2005). Our results point to a presynaptic mechanism of action involving Na_v that occurs independently of GABA-mediated effects which could reduce presynaptic excitability and lead to suppression of neurotransmitter release.

Isoflurane raised the threshold for AP firing to more depolarized membrane potentials. This could affect neuronal excitability by increasing the failure rate for AP

initiation. This could manifest in the axon as decreased sensitivity of a neuron to excitatory stimuli or could cause AP propagation failure at axonal branch points. In dendrites, a higher threshold for Na_v activation could lead to early attenuation of APs backpropagating from the AIS that works as a feedback mechanism to fine-tune incoming stimuli (Jung et al., 1997).

Activity-dependent block of neuronal Na_v

Neuronal signals are transmitted via trains of APs, so activity-dependent block of I_{Na} is a potentially important mechanism of VA action on neuronal networks. Increased block of Na_v at higher stimulation frequencies could contribute to network selectivity of anesthetic effects. The activity-dependence of block could lead to greater sensitivity to isoflurane in fast-firing neuronal networks. By analogy with use-dependent block by local anesthetics, VAs preferentially inhibit more active neurons to selectively suppress fast firing networks (Stewart et al., 1988; Wildsmith et al., 1989). Small reductions in I_{Na} can produce significant effects on oscillatory activity in neuronal networks (Arhem et al., 2003) and so, in fast firing networks, the presence of isoflurane could have significant and selective effects on neuronal activity.

Previous assessments of the role of Na_v inhibition by general anesthetics *in vitro* have not considered the impact of activity-dependent block, which significantly enhances the efficacy of isoflurane inhibition of neuronal Na_v under physiological conditions. For example, the magnitude of tonic I_{Na} inhibition by clinical

concentrations of isoflurane is relatively modest: we observed ~10% reduction of peak I_{Na}, which was comparable to previous reports (Ouyang and Hemmings, 2007; Ouyang et al., 2009; Rehberg et al., 1996; Shiraishi and Harris, 2004). In comparison, we observed an additional ~20% block at 50-Hz stimulation from a physiological V_h of −70 mV. Even modest block of Na_v can strongly affect neuronal transmission, as small reductions in peak I_{Na} alter both frequency of AP firing and neurotransmitter release (Wu et al., 2004).

While the relative sensitivity of the major neuronal isoforms to activity-dependent block by isoflurane remains to be studied, $Na_v1.6$ expressed in *Xenopus* oocytes is potentiated by repetitive firing (Zhou and Goldin, 2004) and does not show activity-dependent depression due to accumulation of inactivated channels. Thus $Na_v1.6$ would not be predicted to show the same response to isoflurane as $Na_v1.2$, which we show is inhibited at higher stimulation frequencies. However, the shift in AP firing threshold may indicate subtype-specific effects on $Na_v1.6$, since $Na_v1.2$ current density does not affect AP firing threshold (Platkiewicz and Brette, 2010). The subcellular localization of Na_v subtypes that differ in their responses to activity-dependent block can be used as a way to regulate different processes within the same cell. Enhanced sensitivity of $Na_v1.6$ peak current to isoflurane (Shiraishi and Harris, 2004) may alter the AP threshold at the AIS which would regulate the overall excitability of the neuron whereas activity-dependent block of $Na_v1.2$ can serve as a mechanism to fine tune responses to incoming stimuli in dendrites or to regulate neurotransmitter release dependent on the activity of specific boutons.

Although the molecular details underlying our proposal that isoflurane stabilizes the fast-inactivated state are beyond the scope of the current investigation, the mechanism could involve isoflurane binding to a freely accessible receptor that allosterically modulates free energy profiles to stabilize the fast-inactivated state. Isoflurane can participate in hydrogen bonding by forming dipoles, and has been shown to bind hydrophobic macromolecules (Zhang and Johansson, 2005) as well as human serum albumin (Eckenhoff et al., 2000). Consistent with this possibility, VA binding has been demonstrated in prokaryotic voltage-gated ion channels (Nury et al., 2011; Spurny et al., 2013), and molecular dynamics simulations of a homology model of the bacterial channel NaChBac revealed a possible pathway for isoflurane to enter the pore via hydrophobic side fenestrations (Payandeh et al., 2011; Raju et al., 2013). Further structural and molecular dynamics studies are necessary to determine where isoflurane binds and what residues are involved in stabilizing the bound state of the channel.

Conclusions and future directions

We show that isoflurane stabilizes the fast-inactivated state of neuronal Na_v such that recovery from fast inactivation is delayed and entry into fast inactivation is accelerated, resulting in activity-dependent inhibition. This enhanced inactivation leads to progressive inhibition of I_{Na} with high-frequency stimulation and contributes significantly to overall inhibition of I_{Na} by isoflurane through activity-dependent

inhibition compared to tonic inhibition. At high stimulus frequencies, Na_v inhibition by isoflurane and probably other anesthetics that exhibit state-dependent inhibition will be greater than that suggested by previous studies of resting block alone.

Future studies investigating the physiological relevance of activity-dependent block by VAs will focus on three areas: 1) effects on the presynaptic AP waveform and exocytosis; 2) effects on backpropogation of APs into the dendrites and stimulus integration; and 3) relative effects on different Na_v subtypes.

To study the effect of activity-dependent block on the presynaptic AP and exocytosis, live-cell imaging of voltage-sensitve fluorescent biosensors could record effects of isoflurane on the AP waveform at the bouton. Conventional electrophysiology techniques cannot readily access small subcellular structures, but recent advances in live-cell imaging techniques revealed that the AP at the bouton has a different waveform than the AP in the soma (Hoppa et al., 2014), reflecting a different ion channel profile. The AP at the bouton directs Ca^{2+} influx and neurotransmitter release, and so it is important to measure changes in AP waveform to understand anesthetic effects on exocytosis. We will use a fluorescently labelled synaptic vesicle protein to identify boutons and a voltage-sensitive fluorescent dye to image the AP (Hoppa et al., 2014). Electrical stimuli can then be applied at various stimulation frequencies to measure the effects of activity-dependent block by isoflurane on the bouton AP.

Future experiments will also analyse the role of the major Na_v subtypes expressed in human brain ($Na_v1.1$, $Na_v1.2$, $Na_v1.3$ and $Na_v1.6$) on neuronal excitability and sensitivity to activity-dependent block by isoflurane. In this study we used rat neonatal hippocampal neurons that demonstrate a pyramidal-like morphology and presumably express $Na_v1.2$ and $Na_v1.6$ as the major Na_v subtypes. To compare Na_v subtype-specific differences in sensitivity to isoflurane, we will transfect TTX-resistant clones into neonatal hippocampal neurons and use TTX to inhibit endogenous Na_v. We can then compare the sensitivities of specific Na_v subtypes to isoflurane and their roles in AP firing frequency and AP waveform, activity-dependent block, and exocytosis. To determine whether activity-dependent block plays a role in regulating exocytosis, we can compare the relative sensitivities of Na_v subtypes to activity-dependent block with the relative sensitivities of Na_v subtype coupled to neurotransmitter release. This analysis of TTX-resistant Na_v subtypes will also provide insight into the specialization of function of Na_v in excitatory vs. inhibitory neurons. While excitatory neurons mainly express $Na_v1.2$, $Na_v1.3$ (in humans) and $Na_v1.6$ (Goldin, 2001), $Na_v1.1$ has been found exclusively in GABAergic inhibitory neurons (Lorincz and Nusser, 2008). We hypothesize that Na_v subtype expression profiles underlie the different responses to VAs of these two cell types. VAs preferentially inhibit the exocytosis of glutamate (Westphalen and Hemmings, 2003), and this could be explained by inhibition of the major excitatory Na_v isoforms $Na_v1.2$ and $Na_v1.6$ and relative insensitivity of $Na_v1.1$.

Future experiments will also investigate whether activity-depedent effects of isoflurane lead to increased potency for fast-firing neurons. Na_v are essential proteins in all excitable cells, yet anesthetic effects arise from specific regions of the CNS. Cell-type dependent effects based on the firing-frequency of the neuron can help explain the specificity of anesthetic effects. These experiments can be performed in a rat preparation such as for the vagus nerve that allows access to A, B, and C fibers that fire at different frequencies (Wildsmith et al., 1989) to measure the relative sensitivities of each nerve fiber at clinical concentrations of isoflurane.

The specificity of VAs for the particular regions of the CNS that give rise to anesthesia remains a mystery. Activity-dependent block of Na_v by isoflurane suggests a novel mechanism for discriminating between different neurons based on firing-frequency. Inhibition of Na_v due to activity-dependent block is relatively modest, but small changes in channel kinetics rather than full block of current might contribute to the mechanism of anesthesia. This is in keeping with the predictions of Franks and Lieb who, based on the immediate onset and ease of reversibility of general anesthetics, predicted that the mechanism of action of these drugs would involve only small changes to the structure of protein targets and modest changes in their activity (Franks and Lieb, 1982).

References

Aldrich, R. W., Corey, D. P. and Stevens, C. F. (1983). A reinterpretation of mammalian sodium channel gating based on single channel recording. *Nature* **306**, 436-441.

Alger, B. E. and Nicoll, R. A. (1982). Pharmacological evidence for two kinds of GABA receptor on rat hippocampal pyramidal cells studied in vitro. *J Physiol* **328**, 125-41.

Alkire, M. T., Haier, R. J. and Fallon, J. H. (2000). Toward a unified theory of narcosis: brain imaging evidence for a thalamocortical switch as the neurophysiologic basis of anesthetic-induced unconsciousness. *Conscious Cogn* **9**, 370-86.

Arhem, P., Klement, G. and Nilsson, J. (2003). Mechanisms of anesthesia: towards integrating network, cellular, and molecular level modeling. *Neuropsychopharmacology* **28 Suppl 1**, S40-7.

Armstrong, C. M. and Bezanilla, F. (1973). Currents related to movement of the gating particles of the sodium channels. *Nature* **242**, 459-61.

Armstrong, C. M. and Bezanilla, F. (1977). Inactivation of the sodium channel. II. Gating current experiments. *The Journal of General Physiology* **70**, 567-590.

Baek, J. H., Cerda, O. and Trimmer, J. S. (2011). Mass spectrometry-based phosphoproteomics reveals multisite phosphorylation on mammalian brain voltage-gated sodium and potassium channels. *Semin Cell Dev Biol* **22**, 153-9.

Barber, A. F., Liang, Q., Amaral, C., Treptow, W. and Covarrubias, M. (2011). Molecular mapping of general anesthetic sites in a voltage-gated ion channel. *Biophys J* **101**, 1613-22.

Bean, B. P. (2007). The action potential in mammalian central neurons. *Nat Rev Neurosci* **8**, 451-65.

Beckh, S., Noda, M., Lubbert, H. and Numa, S. (1989). Differential regulation of three sodium channel messenger RNAs in the rat central nervous system during development. *Embo j* **8**, 3611-6.

Berendt, F. J., Park, K.-S. and Trimmer, J. S. (2010). Multisite Phosphorylation of Voltage-Gated Sodium Channel alpha Subunits from Rat Brain. *Journal of proteome research*.

Berg-Johnsen, J. and Langmoen, I. A. (1986). The effect of isoflurane on unmyelinated and myelinated fibres in the rat brain. *Acta Physiol Scand* **127**, 87-93.

Berg-Johnsen, J. and Langmoen, I. A. (1990). Mechanisms concerned in the direct effect of isoflurane on rat hippocampal and human neocortical neurons. *Brain Res* **507**, 28-34.

Bezanilla, F. and Armstrong, C. (1977). Inactivation of the sodium channel. I. Sodium current experiments. *J Gen Physiol* **70**, 549-566.

Bhattacharji, A., Department of Pathology, A. a. C. B., Jefferson Medical College of Thomas Jefferson University, Philadelphia, PA, USA, and, Klett, N., Department of Pathology, A. a. C. B., Jefferson Medical College of Thomas Jefferson University, Philadelphia, PA, USA, and, Go, R. C. V., Department of Molecular Biosciences and Bioengineering, U. o. H. a. M., Honolulu, Hl, USA, Covarrubias, M. and Department of Pathology, A. a. C. B., Jefferson Medical College of Thomas Jefferson University, Philadelphia, PA, USA, and. (2015). Inhalational anaesthetics and n‐alcohols share a site of action in the neuronal Shaw2 Kv channel. *British Journal of Pharmacology* **159**, 1475-1485.

Boiko, T., Rasband, M. N., Levinson, S. R., Caldwell, J. H., Mandel, G., Trimmer, J. S. and Matthews, G. (2001). Compact myelin dictates the differential targeting of two sodium channel isoforms in the same axon. *Neuron* **30**, 91-104.

Boiko, T., Van Wart, A., Caldwell, J. H., Levinson, S. R., Trimmer, J. S. and Matthews, G. (2003). Functional specialization of the axon initial segment by isoform-specific sodium channel targeting. *Journal of Neuroscience* **23**, 2306-2313.

Borst, J. G. and Sakmann, B. (1999). Effect of changes in action potential shape on calcium currents and transmitter release in a calyx-type synapse of the rat auditory brainstem. *Philos Trans R Soc Lond B Biol Sci* **354**, 347-55.

Boudkkazi, S., Fronzaroli-Molinieres, L. and Debanne, D. (2011). Presynaptic action potential waveform determines cortical synaptic latency. *J Physiol* **589**, 1117-31.

Caldwell, J. H., Schaller, K. L., Lasher, R. S., Peles, E. and Levinson, S. R. (2000). Sodium channel Na(v)1.6 is localized at nodes of ranvier, dendrites, and synapses. *Proceedings of the National Academy of Sciences of the United States of America* **97**, 5616-5620.

Campagna, J. A., Miller, K. W. and Forman, S. A. (2003). Mechanisms of actions of inhaled anesthetics. *N Engl J Med* **348**, 2110-24.

Caraiscos, V. B., Newell, J. G., You-Ten, K. E., Elliott, E. M., Rosahl, T. W., Wafford, K. A., MacDonald, J. F. and Orser, B. A. (2004). Selective enhancement of tonic GABAergic inhibition in murine hippocampal neurons by low concentrations of the volatile anesthetic isoflurane. *J Neurosci* **24**, 8454-8.

Carr, D. B., Cooper, D. C., Ulrich, S. L., Spruston, N. and Surmeier, D. J. (2002). Serotonin receptor activation inhibits sodium current and dendritic excitability in prefrontal cortex via a protein kinase C-dependent mechanism. *J Neurosci* **22**, 6846-6855.

Carras, P. L., Coleman, P. A. and Miller, R. F. (1992). Site of action potential initiation in amphibian retinal ganglion cells.

Catterall, W. (2002). Molecular mechanisms of gating and drug block of sodium channels. *Novartis Found Symp* **241**, 206-18; discussion 218-32.

Cestèle, S., Yarov-Yarovoy, V., Qu, Y., Sampieri, F., Scheuer, T. and Catterall, W. A. (2006). Structure and function of the voltage sensor of sodium channels probed by a beta-scorpion toxin. *The Journal of biological chemistry* **281**, 21332-21344.

Chivukula, S., Grandhi, R. and Friedlander, R. M. (2014). A brief history of early neuroanesthesia. *Neurosurg Focus* **36**, E2.

Cohen, E. N. (1978). Toxicity of inhalation anaesthetic agents. *Br J Anaesth* **50**, 665-75.

Colbert, C. M. and Johnston, D. (1996). Axonal action-potential initiation and Na+ channel densities in the soma and axon initial segment of subicular pyramidal neurons. *J Neurosci* **16**, 6676-86.

Cota, G. and Armstrong, C. M. (1989). Sodium channel gating in clonal pituitary cells. The inactivation step is not voltage dependent. *The Journal of General Physiology* **94**, 213-232.

Davies, J. and Watkins, J. C. (1982). Actions of D and L forms of 2-amino-5-phosphonovalerate and 2-amino-4-phosphonobutyrate in the cat spinal cord. *Brain Res* **235**, 378-86.

de Sousa, S. L., Dickinson, R., Lieb, W. R. and Franks, N. P. (2000). Contrasting synaptic actions of the inhalational general anesthetics isoflurane and xenon. *Anesthesiology* **92**, 1055-66.

Dickinson, R., Franks, N. P. and Lieb, W. R. (1994). Can the stereoselective effects of the anesthetic isoflurane be accounted for by lipid solubility? *Biophysical journal* **66**, 2019-2023.

Eckenhoff, R. G., Petersen, C. E., Ha, C. E. and Bhagavan, N. V. (2000). Inhaled anesthetic binding sites in human serum albumin. *J Biol Chem* **275**, 30439-44.

Eger, E. I., 2nd, Saidman, L. J. and Brandstater, B. (1965). Minimum alveolar anesthetic concentration: a standard of anesthetic potency. *Anesthesiology* **26**, 756-63.

Eger, E. I., Raines, D. E., Shafer, S. L., Hemmings, H. C. and Sonner, J. M. (2008). Is a new paradigm needed to explain how inhaled anesthetics produce immobility? *Anesthesia and analgesia* **107**, 832-848.

El Beheiry, H., Ouanounou, A. and Carlen, P. L. (2007). L-type calcium channel blockade modifies anesthetic actions on aged hippocampal neurons. *Neuroscience* **147**, 117-26.

Engel, D. and Jonas, P. (2005). Presynaptic action potential amplification by voltage-gated Na+ channels in hippocampal mossy fiber boutons. *Neuron* **45**, 405-17.

Fozzard, H. A., Lee, P. J. and Lipkind, G. M. (2005). Mechanism of local anesthetic drug action on voltage-gated sodium channels. *Current pharmaceutical design* **11**, 2671-2686.

Franks, N. P. (2006). Molecular targets underlying general anaesthesia. *British Journal of Pharmacology* **147 Suppl 1**, S72-81.

Franks, N. P. and Lieb, W. R. (1978). Where do general anaesthetics act? *Nature* **274**, 339-42.

Franks, N. P. and Lieb, W. R. (1982). Molecular mechanisms of general anaesthesia. *Nature* **300**, 487-93.

Franks, N. P. and Lieb, W. R. (1984). Do general anaesthetics act by competitive binding to specific receptors? *Nature* **310**, 599-601.

Franks, N. P. and Lieb, W. R. (1988). Volatile general anaesthetics activate a novel neuronal K+ current. *Nature* **333**, 662-4.

Franks, N. P. and Lieb, W. R. (1994). Molecular and cellular mechanisms of general anaesthesia. *Nature* **367**, 607-614.

Friederich, P., Benzenberg, D., Trellakis, S. and Urban, B. W. (2001). Interaction of volatile anesthetics with human Kv channels in relation to clinical concentrations. *Anesthesiology* **95**, 954-8.

Goldin, A. (2001). Resurgence of sodium channel research. *Annu Rev Physiol* **63**, 871-894.

Goldin, A., Barchi, R., Caldwell, J., Hofmann, F., Howe, J., Hunter, J., Kallen, R., Mandel, G., Meisler, M., Netter, Y. et al. (2000). Nomenclature of voltage-gated sodium channels. *Neuron* **28**, 365-368.

Gomez, R. S., Guatimosim, C. and Gomez, M. V. (2003). Mechanism of action of volatile anesthetics: role of protein kinase C. *Cellular and molecular neurobiology* **23**, 877-885.

Gordon, D., Merrick, D., Auld, V., Dunn, R., Goldin, A. L., Davidson, N. and Catterall, W. A. (1987). Tissue-specific expression of the RI and RII sodium channel subtypes. *Proc Natl Acad Sci U S A* **84**, 8682-6.

Grasshoff, C., Drexler, B., Rudolph, U. and Antkowiak, B. (2006). Anaesthetic drugs: linking molecular actions to clinical effects. *Curr Pharm Des* **12**, 3665-79.

Han, B., McCarren, H. S., O'Neill, D. and Kelz, M. B. (2014). Distinctive recruitment of endogenous sleep-promoting neurons by volatile anesthetics and a nonimmobilizer. *Anesthesiology* **121**, 999-1009.

Hemmings, H., Yan, W., Westphalen, R. and Ryan, T. (2005a). The general anesthetic isoflurane depresses synaptic vesicle exocytosis. *Molecular Pharmacology* **67**, 1591-1599.

Hemmings, H. C. (2009). Sodium channels and the synaptic mechanisms of inhaled anaesthetics. *British Journal of Anaesthesia* **103**, 61-69.

Hemmings, H. C. and Adamo, A. I. (1994). Effects of halothane and propofol on purified brain protein kinase C activation. *Anesthesiology* **81**, 147-155.

Hemmings, H. C., Akabas, M. H., Goldstein, P. A., Trudell, J. R., Orser, B. A. and Harrison, N. L. (2005b). Emerging molecular mechanisms of general anesthetic action. *Trends in Pharmacological Sciences* **26**, 503-510.

Hemmings, H. C., Jr., Akabas, M. H., Goldstein, P. A., Trudell, J. R., Orser, B. A. and Harrison, N. L. (2005c). Emerging molecular mechanisms of general anesthetic action. *Trends Pharmacol Sci* **26**, 503-10.

Herold, K. F., Nau, C., Ouyang, W. and Hemmings, H. C. (2009). Isoflurane inhibits the tetrodotoxin-resistant voltage-gated sodium channel Nav1.8. *Anesthesiology* **111**, 591-599.

Hille, B. (1967). The selective inhibition of delayed potassium currents in nerve by tetraethylammonium ion. *J Gen Physiol* **50**, 1287-302.

Hodgkin, A. L. and Huxley, A. F. (1952). The components of membrane conductance in the giant axon of Loligo. *J Physiol* **116**, 473-96.

Honore, T., Davies, S. N., Drejer, J., Fletcher, E. J., Jacobsen, P., Lodge, D. and Nielsen, F. E. (1988). Quinoxalinediones: potent competitive non-NMDA glutamate receptor antagonists. *Science* **241**, 701-3.

Hoppa, M. B., Gouzer, G., Armbruster, M. and Ryan, T. A. (2014). Control and plasticity of the presynaptic action potential waveform at small CNS nerve terminals. *Neuron* **84**, 778-89.

Hu, W., Tian, C., Li, T., Yang, M., Hou, H. and Shu, Y. (2009). Distinct contributions of Na(v)1.6 and Na(v)1.2 in action potential initiation and backpropagation. *Nat Neurosci* **12**, 996-1002.

Hudetz, A. G. (2012). General anesthesia and human brain connectivity. *Brain Connect* **2**, 291-302.

Hudson, A. E., Herold, K. F., Hemmings Jr, H. C. and Egan, H. C. H. D. (2013). Chapter 10 - Pharmacology of Inhaled Anesthetics. In *Pharmacology and Physiology for Anesthesia*, pp. 159-179. Philadelphia: W.B. Saunders.

Huguenard, J. R. (1996). Low-threshold calcium currents in central nervous system neurons. *Annu Rev Physiol* **58**, 329-48.

Isom, L. L. (2001). Sodium channel beta subunits: anything but auxiliary. *Neuroscientist* **7**, 42-54.

Jia, F., Yue, M., Chandra, D., Homanics, G. E., Goldstein, P. A. and Harrison, N. L. (2008). Isoflurane is a potent modulator of extrasynaptic GABA(A) receptors in the thalamus. *J Pharmacol Exp Ther* **324**, 1127-35.

Joksovic, P. M., Weiergraber, M., Lee, W., Struck, H., Schneider, T. and Todorovic, S. M. (2009). Isoflurane-sensitive presynaptic R-type calcium channels contribute to inhibitory synaptic transmission in the rat thalamus. *J Neurosci* **29**, 1434-45.

Jung, H. Y., Mickus, T. and Spruston, N. (1997). Prolonged sodium channel inactivation contributes to dendritic action potential attenuation in hippocampal pyramidal neurons. *J Neurosci* **17**, 6639-6646.

Kay, A. R. and Wong, R. K. (1986). Isolation of neurons suitable for patch-clamping from adult mammalian central nervous systems. *J Neurosci Methods* **16**, 227-38.

Kharasch, E. D. and Thummel, K. E. (1993). Identification of cytochrome P450 2E1 as the predominant enzyme catalyzing human liver

microsomal defluorination of sevoflurane, isoflurane, and methoxyflurane. *Anesthesiology* **79**, 795-807.

Kim, J., Atherley, R., Werner, D. F., Homanics, G. E., Carstens, E. and Antognini, J. F. (2007). Isoflurane depression of spinal nociceptive processing and minimum alveolar anesthetic concentration are not attenuated in mice expressing isoflurane resistant gamma-aminobutyric acid type-A receptors. *Neurosci Lett* **420**, 209-212.

Koblin, D. D., Chortkoff, B. S., Laster, M. J., Eger, E. I., 2nd, Halsey, M. J. and Ionescu, P. (1994). Polyhalogenated and perfluorinated compounds that disobey the Meyer-Overton hypothesis. *Anesth Analg* **79**, 1043-8.

Koblin, D. D., Eger, E. I., 2nd, Johnson, B. H., Collins, P., Harper, M. H., Terrell, R. C. and Speers, L. (1981). Minimum alveolar concentrations and oil/gas partition coefficients of four anesthetic isomers. *Anesthesiology* **54**, 314-7.

Kole, M. H., Ilschner, S. U., Kampa, B. M., Williams, S. R., Ruben, P. C. and Stuart, G. J. (2008). Action potential generation requires a high sodium channel density in the axon initial segment. *Nat Neurosci* **11**, 178-86.

Kole, M. H., Letzkus, J. J. and Stuart, G. J. (2007). Axon initial segment Kv1 channels control axonal action potential waveform and synaptic efficacy. *Neuron* **55**, 633-47.

Kole, M. H. and Stuart, G. J. (2012). Signal processing in the axon initial segment. *Neuron* **73**, 235-47.

Kopp Lugli, A., Yost, C. S. and Kindler, C. H. (2009). Anaesthetic mechanisms: update on the challenge of unravelling the mystery of anaesthesia. *Eur J Anaesthesiol* **26**, 807-20.

Krasowski, M. D. and Harrison, N. L. (1999). General anaesthetic actions on ligand-gated ion channels. *Cell Mol Life Sci* **55**, 1278-303.

Kress, G. J., Dowling, M. J., Eisenman, L. N. and Mennerick, S. (2010). Axonal sodium channel distribution shapes the depolarized action potential threshold of dentate granule neurons. *Hippocampus* **20**, 558-71.

Kungys, G., Kim, J., Jinks, S. L., Atherley, R. J. and Antognini, J. F. (2009). Propofol produces immobility via action in the ventral horn of the spinal cord by a GABAergic mechanism. *Anesthesia and analgesia* **108**, 1531-1537.

Larrabee, M. and Posternak, J. (1952). Selective action of anesthetics on synapses and axons in mammalian sympathetic ganglia. *Journal of neurophysiology* **15**, 91-114.

Laster, M. J., Zhang, Y., Eger, E. I., Shnayderman, D. and Sonner, J. M. (2007). Alterations in spinal, but not cerebral, cerebrospinal fluid Na+ concentrations affect the isoflurane minimum alveolar concentration in rats. *Anesthesia and analgesia* **105**, 661-665.

Leffler, A., Herzog, R. I., Dib-Hajj, S. D., Waxman, S. G. and Cummins, T. R. (2005). Pharmacological properties of neuronal TTX-resistant sodium channels and the role of a critical serine pore residue. *Pflugers Arch* **451**, 454-463.

Li, L. and Zuo, Z. (2009). Isoflurane preconditioning improves short-term and long-term neurological outcome after focal brain ischemia in adult rats. *Neuroscience* **164**, 497-506.

Lorincz, A. and Nusser, Z. (2008). Cell-type-dependent molecular composition of the axon initial segment. *J Neurosci* **28**, 14329-40.

Lorincz, A. and Nusser, Z. (2010). Molecular identity of dendritic voltage-gated sodium channels. *Science* **328**, 906-9.

Lysko, G. S., Robinson, J. L., Casto, R. and Ferrone, R. A. (1994). The stereospecific effects of isoflurane isomers in vivo. *Eur J Pharmacol* **263**, 25-9.

MacIver, M. B., Mikulec, A. A., Amagasu, S. M. and Monroe, F. A. (1996). Volatile anesthetics depress glutamate transmission via presynaptic actions. *Anesthesiology* **85**, 823-34.

Mechaly, I., Scamps, F., Chabbert, C., Sans, A. and Valmier, J. (2005). Molecular diversity of voltage-gated sodium channel alpha subunits expressed in neuronal and non-neuronal excitable cells. *Neuroscience* **130**, 389-96.

Meyer, H. (1899). Zur theorie der alkoholnarkose. *Archiv fur experimentelle Pathologie und Pharmakologie* **42**, 109-118.

Mikulec, A. A., Pittson, S., Amagasu, S. M., Monroe, F. A. and MacIver, M. B. (1998). Halothane depresses action potential conduction in hippocampal axons. *Brain Res* **796**, 231-8.

Nakamura, Y., Nakajima, S. and Grundfest, H. (1965). The action of tetrodotoxin on electrogenic components of squid giant axons. *J Gen Physiol* **48**, 975-96.

Nau, C. and Wang, G. (2004). Interactions of local anesthetics with voltage-gated Na+ channels. *J Membr Biol* **201**, 1-8.

Nishikawa, K. and MacIver, M. B. (2000). Excitatory synaptic transmission mediated by NMDA receptors is more sensitive to isoflurane than are non-NMDA receptor-mediated responses. *Anesthesiology* **92**, 228-36.

Nishikawa, K. and MacIver, M. B. (2001). Agent-selective effects of volatile anesthetics on GABAA receptor-mediated synaptic inhibition in hippocampal interneurons. *Anesthesiology* **94**, 340-7.

Nury, H., Van Renterghem, C., Weng, Y., Tran, A., Baaden, M., Dufresne, V., Changeux, J. P., Sonner, J. M., Delarue, M. and Corringer, P. J. (2011). X-ray structures of general anaesthetics bound to a pentameric ligand-gated ion channel. *Nature* **469**, 428-31.

Orestes, P., Bojadzic, D., Chow, R. M. and Todorovic, S. M. (2009). Mechanisms and functional significance of inhibition of neuronal T-type calcium channels by isoflurane. *Mol Pharmacol* **75**, 542-54.

Orestes, P. and Todorovic, S. M. (2010). Are neuronal voltage-gated calcium channels valid cellular targets for general anesthetics? *Channels (Austin)* **4**, 518-22.

Orser, B. A. (2006). Extrasynaptic GABAA receptors are critical targets for sedative-hypnotic drugs. *J Clin Sleep Med* **2**, S12-8.

Osorio, N., Cathala, L., Meisler, M. H., Crest, M., Magistretti, J. and Delmas, P. (2010). Persistent Nav1.6 current at axon initial segments tunes spike timing of cerebellar granule cells. *J Physiol* **588**, 651-70.

Ouyang, W. and Hemmings, H. (2005). Depression by isoflurane of the action potential and underlying voltage-gated ion currents in isolated rat neurohypophysial nerve terminals. *J Pharmacol Exp Ther* **312**, 801-808.

Ouyang, W. and Hemmings, H. (2007). Isoform-selective effects of isoflurane on voltage-gated Na+ channels. *Anesthesiology* **107**, 91-98.

Ouyang, W., Herold, K. F. and Hemmings, H. C. (2009). Comparative effects of halogenated inhaled anesthetics on voltage-gated Na+ channel function. *Anesthesiology* **110**, 582-590.

Ouyang, W., Wang, G. and Hemmings, H. (2003). Isoflurane and propofol inhibit voltage-gated sodium channels in isolated rat neurohypophysial nerve terminals. *Molecular Pharmacology* **64**, 373-381.

Overton, C. (1901). Studien über die Narkose zugleich ein Beitrag zur allgemeinen Pharmakologie. Jena: Verlag von Gustav Fischer.

Payandeh, J., Scheuer, T., Zheng, N. and Catterall, W. A. (2011). The crystal structure of a voltage-gated sodium channel. *Nature* **475**, 353-8.

Perouansky, M. (2008). Non-immobilizing inhalational anesthetic-like compounds. *Handb Exp Pharmacol*, 209-23.

Perouansky, M. (2012). The quest for a unified model of anesthetic action: a century in Claude Bernard's shadow. *Anesthesiology* **117**, 465-74.

Perouansky, M., Baranov, D., Salman, M. and Yaari, Y. (1995). Effects of halothane on glutamate receptor-mediated excitatory postsynaptic currents. A patch-clamp study in adult mouse hippocampal slices. *Anesthesiology* **83**, 109-19.

Perouansky, M. and Pearce, R. A. (2011). How we recall (or don't): the hippocampal memory machine and anesthetic amnesia. *Can J Anaesth* **58**, 157-66.

Pihlainen, K. and Ojanperä, I. (1998). Analytical toxicology of fluorinated inhalation anaesthetics. *Forensic science international* **97**, 117-133.

Platkiewicz, J. and Brette, R. (2010). A threshold equation for action potential initiation. *PLoS Comput Biol* **6**, e1000850.

Ragsdale, D., McPhee, J., Scheuer, T. and Catterall, W. (1994). Molecular determinants of state-dependent block of Na+ channels by local anesthetics. *Science* **265**, 1724-1728.

Raju, S. G., Barber, A. F., LeBard, D. N., Klein, M. L. and Carnevale, V. (2013). Exploring volatile general anesthetic binding to a closed membrane-bound bacterial voltage-gated sodium channel via computation. *PLoS Comput Biol* **9**, e1003090.

Rampil, I. J. (1994). Anesthetic potency is not altered after hypothermic spinal cord transection in rats. *Anesthesiology* **80**, 606-10.

Rampil, I. J., Mason, P. and Singh, H. (1993). Anesthetic potency (MAC) is independent of forebrain structures in the rat. *Anesthesiology* **78**, 707-712.

Rau, V., Iyer, S. V., Oh, I., Chandra, D., Harrison, N., Eger, E. I., 2nd, Fanselow, M. S., Homanics, G. E. and Sonner, J. M. (2009). Gamma-aminobutyric acid type A receptor alpha 4 subunit knockout mice are resistant to the amnestic effect of isoflurane. *Anesthesia and analgesia* **109**, 1816-22.

Rau, V., Oh, I., Liao, M., Bodarky, C., Fanselow, M. S., Homanics, G. E., Sonner, J. M. and Eger, E. I., 2nd. (2011). Gamma-aminobutyric acid type A receptor beta3 subunit forebrain-specific knockout mice are resistant to the amnestic effect of isoflurane. *Anesth Analg* **113**, 500-4.

Rehberg, B., Xiao, Y. and Duch, D. (1996). Central nervous system sodium channels are significantly suppressed at clinical concentrations of volatile anesthetics. *Anesthesiology* **84**, 1223-33; discussion 27A.

Rudolph, U. and Antkowiak, B. (2004). Molecular and neuronal substrates for general anaesthetics. *Nat Rev Neurosci* **5**, 709-20.

Rush, A. M., Dib-Hajj, S. D. and Waxman, S. G. (2005). Electrophysiological properties of two axonal sodium channels, Nav1.2 and Nav1.6, expressed in mouse spinal sensory neurones. *The Journal of physiology* **564**, 803-815.

Safari, S., Motavaf, M., Seyed Siamdoust, S. A. and Alavian, S. M. (2014). Hepatotoxicity of halogenated inhalational anesthetics. *Iran Red Crescent Med J* **16**, e20153.

.

Scheuer, T. and Catterall, W. (2006). Control of neuronal excitability by phosphorylation and dephosphorylation of sodium channels. *Biochem Soc Trans* **34**, 1299-1302.

Schifilliti, D., Grasso, G., Conti, A. and Fodale, V. (2010). Anaesthetic-related neuroprotection: intravenous or inhalational agents? *CNS Drugs* **24**, 893-907.

Schlame, M. and Hemmings, H. (1995). Inhibition by volatile anesthetics of endogenous glutamate release from synaptosomes by a presynaptic mechanism. *Anesthesiology* **82**, 1406-1416.

Shiraishi, M. and Harris, R. (2004). Effects of alcohols and anesthetics on recombinant voltage-gated Na+ channels. *J Pharmacol Exp Ther* **309**, 987-994.

Sirois, J. E., Lei, Q., Talley, E. M., III, C. L. and Bayliss, D. A. (2000). The TASK-1 Two-Pore Domain K+ Channel Is a Molecular Substrate for Neuronal Effects of Inhalation Anesthetics.

Solt, K. and Forman, S. A. (2007). Correlating the clinical actions and molecular mechanisms of general anesthetics. *Curr Opin Anaesthesiol* **20**, 300-6.

Sonner, J. M., Antognini, J. F., Dutton, R. C., Flood, P., Gray, A. T., Harris, R. A., Homanics, G. E., Kendig, J., Orser, B., Raines, D. E. et al.

(2003). Inhaled anesthetics and immobility: mechanisms, mysteries, and minimum alveolar anesthetic concentration. *Anesth Analg* **97**, 718-40.

Sonner, J. M., Werner, D. F., Elsen, F. P., Xing, Y., Liao, M., Harris, R. A., Harrison, N. L., Fanselow, M. S., Eger, E. I., 2nd and Homanics, G. E. (2007). Effect of isoflurane and other potent inhaled anesthetics on minimum alveolar concentration, learning, and the righting reflex in mice engineered to express alpha1 gamma-aminobutyric acid type A receptors unresponsive to isoflurane. *Anesthesiology* **106**, 107-13.

Spracklin, D. K., Thummel, K. E. and Kharasch, E. D. (1996). Human reductive halothane metabolism in vitro is catalyzed by cytochrome P450 2A6 and 3A4. *Drug Metab Dispos* **24**, 976-83.

Spurny, R., Billen, B., Howard, R. J., Brams, M., Debaveye, S., Price, K. L., Weston, D. A., Strelkov, S. V., Tytgat, J., Bertrand, S. et al. (2013). Multisite binding of a general anesthetic to the prokaryotic pentameric Erwinia chrysanthemi ligand-gated ion channel (ELIC). *J Biol Chem* **288**, 8355-64.

Stewart, A., Lambert, D. H., Concepcion, M. A., Datta, S., Flanagan, H., Migliozzi, R. and Covino, B. G. (1988). Decreased incidence of tourniquet pain during spinal anesthesia with bupivacaine. A possible explanation. *Anesth Analg* **67**, 833-7.

Stuart, G., Schiller, J. and Sakmann, B. (1997). Action potential initiation and propagation in rat neocortical pyramidal neurons. *J Physiol* **505 (Pt 3)**, 617-32.

Sun, M., Deng, B., Zhao, X., Gao, C., Yang, L., Zhao, H., Yu, D., Zhang, F., Xu, L., Chen, L. et al. (2015). Isoflurane preconditioning provides neuroprotection against stroke by regulating the expression of the TLR4 signalling pathway to alleviate microglial activation. *Sci Rep* **5**, 11445.

Tachibana, K., Takita, K., Hashimoto, T., Matsumoto, M., Yoshioka, M. and Morimoto, Y. (2007). Isoflurane bidirectionally modulates the paired-pulse responses in the rat hippocampal CA1 field in vivo. *Anesth Analg* **105**, 1006-11, table of contents.

Taheri, S., Halsey, M., Liu, J., Eger, E., Koblin, D. and Laster, M. (1991). What solvent best represents the site of action of inhaled anesthetics in humans, rats, and dogs? *Anesthesia and analgesia* **72**, 627-634.

Tammaro, P., Shimomura, K. and Proks, P. (2008). Xenopus oocytes as a heterologous expression system for studying ion channels with the patch-clamp technique. *Methods Mol Biol* **491**, 127-39.

Terrell, R. C. (2008). The invention and development of enflurane, isoflurane, sevoflurane, and desflurane. *Anesthesiology* **108**, 531-3.

Urban, B. W. (2008). The site of anesthetic action. *Handb Exp Pharmacol*, 3-29.

Urban, B. W. and Haydon, D. A. (1987). The actions of halogenated ethers on the ionic currents of the squid giant axon. *Proc R Soc Lond B Biol Sci* **231**, 13-26.

Van Wart, A., Trimmer, J. S. and Matthews, G. (2007). Polarized distribution of ion channels within microdomains of the axon initial segment. *J Comp Neurol* **500**, 339-52.

Wakasugi, M., Hirota, K., Roth, S. H. and Ito, Y. (1999). The effects of general anesthetics on excitatory and inhibitory synaptic transmission in area CA1 of the rat hippocampus in vitro. *Anesthesia and analgesia* **88**, 676-80.

Wang, D. S. and Orser, B. A. (2011). Inhibition of learning and memory by general anesthetics. *Can J Anaesth* **58**, 167-77.

Wang, S.-Y., Mitchell, J., Moczydlowski, E. and Wang, G. K. (2004). Block of inactivation-deficient Na+ channels by local anesthetics in stably transfected mammalian cells: evidence for drug binding along the activation pathway. *The Journal of General Physiology* **124**, 691-701.

Werner, D. F., Swihart, A., Rau, V., Jia, F., Borghese, C. M., McCracken, M. L., Iyer, S., Fanselow, M. S., Oh, I., Sonner, J. M. et al. (2011). Inhaled anesthetic responses of recombinant receptors and knockin mice harboring alpha2(S270H/L277A) GABA(A) receptor subunits that are resistant to isoflurane. *J Pharmacol Exp Ther* **336**, 134-44.

Wester, J. C. and Contreras, D. (2013). Biophysical mechanism of spike threshold dependence on the rate of rise of the membrane potential by sodium channel inactivation or subthreshold axonal potassium current. *J Comput Neurosci* **35**, 1-17.

Westphalen, R. and Hemmings, H. (2003). Selective depression by general anesthetics of glutamate versus GABA release from isolated cortical nerve terminals. *J Pharmacol Exp Ther* **304**, 1188-1196.

Westphalen, R. and Hemmings, H. (2006). Volatile anesthetic effects on glutamate versus GABA release from isolated rat cortical nerve terminals: 4-aminopyridine-evoked release. *J Pharmacol Exp Ther* **316**, 216-223.

Westphalen, R., Krivitski, M., Amarosa, A., Guy, N. and Hemmings, H. (2007). Reduced inhibition of cortical glutamate and GABA release by halothane in mice lacking the K+ channel, TREK-1. *British journal of pharmacology* **152**, 939-945.

White, J. A., Alonso, A. and Kay, A. R. (1993). A heart-like Na+ current in the medial entorhinal cortex. *Neuron* **11**, 1037-47.

White, W. F. (1985). The glycine receptor in the mutant mouse spastic (spa): strychnine binding characteristics and pharmacology. *Brain Res* **329**, 1-6.

Wildsmith, J. A., Brown, D. T., Paul, D. and Johnson, S. (1989). Structure-activity relationships in differential nerve block at high and low frequency stimulation. *Br J Anaesth* **63**, 444-52.

Winegar, B. D. and MacIver, M. B. (2006). Isoflurane depresses hippocampal CA1 glutamate nerve terminals without inhibiting fiber volleys. *BMC Neurosci* **7**, 5.

Winegar, B. D., Owen, D. F., Yost, C. S., Forsayeth, J. R. and Mayeri, E. (1996). Volatile general anesthetics produce hyperpolarization of

Aplysia neurons by activation of a discrete population of baseline potassium channels. *Anesthesiology* **85**, 889-900.

Wu, X., Sun, J., Evers, A., Crowder, M. and Wu, L. (2004). Isoflurane inhibits transmitter release and the presynaptic action potential. *Anesthesiology* **100**, 663-670.

Yin, X., Su, B., Zhang, H., Song, W., Wu, H., Chen, X., Zhang, X., Dong, H. and Xiong, L. (2012). TREK1 activation mediates spinal cord ischemic tolerance induced by isoflurane preconditioning in rats. *Neurosci Lett* **515**, 115-20.

Zecharia, A. Y., Nelson, L. E., Gent, T. C., Schumacher, M., Jurd, R., Rudolph, U., Brickley, S. G., Maze, M. and Franks, N. P. (2009). The involvement of hypothalamic sleep pathways in general anesthesia: testing the hypothesis using the GABAA receptor beta3N265M knock-in mouse. *J Neurosci* **29**, 2177-87.

Zhang, T. and Johansson, J. S. (2005). A calorimetric study on the binding of six general anesthetics to the hydrophobic core of a model protein. *Biophys Chem* **113**, 169-74.

Zhang, Y., Guzinski, M., Eger, E. I., Laster, M. J., Sharma, M., Harris, R. A. and Hemmings, H. C. (2010). Bidirectional modulation of isoflurane potency by intrathecal tetrodotoxin and veratridine in rats. *British Journal of Pharmacology* **159**, 872-878.

Zhang, Y., Laster, M. J., Hara, K., Harris, R. A., Eger, E. I., 2nd, Stabernack, C. R. and Sonner, J. M. (2003). Glycine receptors mediate part of the immobility produced by inhaled anesthetics. *Anesth Analg* **96**, 97-101, table of contents.

Zhao, P. and Zuo, Z. (2004). Isoflurane preconditioning induces neuroprotection that is inducible nitric oxide synthase-dependent in neonatal rats. *Anesthesiology* **101**, 695-703.

Zhou, W. and Goldin, A. L. (2004). Use-dependent potentiation of the Nav1.6 sodium channel. *Biophysical journal* **87**, 3862-3872.

Zurek, A. A., Bridgwater, E. M. and Orser, B. A. (2012). Inhibition of alpha5 gamma-Aminobutyric acid type A receptors restores recognition memory after general anesthesia. *Anesth Analg* **114**, 845-55.

APPENDICES

The appendices include work done in Geoffrey Abbott's laboratory at Weill Cornell Medical College. I investigated the role of voltage-gated K^+ channel β subunits belonging to a family of single transmembrane proteins encoded by the *KCNE* genes. We found that these proteins, known as 'MiRPs' and originally discovered in the excitable cells of the heart, are essential in the proper functioning of the epithelial lining of the stomach, thyroid and choroid plexus. KCNE2 and KCNE3, also known as Mirp1 and Mirp2, respectively, convert the voltage-activated KCNQ1 K^+ channel into a voltage-insensitive leak channel that passes K^+ through the membrane of electrically silent epithelial cells and supports acidification of the stomach lumen, production of thyroid hormone and ionic homeostasis of the cerebral spinal fluid.

This work used positron emission tomography to show that KCNE2 is essential for the uptake of iodide into the thyroid and we proposed the *KCNE2* gene as an underlying link between thyroid dysfunction and heart disease. We also investigated the role of KCNE2 in the stomach where it is essential for gastric acid secretion. After finding upregulation of KCNE3 in the stomach of *KCNE2* knock-out mice, we generated a *KCNE3* knock-out mouse line and bred *KCNE2/KCNE3* double knock-out mice to study the effects of these subunits on the trafficking and function of the KCNQ1 channel in the stomach.

APPENDIX I

The KCNQ1-KCNE2 potassium channel is required for thyroid I^- uptake

Kerry Purtell, Monika Paroder-Belenitsky, Andrea Reyna-Neyra, Wade Koba, Eugene Fine, Nancy Carrasco and Geoffrey W. Abbott

Adapted from: *FASEB J*. 2012 Aug;26(8):3252-9.

doi: 10.1096/fj.12-206110

Abstract

The KCNQ1 α subunit and the KCNE2 β subunit form a potassium channel in thyroid epithelial cells. Genetic disruption of KCNQ1-KCNE2 causes hypothyroidism in mice, resulting in cardiac hypertrophy, dwarfism, alopecia, and prenatal mortality. Here, we investigated the mechanistic requirement for KCNQ1-KCNE2 in thyroid hormone biosynthesis, utilizing whole-animal dynamic positron emission tomography. The KCNQ1-specific antagonist (−)-[3R,4S]-chromanol 293B (C293B) significantly impaired thyroid cell I^- uptake, which is mediated by the Na^+/I^- symporter (NIS), *in vivo* (dSUV/dt: vehicle, 0.028±0.004 min^{-1}; 10 mg/kg C293B, 0.009±0.006 min^{-1}) and *in vitro* (EC50: 99±10 μM C293B). Na^+-dependent nicotinate uptake by SMCT, however, was unaffected. *Kcne2* deletion did not alter the balance of free vs. thyroglobulin-bound I^- in the thyroid (distinguished using ClO_4^-, a competitive inhibitor of NIS), indicating that KCNQ1-KCNE2 is not required for Duox/TPO-mediated I^- organification. However, *Kcne2* deletion doubled the rate of free I^- efflux from the thyroid following ClO_4^- injection, a NIS-independent process. Thus, KCNQ1-KCNE2 is necessary for adequate thyroid cell I^- uptake, the most likely explanation being that it is prerequisite for adequate NIS activity.

Introduction

Potassium ion (K^+) channels provide a K^+-selective aqueous pore for the diffusion of K^+ across the plasma membrane, and are essential for function of most if not all mammalian cell types. Voltage-gated potassium (K_v) channels are gated (opened and closed) by changes in membrane potential. They are opened by membrane depolarization and are essential for the timely repolarization of excitable cells. Other K^+ channels are constitutively active, i.e., open at resting membrane potential. Defining the role of constitutively active K^+ channels *in vivo* can be challenging: they contribute an often temporally invariant 'background' K^+ conductance, and may be expressed in cell types resistant to faithful primary culturing or direct electrophysiological analysis. In addition, constitutively active K^+ channels in particular may be important for processes difficult to quantify *in vivo* or *in vitro*, including ion homeostasis, and hormone synthesis and release.

The KCNQ1-KCNE2 potassium channel has an unusual molecular composition for a constitutively active K^+ channel, but is widely studied because its subunits are required for a range of processes essential in human physiology. The KCNQ1 pore-forming (α) subunit contains the S4-based voltage-sensing domain present in voltage-gated K^+, Na^+ and Ca^{2+} channels. However, while homomeric channels formed by a tetramer of KCNQ1 α subunits are voltage-gated, heteromeric channel complexes comprising KCNQ1 together with the single-transmembrane segment KCNE2 β subunit are constitutively active, and relatively voltage-insensitive (1). KCNQ1-KCNE2 channels are essential for the physiology of at least two types of

non-excitable, polarized epithelial cells: gastric parietal cells, which secrete gastric acid, and thyroid epithelial cells, which secrete thyroid hormones. Targeted deletion of either *Kcnq1* or *Kcne2* causes both hypothyroidism and achlorhydria, demonstrating the absolute necessity for both α and β subunits in the native channel complex (2-6).

Kcne2$^{-/-}$ mice also exhibit dwarfism, alopecia (Fig. 1A), prenatal mortality and cardiomegaly, all of which arise from their underlying hypothyroidism (5); *Kcnq1*$^{-/-}$ mice were also recently found to be hypothyroid (6). Human *KCNQ1* and *KCNE2* gene mutations cause potentially fatal ventricular and atrial cardiac arrhythmias, probably primarily due to the role of these subunits in cardiac myocyte K^+ currents (7, 8); however, the discovery of the KCNQ1-KCNE2 channel in mouse and human thyroid suggests a possible endocrine component to these electrical disturbances (5). Here, we sought to elucidate the mechanistic basis for the requirement for KCNQ1-KCNE2 channels in thyroid function. To examine thyroid physiology *in vivo*, we utilized positron emission tomography (PET) to quantitatively image $^{124}I^-$ fluxes in mice genetically and pharmacologically manipulated to isolate different steps in thyroid hormone biosynthesis. We demonstrate that KCNQ1-KCNE2 is required for Na^+/I^- symporter (NIS)-mediated thyroid cell uptake of I^-, an essential step in thyroid hormone biosynthesis.

Materials and Methods

Transgenic mouse generation, care and use

We generated and genotyped the C57BL/6 *Kcne2*$^{-/-}$ mouse line as previously described (4, 5) and housed and used mice according to the US National Institutes of Health *Guide for the Care and Use of Laboratory Animals.* Animal procedures were approved by the Animal Care and Use Committees at Weill Medical College of Cornell University and Albert Einstein College of Medicine.

Positron Emission Tomography (PET) and *Computed Tomography (CT*)

Mice were secured to a bed with a breathing tube over their snout that provided a continuous supply of isoflurane anesthetic throughout the imaging procedure (Fig. 1C). Imaging was performed on an Inveon Multimodality scanner (Siemens), in which CT x-rays were generated by an 80 kV peak voltage difference between cathode and tungsten target at 0.5 mA current and 250 ms exposure time. The CT field of view was 5.5 cm by 8.5 cm with an overall resolution without magnification of 100 µm. Subsequent PET imaging was performed by translating the test subject on the imaging gantry into the PET device which provided a 12.7 cm axial and 10 cm transaxial active field of view. The PET scanner has no septa and acquisitions were performed in 3D list mode. A reconstructed FWHM resolution of <1.4 mm is achievable in the center of the axial field of view. List mode acquisition of data was performed to permit dynamic re-framing for kinetic evaluation of $^{124}I^-$ uptake, where indicated. After each acquisition, data were sorted into 3D sinograms, and images were reconstructed using

a 2D-Ordered Subset Expectation Maximization algorithm. Data were corrected for deadtime counting losses, random coincidences and the measured nonuniformity of detector response (*i.e.*, normalized) but not for attenuation or scatter. After both acquisitions, CT images were coregistered with PET images using a previously stored linear transformation matrix.

Analysis was performed using ASIPRO (Siemens) dedicated software. All image studies were inspected visually in a rotating 3D projection display to examine for interpretability and image artifact. Manual regions of interest (ROI) were defined around the thyroid. Successive scrolling through 2 dimensional slices (each 1.2 mm thick in the axial images) permitted measurement of a radioactivity within defined volumes, and also as profiles in reconstructed image planes. The counts per cc within this volume multiplied by the 3D ROI volume after correction for detector sensitivity, animal weight, and time of injection determined the standardized-uptake value (SUV).

Methimazole (MMI) treatment

Mice were given an intraperitoneal (i.p.) injection of 1 mg MMI (Sigma-Aldrich, St. Louis, MO, USA) in 100 µl total volume filter-sterilized PBS, and overnight *ad libitum* access to drinking water containing 250 mgl^{-1} MMI.

Perchlorate Discharge Assay

Lactating or aging dams, anesthetized with 1.5% isoflurane-oxygen mixture, received 200-300 µCi (7-12 MBq) $^{124}I^-$ in 0.1 ml saline solution via tail-vein injection. Dams

were placed back in their cages for 90 minutes to allow accumulation of the $^{124}I^-$ tracer in the thyroid, then imaged for 10 minutes before, and for the 60 minutes following, injection of 2 mg sodium perchlorate ($NaClO_4$, Sigma Aldrich) in a total volume of 0.1 mL PBS via tail vein. Measurements of thyroid counts taken at 5 minute intervals following $NaClO_4$ injection were normalized to the maximum count value taken from the pre-ClO_4^- image.

Uptake experiments

Stock solutions of 80 mM (-)-[3R,4S]-chromanol 293B (Tocris Biosciences, Cambridge, UK) dissolved in pure DMSO were prepared and stored at -20ºC. The stock was diluted to a final concentration of 2.5 mg ml^{-1} in PBS with 20% DMSO. Vehicle controls contained 20% DMSO in PBS. Mice were injected with 0.1 ml of drug or vehicle 30 minutes before injection with $^{124}I^-$ (150 µCi, 5.55 MBq) dissolved in 0.1 ml saline.

Cell culture, transport, and flow cytometry experiments

FRTL5 cells were grown in Coon's modified Ham's F12 medium supplemented with 5% newborn calf serum (Sigma Aldrich) and 6 different hormones (insulin 10 mg ml^{-1}, transferrin 5 mg ml^{-1}, hydrocortisone 10 nM, tripeptide Gly-L-His-L-Lys 10 ng ml^{-1}, TSH 0.3 mU ml^{-1}, and somatostatin 10 ng ml^{-1}) in a water-saturated atmosphere of 5%

CO_2 and 95% air at 37°C. For transport assays, FRTL5 cells were cultured on 24-well plates.

Uptake experiments were initiated by adding 500 µl HBSS (137 mM NaCl, 5.4 mM KCl, 1.3 mM $CaCl_2$, 0.4 mM $MgSO_4$, 0.4 mM $Na_2HPO_4.7H_2O$, 0.44 mM KH_2PO_4, and 0.55 mM glucose), buffered with 10 mM Hepes-KOH (pH 7.5) containing 20 µM $Na^{125}I^-$ (Perkin Elmer, Wellesley, MA, USA) with a specific activity of 50 Ci/mol, in the presence or absence of (-)-[3R,4S]-chromanol 293B. FRTL5 cells were incubated at 37˚C in a humidified atmosphere for 30 min. Reactions were terminated by aspirating the radioactive solution and washing three times with HBSS. Accumulated $^{125}I^-$ was determined by permeabilizing cells with ethanol for 20 minutes and quantifying the released radioisotope in a gamma counter. Data were standardized per µg of DNA in each well. Concentration of DNA was assessed by the diphenylamine method (9). [^{14}C]nicotinate (Moravek Biochemicals, Brea, CA, USA) uptake was measured using the same procedure, except that cells were incubated with buffered HBSS containing 50 µM [^{14}C]nicotinate. NaCl was replaced with equimolar concentrations of choline chloride to determine the Na^+ dependence of SMCT-mediated nicotinate transport.

For flow cytometry, FRTL-5 cells were transduced with extracellular N-terminal hemagglutinin (HA)-tagged human NIS, as described previously (11). Paraformaldehyde-fixed cells were incubated in PBS containing 0.2% BSA with 3 nM anti-HA (clone 3F10) rat monoclonal IgG (Roche Applied Science, Mannheim, Germany). The fluorescence of 2 × 104 cells/tube was assayed in FACSCalibur flow

cytometer (BD Biosciences, San Jose, CA, USA). Data were analyzed with FlowJo software (Tree Star, Ashland, OR, USA).

COS-7 cells were grown in DMEM supplemented with 10% heat-inactivated FBS (Sigma-Aldrich). Cells were transfected with 10 μg/10-cm dish pcDNA3.1-rNIS or -hNIS cDNA constructs using polyethylenimine. I^- uptake activity was assayed at 48 h post-transfection.

Results

PET imaging of a chemically induced iodine organification defect in mouse thyroid. We previously utilized PET imaging to discover that *Kcne2* deletion in mice impairs thyroid $^{124}I^-$ accumulation (5). Here, we combined PET with other techniques to determine the underlying mechanism for this impairment. Thyrocytes actively take up I^- via the basolateral Na^+/I^- symporter (NIS) (10). I^- next effluxes across the thyrocyte apical membrane to the cell-colloid interface, where it is oxidized and covalently incorporated into specific tyrosyl residues on thyroglobulin – a process termed 'organification' and catalyzed by thyroid peroxidase (TPO) and the NADPH-dependent H_2O_2-generating system (Duox) (Fig. 1 B). Iodinated thyroglobulin (Tg) is then stored in the colloid until demand for thyroid hormones causes Tg to be apically endocytosed and proteolyzed, and thyroid hormones to be basolaterally secreted into the bloodstream (11, 12). To establish the mechanism for impaired thyroid $^{124}I^-$ accumulation in *Kcne2*$^{-/-}$ mice, we needed to distinguish between free I^- and iodine covalently incorporated into Tg, and also between I^- uptake and iodine organification.

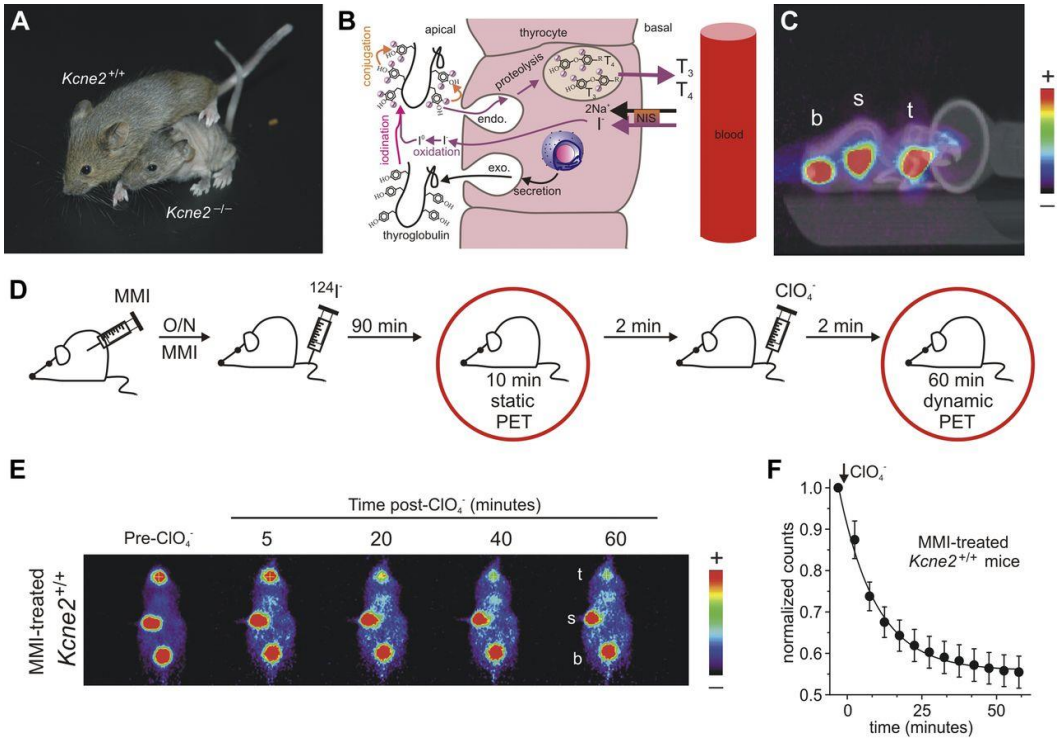

***Figure 1*. PET quantification of ClO_4^--induced $^{124}I^-$ discharge in MMI-treated mice.** *A*) Age-matched 3-wk old *Kcne2*$^{+/+}$ and *Kcne2*$^{-/-}$ pups bred from same-genotype dams, showing dwarfism and alopecia in the latter. *B*) Schematic of I^- uptake and organification in the thyroid. *C*) Exemplar coregistered PET-CT image of a 6-mo-old *Kcne2*$^{+/+}$ mouse, injected with $^{124}I^-$ and positioned in the anesthesia-delivery nose cone. Heat map (scale at right) for PET image shows positioning of the thyroid (t), stomach (s), and bladder (b). CT bony structures are evident in purple color scale. *D*) Schematic showing experimental protocol for validating PET imaging of ClO_4^--induced I^- discharge, using MMI-pretreated mice. *E*) Exemplar pre- and post-ClO_4^- PET images for an MMI-pretreated *Kcne2*$^{+/+}$ mouse (protocol in *D*; 150 μCi of $^{124}I^-$ injected). Tissues labeled as in *C*. Scale bar at right. *F*) Mean thyroid counts normalized to pre-ClO_4^- thyroid counts for MMI-pretreated *Kcne2*$^{+/+}$ mice, demonstrating ClO_4^--induced $^{124}I^-$ discharge (protocol in *D*; *n*=5). Error bars = SEM.

First, we employed co-registered PET and X-ray computed tomography (CT) on mice tail-vein-injected with ^{124}I, to confirm positioning of the thyroid signal compared to other I^--accumulating tissues such as the stomach and bladder (Fig. 1 C).

We then sought to determine whether or not KCNQ1-KCNE2 is required for thyroid I^- organification, using PET in combination with the well-established perchlorate (ClO_4^-) discharge assay (PDA). ClO_4^-, a competitive inhibitor of NIS, that is translocated electroneutrally (13) causes a rapid reduction of free I^- in the thyroid (as I^- can efflux from but not enter the thyrocyte in its presence). When organification is normal, ClO_4^- elicits only moderate thyroid I^- discharge (~15%) because most I^- is rapidly covalently bound to Tg, whereas an organification defect can result in a ClO_4^--induced I^- discharge of 50% or more (14).

We first assessed the suitability of PET for quantifying ClO_4^- discharge in the mouse thyroid, by ascertaining the effect of pretreating 'wild-type' C57BL/6 mice with methimazole (MMI), a thionamide that blocks I^- organification by inhibiting TPO (15, 16). MMI pretreatment involved an intraperitoneal (i.p.) injection of MMI, followed by overnight *ad libitum* access to water supplemented with MMI. The following day, 90 minutes after tail vein injection of $^{124}I^-$, a 10 min static PET image was generated to measure peak $^{124}I^-$ accumulation. Mice immediately received ClO_4^- *via* tail-vein injection and were PET-imaged dynamically at 5 minute intervals for 60 minutes (Fig. 1 D, E). Mean thyroid radioactivity at each 5 minute interval following ClO_4^- injection was normalized to the mean pre-ClO_4^- thyroid radioactivity to quantify discharge. ClO_4^- resulted in a 45 ± 4% discharge of ^{124}I within the first hour after injection in MMI-pretreated mice, thereby confirming successful detection of the chemically induced organification defect and validating the PET assay (n = 5) (Fig. 1F).

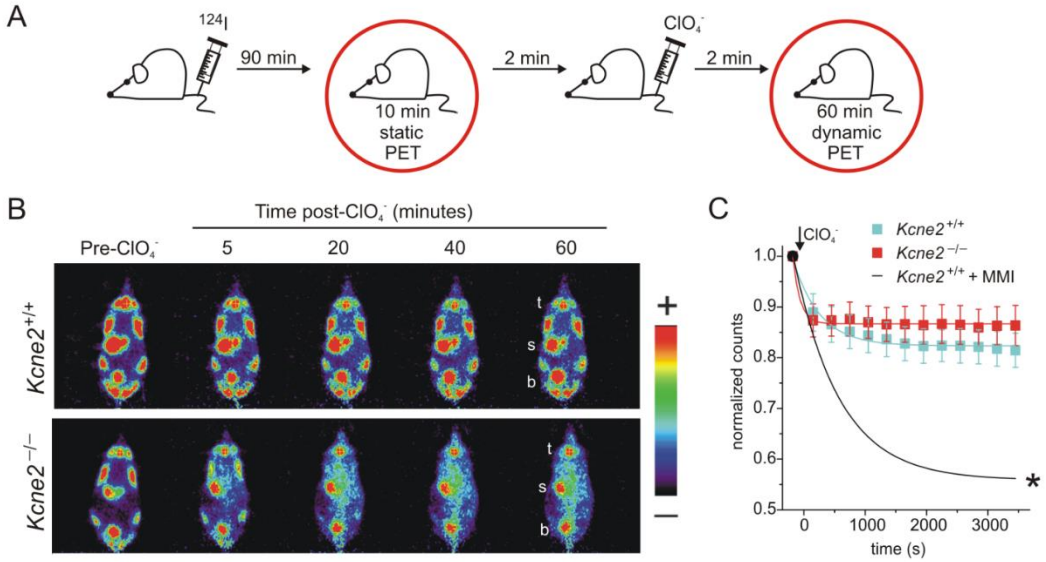

***Figure 2. Kcne2* deletion does not cause an I^- organification defect.** *A*) Schematic showing experimental protocol for PET quantification of ClO_4^- -induced I^- discharge in *Kcne2*$^{+/+}$ and *Kcne2*$^{-/-}$ mice. *B*) Exemplar pre- and post-ClO_4^- PET images for *Kcne2*$^{+/+}$ and *Kcne2*$^{-/-}$ mice (protocol in *A*). Labeled tissues: thyroid (t), stomach (s), and bladder (b). Scale bar at right. *C*) Mean thyroid counts normalized to pre-ClO_4^- thyroid counts for *Kcne2*$^{+/+}$ and *Kcne2*$^{-/-}$ mice as in *B*, compared to data for MMI-pretreated *Kcne2*$^{+/+}$ mice (data from Fig. 1*F*); $n = 5$ mice/group. Error bars = SEM. $^*P < 0.0005$ *vs.* non-MMI-pretreated mice, 60-min time point.

KCNQ1-KCNE2 is not required for I^- organification

We next quantified the effect of targeted deletion of *Kcne2* on ClO_4^--induced discharge of thyroid I^- in non-MMI-treated lactating C57BL/6 mice using PET, following the protocol outlined in Fig. 2 A, and observed 19 ± 3% discharge within the first hour after injection in *Kcne2*$^{+/+}$ mice compared to 14 ± 4% in *Kcne2*$^{-/-}$ mice (*n*

= 5; $P = 0.19$) (Fig. 2 B, C). There was therefore no significant effect of *Kcne2* deletion on organification. Furthermore, both non-MMI-pretreated groups exhibited significantly less discharge than MMI-pretreated *Kcne2*$^{+/+}$ mice ($n = 5$; $P < 0.0005$) (Fig. 2 C). Lactating mice were used for these experiments because hypothyroidism in *Kcne2*$^{-/-}$ mice is most marked during early development, gestation, lactation, and in old age (5).

KCNQ1-KCNE2 is required for efficient I^- uptake

The absence of an organification defect in *Kcne2*$^{-/-}$ mice, combined with our previous finding that *Kcne2* deletion impairs thyroid I^- accumulation (5), suggested KCNQ1-KCNE2 could be important for NIS-mediated I^- uptake. To test this hypothesis, we first used the highly specific KCNQ1 antagonist (-)-[3R,4S]-chromanol 293B (C293B) to acutely inhibit KCNQ1-KCNE2, in *Kcne2*$^{+/+}$ mice pretreated with MMI to inhibit organification, allowing us to assess I^- transport at steady state. This approach dissociated the uptake process from $^{124}I^-$ organification, eliminating radiolabeling of Tg and thus facilitating exclusive imaging of NIS-mediated transport of free $^{124}I^-$ in the thyroid. Following overnight MMI treatment, mice were tail-vein injected with either C293B [(10 $mgkg^{-1}$) or vehicle, then 30 minutes later tail-vein injected with $^{124}I^-$ and immediately dynamically PET imaged for 60 minutes to quantify $^{124}I^-$ uptake (Fig. 3A). Strikingly, C293B (10 $mgkg^{-1}$) impaired $^{124}I^-$ by 42% at 60 min, giving a mean thyroid radioactivity of 0.69 ± 0.11 SUV (standard uptake value, i.e., counts normalized to whole-body mean radioactivity concentration; whole body SUV = 1.00,

by definition) compared to 1.18 ± 0.06 SUV in vehicle-injected mice (n = 5; P < 0.005) (Fig. 3 B,C), signifying ^{124}I uptake and retention. Initial thyroid I^- uptake rates were reduced 3-fold by C293B (10 mg/kg), with the *dSUV/dt* being reduced from 0.028 ± 0.004 min^{-1} (vehicle) to 0.009 ± 0.006 min^{-1} (C293B; n=5, P=0.014; Fig. 3*D*).

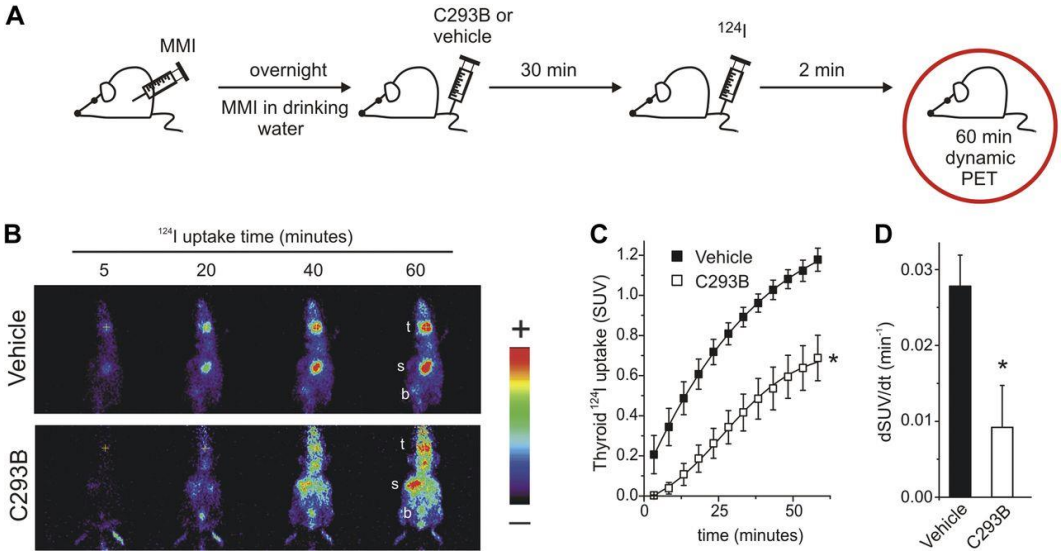

***Figure 3*. Pharmacological inhibition of KCNQ1-KCNE2 impairs thyroid I^- uptake *in vivo*.** *A*) Schematic showing experimental protocol for PET quantification of the effect of C293B (10 mg/kg) on thyroid $^{124}I^-$ uptake in MMI-pretreated *Kcne2*$^{+/+}$ mice. *B*) Exemplar PET images for vehicle- or 10 mg/kg C293B-treated *Kcne2*$^{+/+}$ mice, at the indicated times following $^{124}I^-$ injection (protocol in *A*). Labeled tissues: thyroid (t), stomach (s), and bladder (b). Scale bar at right. *C*) Mean thyroid $^{124}I^-$ counts during the first hour following $^{124}I^-$ injection for MMI-pretreated *Kcne2*$^{+/+}$ mice as in *B*, injected with vehicle or 10 mg/kg C293B 30 min before $^{124}I^-$; n = 5 mice/group. Error bars = SEM. *P < 0.005 *vs.* vehicle-treated, 60-min time point. D) Mean initial (0–13.3 min) thyroid I^- uptake rates determined from graphs as in *C* for individual mice, groups as in *C*; n = 5. *P = 0.014.

To validate this finding in an alternative system, we performed $^{125}I^-$ flux assays using the highly functional rat thyroid-derived FRTL5 cell line (Fig. 4*A***)**, which we previously showed expresses KCNQ1-KCNE2 channel protein and K^+ current (5). FRTL5 cells exhibit minimal I^- organification, but express NIS and efficiently transport I^-. Increasing concentrations of C293B inhibited NIS-mediated I^- uptake in a dose-dependent manner (EC_{50}: 99±10 μM C293B; *n*=4; Fig. 4*B*); in contrast, they did not affect another Na^+-driven transport process, namely SMCT-mediated nicotinate uptake (Fig. 4*B*), demonstrating the specificity of the inhibition of I^- uptake and also indicating that impaired NIS function arising from KCNQ1-KCNE2 inhibition does not stem from a disrupted Na^+ gradient. In support of the KCNQ1-dependence of action of C293B, it did not inhibit cell-surface expression of HA-tagged NIS in FRTL-5 cells, as quantified by flow cytometry, indicating that the decrease of I^- uptake caused by C293B is not due to fewer NIS molecules at the plasma membrane (Fig. 4*C*). Likewise, C293B had no effect on I^- uptake through rat or human NIS when heterologously expressed, without KCNQ1 overexpression, in COS-7 cells (Fig. 4*D*).

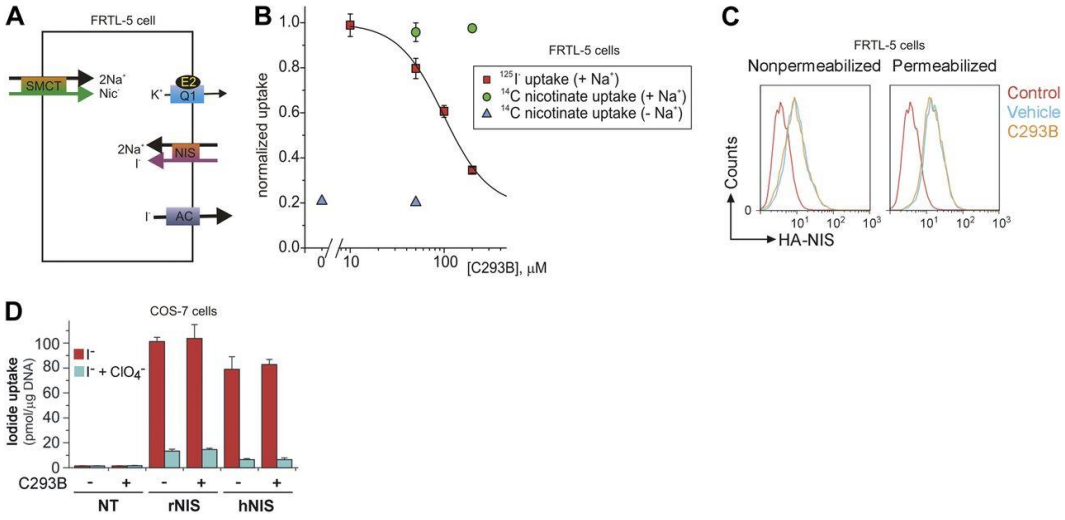

***Figure 4*. Pharmacological inhibition of KCNQ1-KCNE2 specifically impairs I^- uptake *in vitro*.** *A*) FRTL-5 cell simplified model to illustrate various key ion fluxes. AC, anion channel; E2, KCNE2; Q1, KCNQ1; Nic^-, nicotinate; NIS, Na^+/I^- symporter; SMCT, sodium/monocarboxylate transporter. *B*) C293B inhibition of $^{125}I^-$ steady-state uptake by FRTL5 cells (red squares) for various C293B concentrations. Values were normalized to steady-state uptake of $^{125}I^-$ by FRTL5 cells bathed in DMSO as a vehicle control. Data are means of 4 independent experiments/concentration, each performed in triplicate. $^{125}I^-$ uptake values in the presence of ClO_4^- were <3.7% (data not shown). Dose response was fitted with a sigmoidal function. Also shown: [^{14}C]nicotinate steady-state uptake in FRTL-5 cells bathed in medium containing 50 μM [^{14}C]nicotinate, and either Na^+ (green circles) or choline (blue triangles), to assess effects of C293B on the function of SMCT. *C*) FRTL-5 cells expressing extracellular HA-tagged NIS were incubated with 100 μM C293B or vehicle for 1 h. Histograms indicate NIS expression at the plasma membrane quantified by flow cytometry using an anti-HA antibody under nonpermeabilized conditions (left) or permeabilized conditions as a control for total protein (right). Unstained control cells in red, DMSO-treated cells in cyan, and C293B-treated cells in orange. Data are representative of 2 experiments, each performed in duplicate. *D*) I^- steady-state uptake in rNIS- or hNIS-transfected COS-7 cells incubated with 20 μM $^{125}I^-$, 100 μM C293B, or vehicle as indicated, and in the absence (red) or presence (blue) of 40 μM ClO_4^-. Data are representative of 3 independent experiments, each performed in triplicate. Error bars = SD.

Discussion

After initially being recognized for their respective roles in voltage-dependent K^+ channels in cardiac myocytes, KCNQ1 and KCNE2 were found to form a constitutively active K^+ channel (1), subsequently identified in gastric parietal cells (3, 17). KCNQ1-KCNE2 recycles K^+ from the parietal cell to the stomach lumen, facilitating the 1:1 exchange of H^+ ions for K^+ ions required by the H^+/K^+-ATPase for gastric acid secretion (3, 17, 18). Thus, genetic disruption of either *Kcnq1* or *Kcne2* in mice causes achlorhydria and gastric hyperplasia owing to an inability to secrete gastric acid (2, 4). Following up on our recent discovery that the KCNQ1-KCNE2 K^+ channel is important for thyroid hormone biosynthesis (5), we have now utilized PET to uncover the mechanistic basis for this requirement: without functional KCNQ1-KCNE2, I^- uptake into the thyroid is impaired, with no direct effect on I^- organification (Fig. 5).

The requirement for KCNQ1-KCNE2 for thyroidal I^- uptake may indicate that KCNQ1-KCNE2 is necessary for adequate function of NIS, the primary thyrocyte I^- uptake conduit. This functional requirement almost certainly does not involve a need for KCNQ1-KCNE2 to supply the thyrocyte basolateral Na^+/K^+ ATPase with K^+ so that it can maintain a Na^+ gradient for NIS, because KCNQ1 inhibition did not affect function of another Na^+-driven transporter, SMCT (Fig. 4*B*).

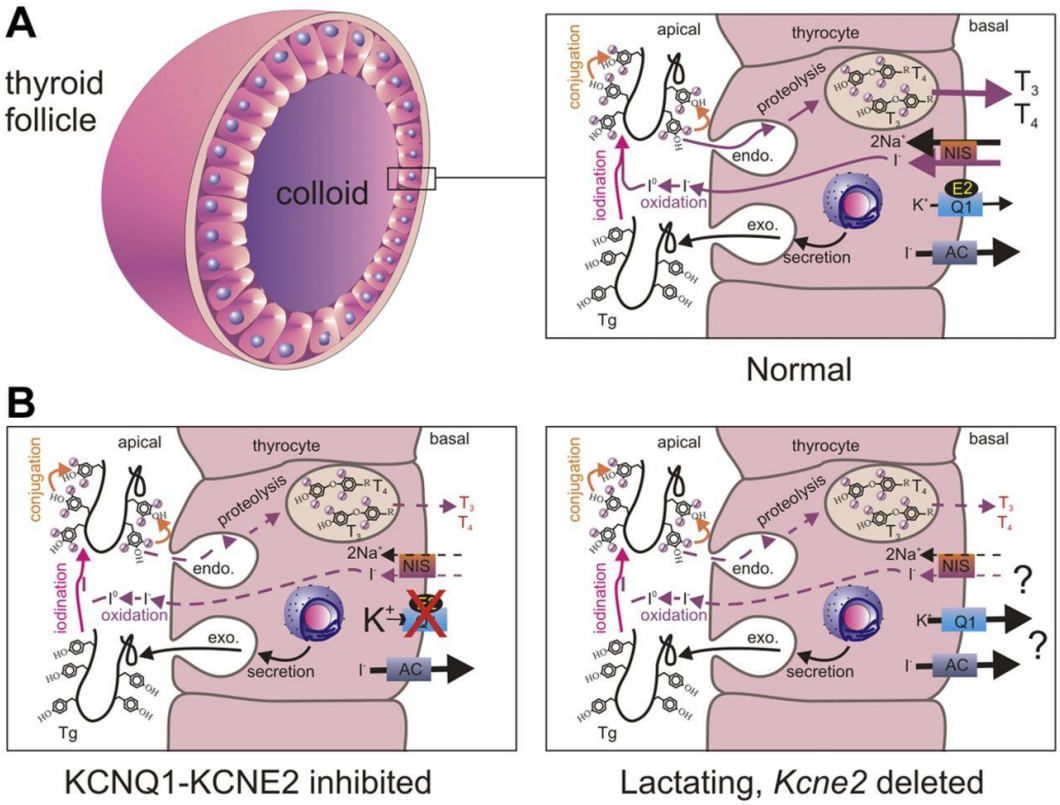

***Figure 5*. Summary of effects of KCNQ1-KCNE2 disruption on thyrocyte function.** *A*) In the normal thyroid, basolateral uptake through NIS supplies I^- for apical organification (iodination of Tg) and thyroid hormone biosynthesis. KCNQ1-KCNE2 is expressed on the basolateral surface. *B*) Left panel: when KCNQ1-KCNE2 is pharmacologically inhibited, organification is not directly impaired, but I^- uptake is reduced, reducing thyroid hormone biosynthesis, while SMCT function is maintained. Right panel: *Kcne2* deletion also reduces I^- uptake without affecting organification. Impaired NIS function is the prime candidate, but it is possible that *Kcne2* deletion also increases I^- leak through anion channels, as suggested by an increased rate of I^- efflux following NIS inhibition by ClO_4^- *in vivo*.

One possible mechanism is that KCNQ1-KCNE2 is required to regulate thyrocyte membrane potential *in vivo*, and that with *Kcne2* or *Kcnq1* deleted, or the channel pharmacologically inhibited, this function is perturbed. NIS-mediated I^- uptake is electrogenic, with two Na^+ entering for every I^-, therefore, its activity would depolarize the cell in the absence of other regulatory ion fluxes. Given that KCNQ1-

KCNE2 is constitutively active, it has the capacity to permit K^+ efflux to help maintain a negative membrane potential. If this channel is pharmacologically blocked (Fig. 5*B*), or if the *Kcnq1* gene itself is deleted, the thyrocyte could become depolarized, and NIS function could therefore be impaired due to a decrease in the membrane potential, one of the two components of the electrochemical driving force of NIS.

Deletion of *Kcne2* may have slightly different effects, albeit still resulting in impaired thyroid hormone biosynthesis. We recently found that KCNE2 is expressed in the choroid plexus epithelium, where it forms K^+ channels with KCNQ1 and with Kv1.3 (KCNA3) (19). When *Kcne2* is deleted, choroid plexus epithelial outward K^+ currents actually increase, because KCNE2 normally partially suppresses Kv1.3 and KCNQ1outward currents (although endowing the latter with the ability to remain open at very negative potentials). This hyperpolarizes the choroid plexus cells, and may contribute to the higher cerebrospinal fluid [Cl^-] we observe in *Kcne2*$^{-/-}$ mice (19). It is possible that this effect also occurs in the thyroid of *Kcne2*$^{-/-}$ mice, possibly favoring I^- loss through nonspecific anion channels. Significantly, the loss of I^- from the thyrocyte which is clearly observed following competitive inhibition of NIS with ClO_4^- occurs *via* a NIS-independent mechanism, probably through one or more types of anion channel and down the I^- electrochemical gradient. *Kcne2* deletion doubled the rate of this I^- efflux (Fig. 2*C*), and we speculate that thyrocyte I^- 'leak' arising from hyperpolarization in *Kcne2*$^{-/-}$ mice could contribute to their inability to accumulate I^- as efficiently as their wild-type counterparts. Future studies will be aimed at further

dissecting the molecular basis of the requirement for KCNQ1-KCNE2 in NIS-mediated I^- uptake.

In summary, we demonstrate here that state-of-the-art imaging techniques can be combined with genetically tractable small animal models, pharmacological tools, and in this case a standard clinical assay for organification deficiency (the ClO_4^- discharge test) to discern physiologically and pathophysiologically important mechanisms *in vivo*. The discovery of this link between a K^+ channel and a plasma membrane transporter suggests that similar such links may yet be found in a wide variety of cell types. The findings also present proof-of-principle that pharmacological inhibition of KCNQ1-KCNE2 can be used to alter thyroid function – opening up potential novel therapeutic avenues for thyroid disorders.

References

1. Tinel, N., Diochot, S., Borsotto, M., Lazdunski, M., and Barhanin, J. (2000) KCNE2 confers background current characteristics to the cardiac KCNQ1 potassium channel. *The EMBO journal* **19**, 6326-6330
2. Lee, M. P., Ravenel, J. D., Hu, R. J., Lustig, L. R., Tomaselli, G., Berger, R. D., Brandenburg, S. A., Litzi, T. J., Bunton, T. E., Limb, C., Francis, H., Gorelikow, M., Gu, H., Washington, K., Argani, P., Goldenring, J. R., Coffey, R. J., and Feinberg, A. P. (2000) Targeted disruption of the Kvlqt1 gene causes deafness and gastric hyperplasia in mice. *The Journal of clinical investigation* **106**, 1447-1455
3. Grahammer, F., Herling, A. W., Lang, H. J., Schmitt-Graff, A., Wittekindt, O. H., Nitschke, R., Bleich, M., Barhanin, J., and Warth, R. (2001) The cardiac K^+ channel KCNQ1 is essential for gastric acid secretion. *Gastroenterology* **120**, 1363-1371
4. Roepke, T. K., Anantharam, A., Kirchhoff, P., Busque, S. M., Young, J. B., Geibel, J. P., Lerner, D. J., and Abbott, G. W. (2006) The KCNE2 potassium channel ancillary subunit is essential for gastric acid secretion. *The Journal of biological chemistry* **281**, 23740-23747
5. Roepke, T. K., King, E. C., Reyna-Neyra, A., Paroder, M., Purtell, K., Koba, W., Fine, E., Lerner, D. J., Carrasco, N., and Abbott, G. W. (2009) Kcne2 deletion uncovers its crucial role in thyroid hormone biosynthesis. *Nature medicine* **15**, 1186-1194

6. Frohlich, H., Boini, K. M., Seebohm, G., Strutz-Seebohm, N., Ureche, O. N., Foller, M., Eichenmuller, M., Shumilina, E., Pathare, G., Singh, A. K., Seidler, U., Pfeifer, K. E., and Lang, F. (2011) Hypothyroidism of gene-targeted mice lacking Kcnq1. *Pflugers Archiv : European journal of physiology* **461**, 45-52

7. Wang, Q., Curran, M. E., Splawski, I., Burn, T. C., Millholland, J. M., VanRaay, T. J., Shen, J., Timothy, K. W., Vincent, G. M., de Jager, T., Schwartz, P. J., Toubin, J. A., Moss, A. J., Atkinson, D. L., Landes, G. M., Connors, T. D., and Keating, M. T. (1996) Positional cloning of a novel potassium channel gene: KVLQT1 mutations cause cardiac arrhythmias. *Nature genetics* **12**, 17-23

8. Abbott, G. W., Sesti, F., Splawski, I., Buck, M. E., Lehmann, M. H., Timothy, K. W., Keating, M. T., and Goldstein, S. A. (1999) MiRP1 forms IKr potassium channels with HERG and is associated with cardiac arrhythmia. *Cell* **97**, 175-187

9. Kissane, J. M., and Robins, E. (1958) The fluorometric measurement of deoxyribonucleic acid in animal tissues with special reference to the central nervous system. *The Journal of biological chemistry* **233**, 184-188

10. Dai, G., Levy, O., and Carrasco, N. (1996) Cloning and characterization of the thyroid iodide transporter. *Nature* **379**, 458-460

11. Ris-Stalpers, C. (2006) Physiology and pathophysiology of the DUOXes. *Antioxidants & redox signaling* **8**, 1563-1572

12. Dadachova, E., and Carrasco, N. (2004) The Na/I symporter (NIS): imaging and therapeutic applications. *Seminars in nuclear medicine* **34**, 23-31

13. Dohan, O., Portulano, C., Basquin, C., Reyna-Neyra, A., Amzel, L. M., and Carrasco, N. (2007) The Na+/I symporter (NIS) mediates electroneutral active transport of the environmental pollutant perchlorate. *Proceedings of the National Academy of Sciences of the United States of America* **104**, 20250-20255

14. Takeuchi, K., Suzuki, H., Horiuchi, Y., and Mashimo, K. (1970) Significance of iodide-perchlorate discharge test for detection of iodine organification defect of the thyroid. *The Journal of clinical endocrinology and metabolism* **31**, 144-146

15. Engler, H., Taurog, A., and Dorris, M. L. (1982) Preferential inhibition of thyroxine and 3,5,3'-triiodothyronine formation by propylthiouracil and methylmercaptoimidazole in thyroid peroxidase-catalyzed iodination of thyroglobulin. *Endocrinology* **110**, 190-197

16. McDonald, D. O., and Pearce, S. H. (2009) Thyroid peroxidase forms thionamide-sensitive homodimers: relevance for immunomodulation of thyroid autoimmunity. *J Mol Med (Berl)* **87**, 971-980

17. Dedek, K., and Waldegger, S. (2001) Colocalization of KCNQ1/KCNE channel subunits in the mouse gastrointestinal tract. *Pflugers Archiv : European journal of physiology* **442**, 896-902

18. Geibel, J. P. (2005) Role of potassium in acid secretion. *World journal of gastroenterology : WJG* **11**, 5259-5265

19. Roepke, T. K., Kanda, V. A., Purtell, K., King, E. C., Lerner, D. J., and Abbott, G. W. (2011) KCNE2 forms potassium channels with KCNA3 and KCNQ1 in the choroid plexus epithelium. *FASEB J* **12**, 4264-4273

20. Peeters, R. P. (2009) Thyroid function and longevity: new insights into an old dilemma. *The Journal of clinical endocrinology and metabolism* **94**, 4658-4660

APPENDIX II

Cardiac arrhythmia and thyroid dysfunction: a novel genetic link

Kerry Purtell, Torsten K. Roepke, and Geoffrey W. Abbott

Adapted from: *Int J Biochem Cell Biol*. 2010 Nov;42(11):1767-70.

doi: 10.1016/j.biocel.2010.07.013

Summary

Inherited Long QT Syndrome (LQTS), a cardiac arrhythmia that predisposes to the often lethal ventricular fibrillation, is commonly linked to mutations in KCNQ1. The KCNQ1 voltage-gated K^+ channel α subunit passes ventricular myocyte K^+ current that helps bring a timely end to each heart-beat. KCNQ1, like many K^+ channel α subunits, is regulated by KCNE β subunits, inherited mutations in which also associate with LQTS. KCNQ1 and KCNE mutations are also associated with atrial fibrillation. It has long been known that thyroid status strongly influences cardiac function, and that thyroid dysfunction causes abnormal cardiac structure and rhythm. We recently discovered that KCNQ1 and KCNE2 form a thyroid-stimulating hormone-stimulated K^+ channel in the thyroid that is required for normal thyroid hormone biosynthesis. Here, we review this novel genetic link between cardiac and thyroid physiology and pathology, and its potential influence upon future therapeutic strategies in cardiac and thyroid disease.

1. Introduction

Excitable cells facilitate dynamic processes such as electrical signaling in the brain and rhythmic beating of the heart. Excitability, defined in this context as the ability to sustain action potentials, requires voltage-gated sodium (Na_V) channels for the depolarization phase (upstroke) and voltage-gated potassium (K_V) channels for the repolarization phase (downstroke) (Fig. 1A). The ventricles of the human heart provide most of the contractile force for pumping blood to the lungs and around the

rest of the body, and the integrity of the ventricular myocyte action potential is therefore crucial for life. Influx of Na^+ ions through $Na_V1.5$ (encoded by SCN5A) depolarizes human ventricular myocytes, and K^+ efflux through a variety of K^+ channel types, primarily K_V channels, facilitates myocyte repolarization. The most prominent repolarization phase, Phase 3, is coordinated primarily by two K_V α subunits: hERG and KCNQ1, which respectively generate the I_{Kr} and I_{Ks} repolarization currents (Fig. 1B). The completion of ventricular repolarization manifests on a surface electrocardiogram (ECG) as the end of the T wave (Fig. 1C). KCNQ1 and hERG, as with all other K_V α subunits, each contain six transmembrane helices within which is a voltage sensor that moves upon membrane depolarization – a conformational shift transmitted to the channel pore, or gate, which then opens to permit ion flux; four K_V α subunits are necessary and sufficient to form a functional (tetrameric) pore. However, *in vivo*, hERG and KCNQ1 each form complexes with KCNE β subunits, also referred to as MinK-related peptides (MiRPs). KCNE subunits are single-transmembrane-segment (TMS) proteins that do not pass current alone, but co-assemble with pore-forming K_V α subunits to regulate their trafficking, gating, conductance, regulation by other proteins, and pharmacology (Fig. 2). Importantly, both the KCNE β subunits and the K_V α subunits are promiscuous, helping to create K^+ current diversity but also hampering efforts to determine molecular correlates of native currents.

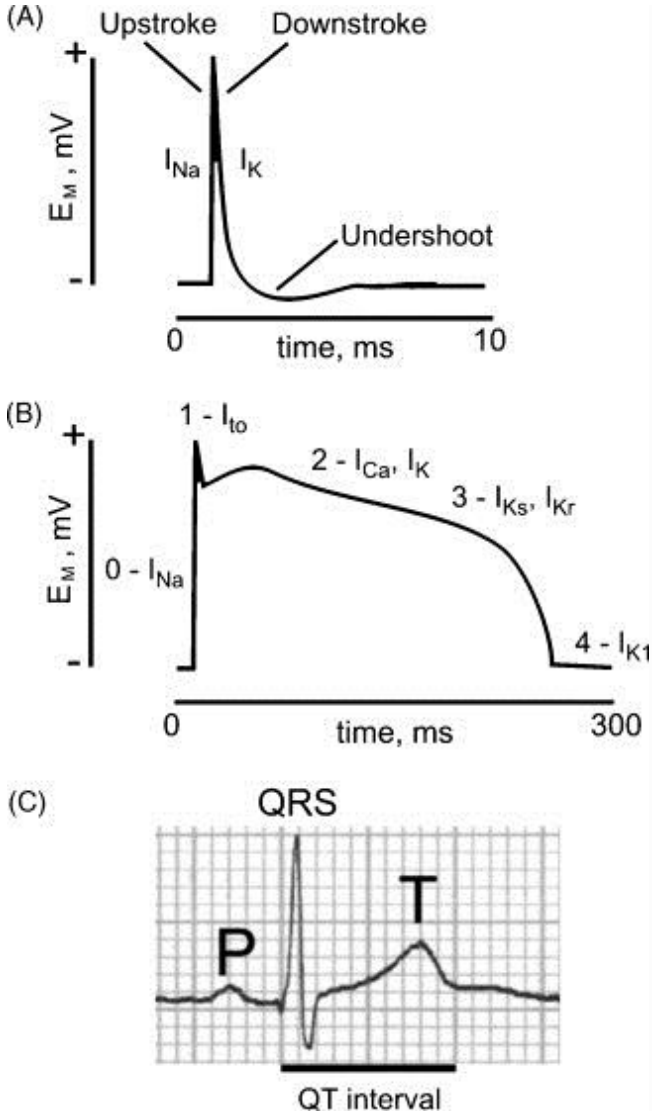

Figure 1. Action potentials and the surface electrocardiogram. (A) An idealized neuronal action potential. I_{Na}, sodium current; I_K, potassium current; E_M, membrane potential. (B) An idealized human ventricular myocyte action potential. Phases 0–4 are indicated, together with prominent currents during these phases: I_{Na}, sodium current; I_{to}, transient outward K_V current (generated by K_V 4.3); I_{Ca}, voltage-gated calcium current (generated by CACNA1C, also termed Ca_V 1.2); I_K, potassium current (generated by various K^+ channels); I_{Ks}, slowly activating K^+ current (generated by KCNQ1-KCNE1); I_{Kr}, rapidly activating K^+ current (generated by hERG-KCNE2); I_{K1}, inward rectifier K^+ current (generated by Kir2.x subfamily α subunits); E_M, membrane potential. (C) A surface electrocardiogram showing the P and T waves, the QRS complex, and the QT interval.

Thus, the KCNQ1-KCNE1 channel activates more slowly and at more positive membrane potentials than homomeric KCNQ1, and generates the I_{Ks} human ventricular repolarization current (with possible contributions from other KCNQ1-KCNE complexes). hERG, the α subunit that generates human ventricular I_{Kr}, may be regulated by KCNE1, KCNE2 and potentially other KCNEs *in vivo*; for review, see (McCrossan and Abbott, 2004).

KCNQ1 has a property unique among K_V α subunits: it can be converted to a constitutively open K^+ leak channel (i.e., one that does not require membrane depolarization to open) by co-assembly with the KCNE2 or KCNE3 ancillary subunits (Schroeder et al., 2000 and Tinel et al., 2000). While it is not yet known whether KCNQ1 forms leak channels in human heart with KCNE2 or KCNE3, the ability to open constitutively has been shown to facilitate functional roles for KCNQ1-KCNE complexes in non-excitable, polarized epithelia *in vivo*. In gastric parietal cells, KCNQ1-KCNE2 channels provide an apical K^+ recycling pathway required for gastric acidification by the apical gastric H^+/K^+ATPase (Lee et al., 2000, Heitzmann et al., 2004 and Roepke et al., 2006). In the colon, basolateral KCNQ1-KCNE3 channels help provide a driving force for cAMP-stimulated Cl^- secretion (Schroeder et al., 2000). Recently, we also discovered that KCNQ1 and KCNE2 form a constitutively active K^+ channel in thyrocytes, and that the KCNQ1-KCNE2 channel is required for normal thyroid hormone (TH) biosynthesis (Roepke et al., 2009). Because the heart is strongly influenced by the thyroid, the finding suggests that these two K^+ channel

subunits could influence cardiac function both directly, due to their roles in cardiac myocytes, and indirectly, by virtue of their role in thyroid physiology.

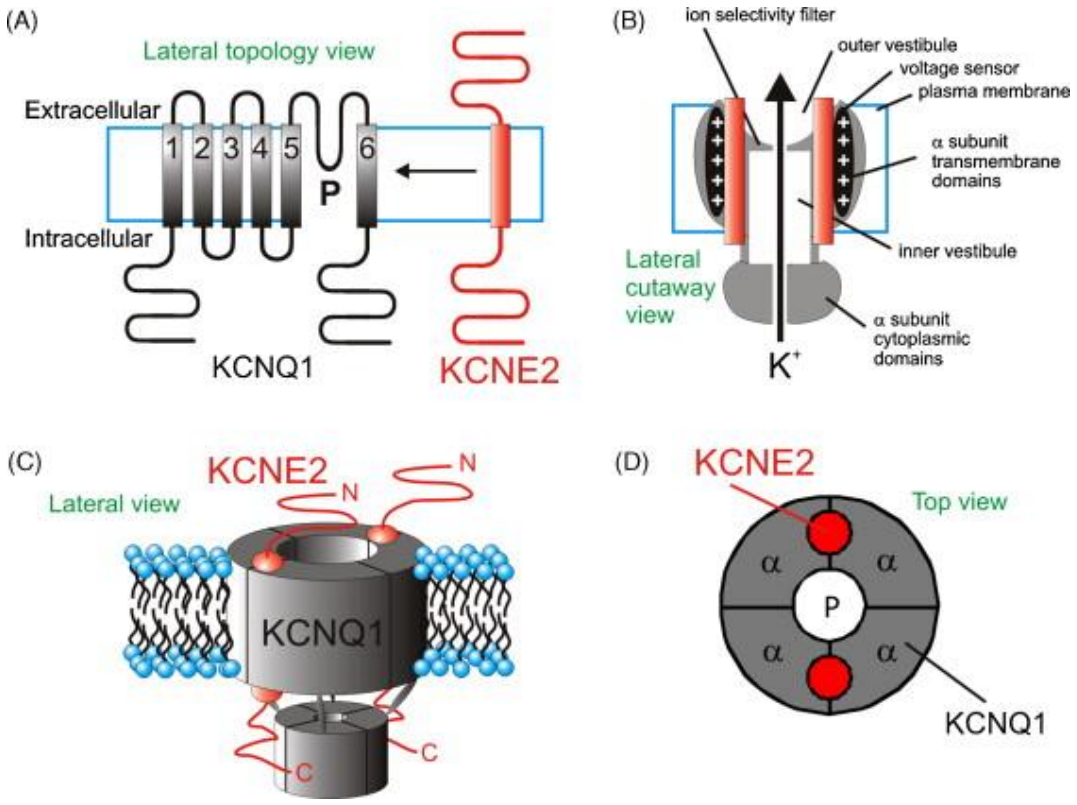

Figure 2. KCNE2 and KCNQ1. (A) Topology of KCNQ1 and KCNE2 with respect to the cell membrane. (B) Idealized cutaway lateral view of a KCNQ1-KCNE2 complex (KCNQ1, grey; KCNE2, red). (C) Cartoon lateral view of a KCNQ1-KCNE2 channel complex, stoichiometry as determined for KCNQ1-KCNE1 (Chen et al., 2003a). (D) Cartoon top view of a KCNQ1-KCNE2 complex suggesting a possible juxtaposition of the two subunit types.

2. Pathogenesis

Mutations in human KCNQ1 and KCNE2 are associated with cardiac arrhythmias, thought to be primarily due to disruption of their function in the heart (Wang et al., 1996 and Abbott et al., 1999). KCNQ1 mutations underlie LQTS Type 1 (LQT1), sub-classified as Romano Ward Syndrome (RWS; autosomal dominant) and Jervell Lange-Nielsen Syndrome (JLNS; typically autosomal recessive). Loss-of-function mutations in KCNQ1 reduce ventricular repolarization capacity, and therefore extend the QT interval on the surface electrocardiogram, hence LQTS. JLNS manifests as both LQTS and profound sensorineural deafness – because KCNQ1-KCNE1 channels are important not only for ventricular repolarization, but also for K^+ secretion into the endolymph of the inner ear. Accordingly, loss-of-function KCNE1 mutations, which underlie LQT5, also cause either RWS or JLNS; for review, see (Keating and Sanguinetti, 2001). Interestingly, gain-of-function mutations in KCNQ1 (and perhaps in some KCNE genes) appear to underlie some cases of lone atrial fibrillation (AF), probably because they shorten the atrial effective refractory period (Chen et al., 2003b and Yang et al., 2004).

We originally identified KCNE2 as a partner for hERG (KCNH2) and found that KCNE2 mutations associate with inherited and drug-induced LQTS, a cardiac arrhythmia that predisposes to the often lethal ventricular fibrillation. KCNE2-associated LQTS is classified LQT6. The presumed mechanism is disruption of ventricular myocyte hERG-KCNE2 channels (Abbott et al., 1999). Despite initial controversy surrounding these findings, KCNE2 has also since been found by others to

regulate I_{Kr} *in vivo* in canine ventricles (Jiang et al., 2004) and mouse sinoatrial node (Hesketh et al., 2005). We also found that 3-month-old *Kcne2*$^{-/-}$ mice (which are euthyroid at this age, when bred from *Kcne2*$^{+/-}$ dams) have impaired ventricular myocyte repolarization due to loss of KCNE2 from myocyte channel complexes with the $K_V4.2$ and $K_V1.5$ α subunits (Roepke et al., 2008). After these cardiac roles for KCNE2 were identified, we discovered that breeding of *Kcne2*$^{-/-}$ dams results in hypothyroidism in both the pregnant dams and their pups, due to a previously unreported role for the KCNQ1-KCNE2 K^+ channel in thyrocytes (Roepke et al., 2009). By 3 weeks of age, *Kcne2*$^{-/-}$ mice born to *Kcne2*$^{-/-}$ dams show marked cardiac abnormalities including cardiomegaly, hypertrophy and impaired contractility. These mice also exhibit alopecia, defective skeletal development, 50% embryonic lethality, and delayed growth resulting in dwarfism (Roepke et al., 2009); these are all symptoms observed in human congenital hypothyroidism (Lafranchi, 2010). While *Kcne2*$^{-/-}$ pups born to *Kcne2*$^{+/-}$ dams appear to develop normally, and by three months are euthyroid (indicating a strong influence of maternal genotype on phenotype), they exhibit latent hypothyroidism with cardiomegaly, alopecia, diminished T4 and elevated TSH levels by 1 year of age (Roepke et al., 2009) (Fig. 3A–D). As previously observed in hypothyroid rats (Hapon et al., 2003), *Kcne2*$^{-/-}$ dams have impaired milk ejection – alleviated by oxytocin injection – partially explaining the influence of maternal genotype in *Kcne2*$^{-/-}$ mouse phenotype severity (Roepke et al., 2009).

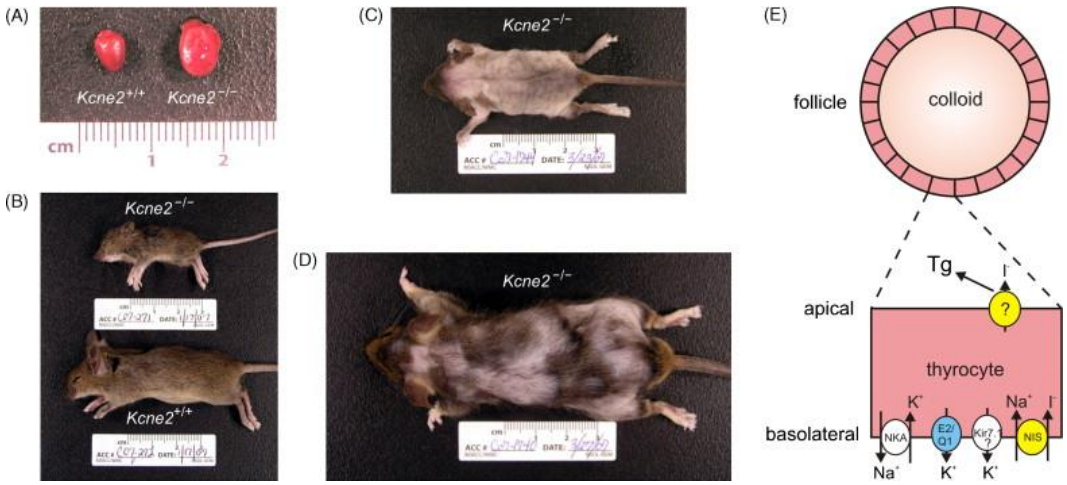

Figure 3. Manifestations of thyroid pathology in the *Kcne2*$^{-/-}$ mouse. *Kcne2*$^{-/-}$ mice have a complex pathophysiology. The primary hypothyroidism due to dysfunction of thyrocyte KCNQ1-KCNE2 causes, among other defects: (A) cardiomegaly; (B) retarded growth; and alopecia in (C) *Kcne2*$^{-/-}$ pups from *Kcne2*$^{-/-}$ dams, and (D) 1-year-old *Kcne2*$^{-/-}$ mice originally bred from *Kcne2*$^{+/-}$ dams. (E) The putative role for KCNQ1-KCNE2 (blue) in thyrocytes is to facilitate K^+ efflux basolaterally. A subset of other channels and transporters are shown for context: Kir7.1, inward rectifier K^+ channel; NKA, Na^+/K^+/ATPase; NIS, Na^+/I^- symporter (yellow). At the apical membrane, I^- passes from the thyrocyte to the colloid for organification, through pendrin or another, unspecified protein (yellow), resulting in formation of thyroglobulin (Tg).

The thyroid hormones (THs), thyroxine (T4) and triiodothyronine (T3), are crucial for proper growth and development, and play an integral role throughout adulthood in maintenance of cognitive function, metabolism, and cardiac function. As iodide (I^-) is an essential component of TH, the scarcity of dietary I^- is a universal health concern monitored by the WHO, UNICEF, and the International Council for Control of Iodine Deficiency (ICCID) (Zimmermann et al., 2008). I^- deficiency manifests most severely during pregnancy, when the demand for TH is increased as

the early fetus is unable to synthesize TH on its own and must rely on a supply of maternal T4 for proper development. Inability to supply the growing fetus with T4 can result in fetal mortality, defective neuronal myelination and synapse formation, retarded growth and a form of mental retardation known as cretinism (Zimmermann et al., 2008). Though severe, defects resulting from hypothyroidism are highly preventable with proper intervention. However, controversies surround research aimed at determining the population at risk, effective treatment dosage, and the crucial point in gestation at which to implement treatment, necessitating further study to elucidate the etiology of hypothyroidism, and safe, effective means of its prevention (Loh et al., 2009). The Na^+/I^- symporter (NIS) is responsible for the accumulation of I^- in thyrocytes in the first step of TH biosynthesis. I^- is then transported apically into the colloid in the thyroid lumen where it is organified into thyroglobin (Tg) and subsequently incorporated into T3 and T4. NIS uses the movement of Na+ down its concentration gradient to accumulate I^- into thyrocytes. While it has previously been established that the Na^+/K^+ATPase, which co-localizes with NIS at the basolateral membrane, generates this gradient by pumping Na^+ out in exchange for moving K^+ in (Dohan et al., 2003), the pathway responsible for moving K^+ back out of the cell has remained enigmatic. Our recent findings show that KCNE2, probably primarily in complexes with KCNQ1, is required for normal I^- accumulation in the thyroid, suggesting that the KCNQ1-KCNE2 channel may form the aforementioned thyrocyte K^+ efflux pathway (Fig. 3 E).

3. Therapy

Despite there being a long-recognized link between thyroid dysfunction and cardiovascular risk, and an awareness that THs regulate expression of K^+ channels in the heart (Klein and Ojamaa, 2001 and Tribulova et al., 2010), our recent discovery of a crucial role for KCNE2 and KCNQ1 in TH biosynthesis presents a novel and unexpected genetic link between thyroid dysfunction and cardiac arrhythmias. Mutations in KCNE2 and/or KCNQ1 have previously been associated with LQTS, AF, and even early-onset myocardial infarction (Wang et al., 1996, Abbott et al., 1999, Chen et al., 2003b, Yang et al., 2004 and Kathiresan et al., 2009), each of which is also predisposed to by thyroid dysfunction in the general population (Forfar et al., 1979, Hak et al., 2000 and Bakiner et al., 2008), suggesting the intriguing possibility of an endocrine component to some KCNE2- and KCNQ1-associated human cardiac disease. Whether or not the discovery of KCNQ1-KCNE2 in the thyroid and its role in TH biosynthesis leads to use of KCNQ1-KCNE2 modulators to treat thyroid dysfunction remains to be seen, but these findings should at least be a consideration in future studies of thyroid-related cardiac disease, its molecular etiology and therapy.

It is noteworthy that subclinical hypothyroidism is associated with prolongation of the QTc (QT interval corrected for heart rate) (Tribulova et al., 2010), especially given that loss-of-function mutations in KCNQ1 are the joint most commonly identified cause of inherited LQTS (Keating and Sanguinetti, 2001), and would also be predicted to impair TH biosynthesis by loss-of-function of thyroid

KCNQ1-KCNE2 channels, as is achieved by genetic disruption of *Kcne2* (Roepke et al., 2009). Conversely, ~10% of AF patients show biochemical evidence of hyperthyroidism, and in two-thirds of patients diagnosed with both idiopathic AF and hyperthyroidism, successful therapeutic conversion to a euthyroid state is accompanied by a return to normal sinus rhythm (Klein and Ojamaa, 2001). One genetic cause of AF is gain-of-function of KCNQ1, which shortens the atrial effective refractory period, predisposing to AF (Chen et al., 2003b). This raises the interesting question of whether increased KCNQ1 function in the thyroid might actually increase TH production, something which can initially be tested in mouse models, using existing KCNQ1 openers such as the benzodiazepine RL-3.

In summary, the KCNQ1-KCNE2 K^+ channel appears important for normal TH biosynthesis in mice, by an as yet incompletely defined mechanism. KCNQ1 and KCNE2 are also expressed in human thyroid but we do not yet know their function there, or the consequences of their disruption. Disruption of thyrocyte KCNQ1-KCNE2 in mice is most deleterious to health in pregnant and lactating dams and their offspring, and in older mice. A possible role for thyroid dysfunction in KCNQ1- and KCNE2-associated cardiac arrhythmias and myocardial infarction warrants consideration in future anti-arrhythmic regimes involving pharmacologic modulation of KCNQ1.

References

Abbott GW, Sesti F, Splawski I, Buck ME, Lehmann MH, Timothy KW, et al. MiRP1 forms I_{Kr} potassium channels with HERG and is associated with cardiac arrhythmia. *Cell* 1999;97(2):175–87.

Bakiner O, Ertorer ME, Haydardedeoglu FE, Bozkirli E, Tutuncu NB, Demirag NG. Subclinical hypothyroidism is characterized by increased QT interval dispersion among women. *Med Princ Pract* 2008;17(5):390–4.

Chen H, Kim LA, Rajan S, Xu S, Goldstein SA. Charybdotoxin binding in the I(Ks) pore demonstrates two MinK subunits in each channel complex. *Neuron* 2003a;40(1):15–23. Chen YH, Xu SJ, Bendahhou S, Wang XL, Wang Y, Xu WY, et al. KCNQ1 gainof-function mutation in familial atrial fibrillation. *Science* 2003b;299(5604): 251–4.

Dohan O, De la Vieja A, Paroder V, Riedel C, Artani M, Reed M, et al. The sodium/iodide Symporter (NIS): characterization, regulation, and medical significance. *Endocr Rev* 2003;24(1):48–77.

Forfar JC,Miller HC, Toft AD. Occult thyrotoxicosis: a correctable cause of "idiopathic" atrial fibrillation. *Am J Cardiol* 1979;44(1):9–12.

Hak AE, Pols HA, Visser TJ, Drexhage HA, Hofman A, Witteman JC. Subclinical hypothyroidism is an independent risk factor for atherosclerosis and myocardial infarction in elderly women: the Rotterdam Study. *Ann Intern Med* 2000;132(4):270–8.

Hapon MB, Simoncini M, Via G, Jahn GA. Effect of hypothyroidism on hormone profiles in virgin, pregnant and lactating rats, and on lactation. *Reproduction* 2003;126(3):371–82.

Heitzmann D, Grahammer F, von Hahn T, Schmitt-Graff A, Romeo E, Nitschke R, et al. Heteromeric KCNE2/KCNQ1 potassium channels in the luminal membrane of gastric parietal cells. *J Physiol* 2004;561(Pt 2):547–57.

Hesketh JC, Qi X, Li D, Levesque P, Nattel S. Cardiac function of KCNE2 subunits revealed by targeted deletion in mice. Am Heart Assoc Sci Sessions 2005 [session number AOP.16.2a (presentation number 278)].

Jiang M, Zhang M, Tang DG, Clemo HF, Liu J, Holwitt D, et al. KCNE2 protein is expressed in ventricles of different species, and changes in its expression contribute to electrical remodeling in diseased hearts. *Circulation* 2004;109(14):1783–8.

Kathiresan S, Voight BF, Purcell S, Musunuru K, Ardissino D, Mannucci PM, et al. Genome-wide association of early-onset myocardial infarction with single nucleotide polymorphisms and copy number variants. *Nat Genet* 2009;41(3):334–41.

Keating MT, Sanguinetti MC. Molecular and cellular mechanisms of cardiac arrhythmias. *Cell* 2001;104(4):569–80.

Klein I, Ojamaa K. Thyroid hormone and the cardiovascular system. *N Engl J Med* 2001;344(7):501–9.

Lafranchi SF. Newborn screening strategies for congenital hypothyroidism: an update. *J Inherit Metab* 2010 [Dis. epub ahead of print (March 2nd)].

Lee MP, Ravenel JD, Hu RJ, Lustig LR, Tomaselli G, Berger RD, et al. Targeted disruption of the Kvlqt1 gene causes deafness and gastric hyperplasia in mice. *J Clin Invest* 2000;106(12):1447–55.

Loh JA, Wartofsky L, Jonklaas J, Burman KD. The magnitude of increased levothyroxine requirements in hypothyroid pregnant women depends upon the etiology of the hypothyroidism. *Thyroid* 2009;19(3):269–75.

McCrossan ZA, Abbott GW. The MinK-related peptides. *Neuropharmacology* 2004;47(6):787–821.

Roepke TK, Anantharam A, Kirchhoff P, Busque SM, Young JB, Geibel JP, et al. The KCNE2 potassium channel ancillary subunit is essential for gastric acid secretion. *J Biol Chem* 2006;281(33):23740–7.

Roepke TK, King EC, Reyna-Neyra A, Paroder M, Purtell K, Koba W, et al. Kcne2 deletion uncovers its crucial role in thyroid hormone biosynthesis. *Nat Med* 2009;15(10):1186–94.

Roepke TK, Kontogeorgis A, Ovanez C, Xu X, Young JB, Purtell K, et al. Targeted deletion of kcne2 impairs ventricular repolarization via disruption of $I_{(K,slow1)}$ and $I_{(to,f)}$. *FASEB J* 2008;22(10):3648–60.

Schroeder BC, Waldegger S, Fehr S, Bleich M, Warth R, Greger R, et al. A constitutively open potassium channel formed by KCNQ1 and KCNE3. *Nature* 2000;403(6766):196–9.

Tinel N, Diochot S, Borsotto M, Lazdunski M, Barhanin J. KCNE2 confers background current characteristics to the cardiac KCNQ1 potassium channel. *EMBO J* 2000;19(23):6326–30.

Tribulova N, Knezl V, Shainberg A, Seki S, Soukup T. Thyroid hormones and cardiac arrhythmias. *Vasc Pharmacol* 2010;52(3–4):102–12.

Wang Q, Curran ME, Splawski I, Burn TC, Millholland JM, VanRaay TJ, et al. Positional cloning of a novel potassium channel gene: KVLQT1 mutations cause cardiac arrhythmias. *Nat Genet* 1996;12(1):17–23.

Yang Y, Xia M, Jin Q, Bendahhou S, Shi J, Chen Y, et al. Identification of a KCNE2 gain-of-function mutation in patients with familial atrial fibrillation. *Am J Hum Genet* 2004;75(5):899–905.

Zimmermann MB, Jooste PL, Pandav CS. Iodine-deficiency disorders. *Lancet* 2008;372(9645):1251–62.

APPENDIX III

Genetic dissection reveals unexpected influence of β subunits on KCNQ1 K^+ channel polarized trafficking *in vivo*

Torsten K. Roepke, Elizabeth C. King, Kerry Purtell, Vikram A. Kanda, Daniel J. Lerner and Geoffrey W. Abbott

Adapted from: *FASEB J*. 2011 Feb;25(2):727-36.

doi: 10.1096/fj.10-173682

Abstract

Targeted deletion of the *Kcne2* potassium channel β subunit gene ablates gastric acid secretion and predisposes to gastric neoplasia in mice. Here, we discovered that *Kcne2* deletion basolaterally reroutes the Kcnq1 α subunit *in vivo* in parietal cells (PCs), in which the normally apical location of the Kcnq1-Kcne2 channel facilitates its essential role in gastric acid secretion. Quantitative RT-PCR and Western blotting revealed that *Kcne2* deletion remodeled fundic *Kcne3* (2.9±0.8-fold mRNA increase, *n*=10; 5.3±0.4-fold protein increase, *n*=7) but not *Kcne1*, *4*, or *5*, and resulted in basolateral Kcnq1-Kcne3 complex formation in *Kcne2*$^{-/-}$ PCs. Concomitant targeted deletion of *Kcne3* (creating *Kcne2*$^{-/-}$ *Kcne3*$^{-/-}$ mice) restored PC apical Kcnq1 localization without *Kcne1*, *4*, or *5* remodeling (assessed by quantitative RT-PCR; *n*=5-10), indicating Kcne3 actively, basolaterally rerouted Kcnq1 in *Kcne2*$^{-/-}$ PCs. Despite this, *Kcne3* deletion exacerbated gastric hyperplasia in *Kcne2*$^{-/-}$ mice, and both hypochlorhydria and hyperplasia in *Kcne2*$^{+/-}$ mice, suggesting that Kcne3 up-regulation was beneficial in *Kcne2*-depleted PCs. The findings reveal, *in vivo*, Kcne-dependent α subunit polarized trafficking and the existence and consequences of potassium channel β subunit remodeling.

Introduction

Parietal cells (PCs) achieve gastric acidification by virtue of an apical H^+/K^+ATPase (HKA) that pumps protons into the stomach lumen in exchange for K^+ ions. To maintain this activity, K^+ ions that enter the PC through the HKA must travel back into the stomach lumen across the apical membrane. This K^+ ion efflux occurs primarily through the heteromeric KCNQ1-KCNE2 K^+ channel (1, 2), with other K^+ channels also possibly contributing (3, 4). KCNQ1 is a six-transmembrane segment (TMS) α subunit from the S4 superfamily that forms functional, voltage-gated, homotetrameric K^+-selective channels in heterologous expression studies (5, 6). KCNE2, originally termed MinK-related peptide 1 (MiRP1), is a 1-TMS ancillary subunit from the KCNE gene family (7) (Fig. 1 A). All five known *KCNE* gene products have been shown to regulate KCNQ1 function in heterologous expression studies (8). Two of these - KCNE2 and KCNE3, originally named MiRP2 (7) - endow KCNQ1 with constitutive activation, probably by favoring the activated conformation of the KCNQ1 voltage sensor (9-11). While KCNE2 and KCNQ1 co-localize in the PC apical membrane (Fig. 1 B), KCNQ1-KCNE3 channels target to the basolateral membrane of colonic epithelial cells, where they regulate cAMP-stimulated chloride secretion (10, 13, 14).

Kcnq1$^{-/-}$ mice and *Kcne2*$^{-/-}$ mice show similar gastric phenotypes, characterized by achlorhydria, hypergastrinemia and gastric glandular hyperplasia (1, 2, 12). PCs from either null show ~10-fold reduced capacity to recover from proton

loading, suggesting a primary defect in gastric acid secretion. The achlorhydria we previously observed in *Kcne2*$^{-/-}$ mice was striking given that KCNQ1, the pore-forming subunit of the complex, was still present, and in fact was strongly expressed in double the number of cells per gastric gland in *Kcne2*$^{-/-}$ mice compared to *Kcne2*$^{+/+}$ mice (2). PCs are non-excitable and their membrane potential reportedly varies from -20 to -40 mV, with stimulation by secretagogues such as gastrin, histamine or carbachol causing a shift to the hyperpolarized end of this spectrum (15). Current-voltage relationships measured using patch clamp of KCNQ1 alone or with KCNE2 in mammalian cell lines indicate that KCNE2 reduces the voltage dependence of KCNQ1 activation (11); however, in the crucial -20 to -40 mV range, homomeric KCNQ1 channels appear to actually pass more current (in e.g. 3-second pulses) at neutral pH than KCNE2-KCNQ1 complexes. While KCNQ1 channels are partially inhibited at low extracellular pH, KCNE2-KCNQ1 channel currents are increased, but the former still pass current even at pH 3, and low pH reduces homomeric KCNQ1 inactivation (16). The polarity of KCNQ1 trafficking would be expected to be fundamental to its role in PCs, and disruption of this trafficking an interesting candidate mechanism for the profound gastric effects of *Kcne2* deletion. However, previous studies failed to find any effects of KCNE subunits on KCNQ1 localization *in vitro* in Madin-Darby Canine Kidney (MDCK) cells (in which KCNQ1 remained basolateral regardless of co-expression with each of KCNE1-5) or *in vivo* in the colonic epithelium (in which KCNQ1 was basolateral in both wild-type and *Kcne3*$^{-/-}$ mice) (14, 17). Further, we recently discovered that KCNQ1-KCNE2 plays a crucial role in thyroid hormone

biosynthesis, and that this channel appears to be basolaterally located in thyrocytes (18), contrasting with its apical localization in PCs. These apparent paradoxes, and the relative lack of understanding of the mechanisms underlying polarized trafficking of ion channels in general, prompted us to determine the effects of *Kcne* gene deletion on KCNQ1 trafficking in mouse PCs *in vivo*.

Materials and Methods

Generation of gene-targeted mice

All mice used were housed and utilized according to the NIH Guide for the Care and Use of Laboratory Animals and Weill Medical College of Cornell University animal care and use policies. *Kcne2*$^{-/-}$ mice were generated as described previously from *Kcne2*$^{+/-}$ × *Kcne2*$^{+/-}$ crosses (2). *Kcne3* was disrupted through homologous recombination, using a targeting vector to replace the entire coding region, contained within the fourth exon, of the *Kcne3* gene. Two homologous arms, a 3.9-kb sequence homologous to the 5′ region upstream from exon 4 and a 3.0-kb sequence homologous to the 3′ downstream region, were subcloned into a pVBTk-loxP-knockout backbone vector. The vector contained a neomycin resistance (Neo_r) cassette flanked by LoxP sites, allowing for the removal of the cassette on expression of Cre-recombinase, and a TK− selection marker (see Fig. 4 A). The targeting vector was linearized at a unique I-Ceu1 restriction enzyme site outside of the homologous region and electroporated into Albino C57BL/6 (C2J) ES cells. Clones were positively selected for Neo_r, and

integration of the null vector was confirmed through Southern blot analysis with a 5′ probe directed at a 126-bp sequence located outside the recombined region. The probe was amplified by PCR using the following primers: forward 5′-GCAGAAGGTAGGCACTTGGG-3′ and reverse 5′-ACTGGGGGAGACAATAGGCG-3′. Correctly targeted ES cells were injected into C57BL/6 blastocysts and implanted into female mice, which were bred with C57BL/6 males to generate chimeric progeny of a 50:50 C57BL/6:Albino B6 (C2J) genetic background. Chimeras were interbred to produce *Kcne3*$^{+/-}$ mice. The *Kcne3*$^{-/-}$ mice used in this study were bred from *Kcne3*$^{+/-}$ × *Kcne3*$^{+/-}$ crosses.

To generate litters of *Kcne2*$^{+/-}$*Kcne3*$^{+/-}$ mice, male *Kcne2*$^{-/-}$ mice were bred with female *Kcne3*$^{-/-}$ mice. All double-heterozygous mice appeared superficially normal and were interbred to yield the *Kcne2*$^{-/-}$*Kcne3*$^{-/-}$ and *Kcne2*$^{+/-}$*Kcne3*$^{-/-}$ mice used in experiments. Genotyping for *Kcne2* was performed by PCR using the following oligonucleotide primers: 5′-CTGGAGGTAGCCAAATGGAGGAAG-3′, 5′-TCCTGCCAATC TTCCACGATGTAC-3′, and 5′-CGCTCCCGATTCGCAGCGCATC-3′, which generated a wild-type band of 382 bp and a knockout band of 680 bp. Genotyping for *Kcne3* was performed by PCR using the following oligonucleotide primers: 5′-CTATTCTACACGCACTGTGGGATG-3′, 5′-CGTTGGAAGTCT CCATAGCAACAG-3′, and 5′-CGCTCCCGATTCGCAGCGCATC-3′, which generated a wild-type band of 280 bp and a knockout band of 1000 bp.

Quantitative RT-PCR (qRT-PCR)

Tissue extraction: Mice were euthanized by CO_2 asphyxiation. Stomachs were excised and washed in PBS, and the fundus was removed. Tissue was flash-frozen in liquid nitrogen and stored at −80°C until use. In preparation for RNA extraction, frozen tissue sections were submerged overnight or for 8 h in RNAlater Ice (Ambion, Austin, TX, USA) at −20°C.

RNA extraction: RNA was extracted from 30 mg of tissue with RNeasy Mini Kit (Qiagen, Valencia, CA, USA) according to the manufacturer's protocol. Tissue homogenization was achieved using a pestle grinder system (Fisher Scientific, Hampton, NH, USA). RNA yield and purity (A260/A280) were assessed by NanoDrop 2000 spectrophotometer (ThermoScientific, Waltham, MA, USA). RNA samples with A260/A280 absorbance ratios between 1.80 and 2.10 were considered acceptable for cDNA synthesis.

cDNA synthesis: cDNA was synthesized from 1 μg of RNA with Quantitect Reverse Transcriptase (Qiagen) according to the manufacturer's protocol. To remove genomic DNA, template RNA was mixed with gDNA Wipeout Buffer (Qiagen) and incubated at 42°C for 2 min. Quantitect Reverse Transciptase containing an RNase inhibitor and Quantiscript RT Buffer containing Mg2+ and dNTPs were then added to the genomic DNA elimination reaction and incubated at 42°C for 15 min. The reverse transcription

reaction was inactivated with a 3-min incubation at 95°C. Synthesized cDNA was analyzed immediately thereafter by qPCR or stored at −20°C until use.

Targeting information: qRT-PCR was conducted adhering as closely as possible to MIQE guidelines (19). Primer pairs for target gene *Kcne1* [National Center for Biotechnology Information (NCBI) GeneID 16509] produced an amplicon of 108 bp; match position of the expected sequence was number 1 out of 123 Basic Local Alignment Search Tool (BLAST; U.S. National Institutes of Health, Bethesda, MD, USA) matches. Primer pairs for target gene *Kcne3* (NCBI GeneID 57442) produced an amplicon of 143 bp; match position of the expected sequence was number 1 out of 1001 BLAST matches. Primer pairs for target gene *Kcne4* (NCBI GeneID 57814) produced an amplicon of 126 bp. Primer pairs for target gene *Kcne5* (NCBI GeneID 66240) produced an amplicon of 113 bp; match position of the expected sequence was number 1 out of 428 BLAST matches. Primer pairs for reference gene glyceraldehyde 3-phosphate dehydrogenase (GAPDH; NCBI Gene ID 14433) produced an amplicon of 123 bp; match position of the expected sequence is number 1 out of 251 BLAST matches.

Primer information: Primer sequences for qPCR analysis were acquired from the Harvard Medical School PrimerBank (Boston, MA, USA; ref. 20) and were as follows: *Kcne1*, forward 5′-ATGAGCCTGCCCAATTCCAC-3′ and reverse 5′-GAGCTGAGACTTACGAGCCA-3′; *Kcne2*, forward 5′-

CACATTAGCCAATTTGACCCAGA-3′ and reverse 5′-GAACATGCCGATCATCACCAT-3′; *Kcne3*, forward 5′-CTTTGCTCGATGGAAGGGGAC-3′ and reverse 5′-GCTGTCGTTGAGAGGCGTC-3′; *Kcne4*, forward 5′-CTGAGGATGGAGCCTCTGAAC-3′ and reverse 5′-AGCAAATCGAAACGAGTCCTTC-3′; *Kcne5*, forward 5′-AGATCCGCTGTCCTCCTCATT-3′ and reverse 5′-GGGTTCTGACCTCTCATCATCTT-3′; and *GAPDH*, forward 5′-AGGTCGGTGTGAACGGATTTG-3′ and reverse 5′-TGTAGACCATGTAGTTGAGGTCA-3′. Primers (50-nm synthesis scale, desalted) were acquired from Invitrogen (Carlsbad, CA, USA).

Assay details: qPCR analysis was performed on the Roche Light Cycler 480 System using LightCycler 480 SYBR Green I Master Mix and LightCycler 480 96-well white plates (Roche Diagnostics, Indianapolis, IN, USA). Each reaction contained ~75 ng of cDNA, 1 µl of PCR-grade water, 2 µl of 10 µM forward primer, 2 µl of 10 µM reverse primer, and 10 µl 2X Master Mix, which was comprised of dNTP mix, $MgCl_2$, FastStart TaqDNA Polymerase, reaction buffer, and SYBR Green I dye.

Cycling conditions: Thermocycling parameters were as follows: for amplification, 1 cycle at 95°C (10 min); 45 cycles at 95°C (5 s), 68°C (5 s), and 72°C (25 s); for

melting curve, 95°C (1 s), 65°C (1 s), 95°C (continuous); for cooling, 1 cycle 45°C (15 s).

Data analysis: Advanced relative quantification was used to obtain normalized changes in expression levels of target genes (*Kcne1–5*) relative to controls (*GAPDH*) using LightCycler 480 1.5 software. Primer pairs were previously validated by PrimerBank with amplification plots, dissociation curves, and 2% agarose gel analysis. Primer pair amplification efficiency was also established with calibration curves within the laboratory on LightCycler 480 equipment, and deemed satisfactory for experimentation. The calibration curve for *GAPDH* yielded a slope of −3.334 and efficiency of 1.995. The calibration curve for *Kcne1* yielded a slope of −3.386 and efficiency of 1.974. The calibration curve for *Kcne3* yielded a slope of −3.362 and efficiency of 1.983. The calibration curve for *Kcne4* yielded a slope of −3.110 and efficiency of 2.097. The calibration curve for *Kcne5* yielded a slope of −3.315 and efficiency of 2.003. Each sample was run in triplicate as a quality control measure, and triplicates varying from one another by >1 cycle were discarded. Melting curves were assessed for each reaction to verify the amplification of a single product. Final analysis of statistical significance was calculated using 1-way analysis of variance (ANOVA) test (Origin).

Semiquantitative RT-PCR

The observation of *Kcne3* up-regulation in *Kcne2*$^{-/-}$ mouse fundus using qPCR was recapitulated using conventional semiquantitative RT-PCR on fundic cDNA, using different primer sequences to those used for qPCR, and an alternative reference gene: hypoxanthine-guanine phosphoribosyltransferase (HPRT). Briefly, RNA was extracted from 4 separate stomach fundi/genotype using an RNAeasy kit (Qiagen), then samples were diluted to give equal RNA concentrations, as assessed by spectrophotometry, before reverse-transcription to give cDNA as before (21). Primers used were as follows: *HPRT*, forward 5′-TGGAAAGAATGTCTTGATTGTTGA-3′ and reverse 5′-ACTTCGAGAGGTCCTTTTCACC-3′, which gives a 130-bp product; *Kcne3*, forward 5′-GGCTCTGAACACAACCCTTC-3′ and reverse 5′-TTTGTCCACTTTGCGTGAAC-3′, which gives a 205-bp product. Band densities of PCR products obtained with specific primers for HPRT transcript, run on a 1% agarose gel and stained with ethidium bromide, were measured using a Fluor-S MultiImager (Bio-Rad, Hercules, CA, USA) to confirm that the RNA-concentration-normalized samples each yielded similar amounts of this reference transcript. In parallel, cDNA samples from the same preps were amplified with Kcne3-specific primers, and optical density was measured. Results are expressed as mean optical density for each amplicon, with statistical analysis performed using 1-way ANOVA with statistical significance set at $P < 0.05$.

Immunostaining (IS) and immunofluorescence (IF)

KCNQ1 IS (Fig. 1 C–E) was performed as we previously described (2). IF detection of HKA β, the $Na^+K^+2Cl^-$ cotransporter (NKCC1), KCNQ1, and KCNE3 was performed using a Discovery XT processor (Ventana Medical Systems, Tucson, AZ, USA). The primary antibody concentrations used were: 0.5 mg/ml anti-HKA β (mouse monoclonal; Affinity Bioreagents, Golden, CO, USA), 0.5 mg/ml anti-NKCC1 (goat polyclonal, Santa Cruz Biotechnology, Santa Cruz, CA, USA), and 1 mg/ml anti-KCNQ1 (rabbit or goat polyclonal; Chemicon, Temecula, CA, USA); in-house anti-KCNE3 serum was used at a 1:500 dilution after column-enriching IgG. Preceding the primary antibody incubation, the tissue sections were blocked for 30 min in 10% normal goat serum, 2% BSA in PBS, followed by 8 min avidin/biotin block. The primary antibody incubation (3 h) was followed by 32 min incubation with biotinylated anti-mouse IgG (Vectastain ABC kit; Vector Laboratories, Burlingame, CA, USA) for HKA β, 60 min incubation with biotinylated anti-goat IgG (Vectastain ABC kit) for NKCC1 (and for KCNQ1 for KCNE3 colocalization analysis), and biotinylated anti-rabbit or antibody at 1:200 dilution (Vectastain ABC kit) for KCNQ1 (for HKA and NKCC1 colocalization analysis). The secondary detection was performed with Streptavidin-HRP D (Ventana Medical Systems), followed by incubation with Tyramide-Alexa Fluor 488 (Invitrogen) or Tyramide Alexa Fluor 568 (Invitrogen). Stained slides were viewed with a Zeiss Axiovert 200 widefield microscope (Carl Zeiss, Oberkochen, Germany), and pictures were acquired using MetaMorph 7.1 software (Molecular Devices, Sunnyvale, CA, USA).

Western blotting and coimmunoprecipitation (co-IP)

For Western blotting, gastric membrane fractions were prepared as we previously described (2). Protein concentration of the supernatant was measured according to the Bradford method. Total protein (40 μg/lane) was loaded into a precast Tris-glycine 4–20% gel (Bio-Rad) and separated by electrophoresis. Proteins were then transferred onto a PVDF membrane (Bio-Rad) and blocked with 5% milk and 0.05% Tween-20 in PBS at 4°C on a rocker either for 1–2 h or overnight. Primary antibody incubations (4 h, room temperature, in 1% milk and 0.05% Tween-20 in PBS) were 1:1000 anti-KCNQ1 (Chemicon); 1:500 anti-KCNE3 (in-house anti-KCNE3 N terminus or anti-KCNE3 C terminus from Alomone Labs, Jerusalem, Israel); 1 mg/ml anti-NKCC1 (Santa Cruz Biotechnology). Membranes were washed 4 times, 20 min each, with antibody incubation buffer; incubated with the appropriate secondary antibodies (Bio-Rad), diluted 1:10,000 in buffer A, for 2 h at room temperature; then washed 4 times, 20 min each, with buffer A and once for 5 min with PBS. Membranes were incubated for 1 min with the SuperSignal ECL reagent (Pierce Biotechnology, Rockford, IL, USA), then exposed on BioMax Light Film (Kodak, Rochester, NY, USA) and developed using an RP X-OMAT processor (Kodak). For co-IPs, membrane fractions in buffer A—150 mM NaCl, 50 mM Tris-HCL (pH 7.4), 20 mM NaF, 10 mM $NaVO_4$, 1 mM phenylmethylsulfonyl fluoride (Fisher Scientific), 1% Nonidet P-40 (Pierce), 1% CHAPS (Sigma, St. Louis, MO, USA), 1% Triton X-100 (Fisher Scientific), and 0.5% SDS (Sigma)—were precleared with Protein A Sepharose beads (Amersham Bioscience), incubated with antibodies raised against KCNQ1 or NKCC1, and

precipitated with Protein A Sepharose beads; then beads were washed with buffer A, and bound proteins were eluted with SDS-PAGE loading buffer for Western blotting as above.

Histology

For histology and stomach mass quantification, mice were killed using CO_2 asphyxiation (5–10/genotype). Stomachs and colons were removed postmortem, stomach mass was determined, and stomach and colon tissue was fixed in 10% neutral buffered formalin, processed by routine methods, and embedded in paraffin wax. Gastric mucosal and colonic epithelial sections were cut at 5-μm intervals, placed on positively charged Superfrost slides, stained with hematoxylin and eosin (H&E), and evaluated with an Olympus BX45 microscope (New York/New Jersey Scientific Inc., Middlebush, NJ, USA).

Whole-stomach pH measurements

Mice were killed by CO_2 asphyxiation. Stomachs were ligated *ex vivo* at the esophageal and duodenal junctures and excised. Stomachs were then incubated for 1 h in oxygenated HEPES-buffered Ringer's solution with or without 300 μM histamine (Sigma). After 1 h incubation time, stomach contents were aspirated, and pH was measured using a microcombination pH probe (Microelectrodes Inc., Bedford, NH, USA).

Results

Kcne2 deletion reverses the polarity of Kcnq1 trafficking in PCs

Having previously determined that Kcnq1 expression in the gastric mucosa is increased after targeted deletion of *Kcne2* (2), here we examined the effects of *Kcne2* deletion on the intracellular localization of Kcnq1 in PCs. In 3-mo-old *Kcne2*$^{-/-}$ mouse gastric mucosa, Kcnq1 IS demonstrated an apparent sharply basolateral localization in PCs across the mucosa, in contrast to its diffuse staining in *Kcne2*$^{+/+}$ PCs due to localization in the highly convoluted and invaginated apical membrane (Fig. 1C–E). Double IF staining confirmed that Kcnq1 was expressed in the apical side of PCs from 3-mo-old *Kcne2*$^{+/+}$ mice, colocalizing with the H^+/K^+ATPase β subunit (HKA β), a PC apical membrane marker, but not with NKCC1, a marker for basolateral membrane in PCs (22) (Fig. 1F, G). In contrast, in age-matched *Kcne2*$^{-/-}$ mouse gastric sections, Kcnq1 was still expressed in PCs (which were identified by midgastric gland location and HKA β expression), but was colocalized with NKCC1 at the PC basolateral membrane (Fig. 1F, G). HKA β was still expressed in the apical membrane of PCs, as described previously (23), and did not colocalize with NKCC1 in either *Kcne2*$^{+/+}$ or *Kcne2*$^{-/-}$ sections, demonstrating that *Kcne2* deletion did not globally disrupt PC polarity (Fig. 1H).

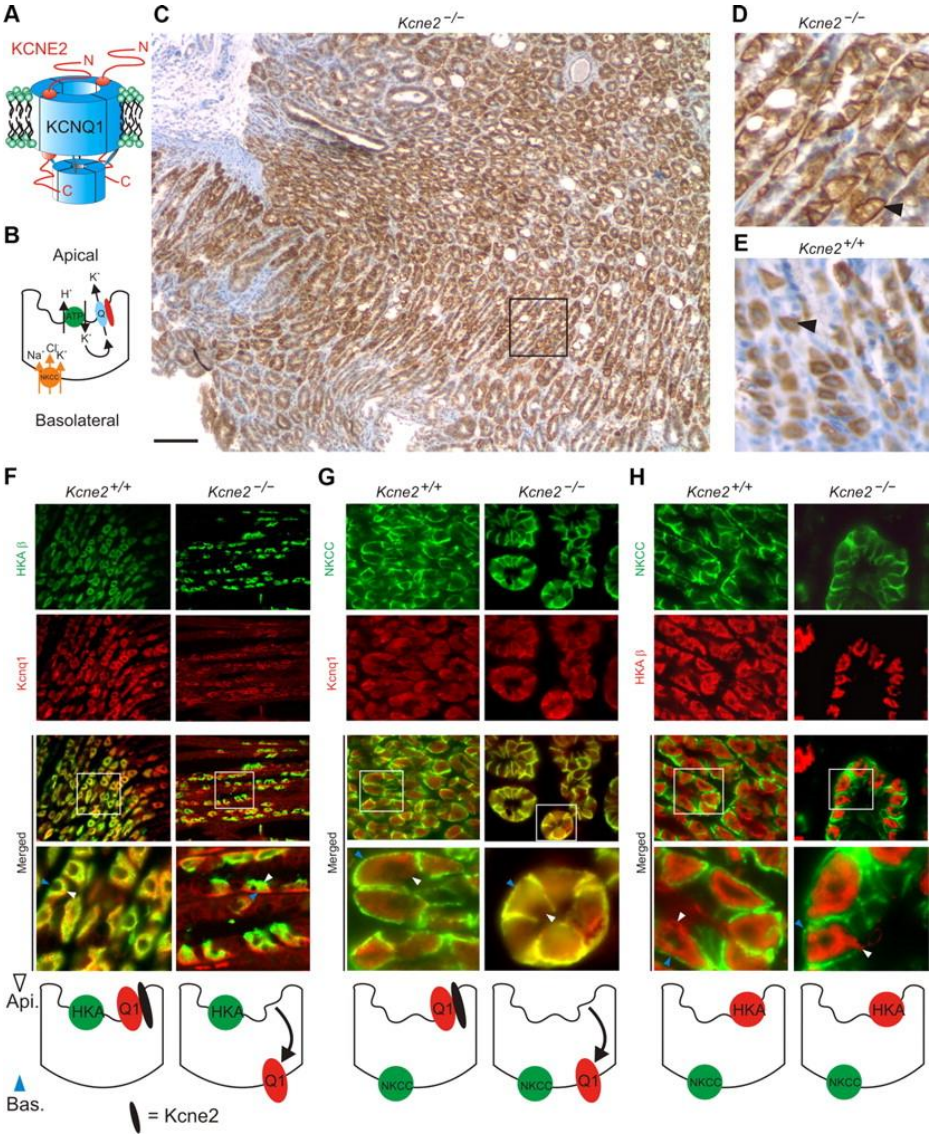

Figure 1. Reversed Kcnq1 trafficking in PCs of *Kcne2*$^{-/-}$ mice. A) Cartoon of a KCNQ1–KCNE2 complex. B) Cartoon of a PC showing HKA, NKCC1, and KCNQ1–KCNE2. C) KCNQ1 immunostaining (IS) in *Kcne2*$^{-/-}$ gastric mucosa. Scale bar = 100 µm. D) Expanded view of black box from panel *C*. Arrowhead indicates basolateral KCNQ1 staining. E) KCNQ1 IS in *Kcne2*$^{+/+}$ gastric mucosa (same scale as panel *D*). Arrowhead indicates diffuse KCNQ1 staining due to localization at the invaginated apical membrane. F–H) *Top:* exemplar IF colabeling of *Kcne2*$^{+/+}$ and *Kcne2*$^{-/-}$ gastric glands as indicated. Bottom merged panel shows expanded view of the boxed region in the top merged panel. Width of view (except bottom merge): 100 µm (F); 75 µm (G, H). Blue arrowheads, PC basolateral side; white arrowheads, PC apical side. Representative of results from ≥2 mice, 3–5 sections/mouse/genotype. *Bottom:* cartoons summarizing IF data.

Kcne2 deletion selectively up-regulates fundic Kcne3

We considered two possible mechanisms underlying the observed switch in Kcnq1 location on *Kcne2* deletion: passive, arising from homomeric Kcnq1 trafficking to the basolateral membrane in the absence of a required chaperone (postulated to be Kcne2) to target its expression to the apical side; or active, due to hijacking by another Kcne subunit. We therefore next investigated possible Kcne remodeling in *Kcne2*$^{-/-}$ gastric fundus tissue, using qRT-PCR analysis of transcripts for each of the four remaining Kcne genes, with GAPDH serving as a reference gene. Strikingly, we observed that fundic *Kcne3* transcript expression was increased 3-fold at 3 mo of age by targeted deletion of *Kcne2* (n=10 mice/genotype; P<0.05), whereas there were no significant changes in the fundic expression of transcripts for *Kcne1*, *Kcne4*, or *Kcne5* (n=10 mice/genotype; $P > 0.4$) (Fig. 2A). The observation that *Kcne3* mRNA was upregulated in *Kcne2*$^{-/-}$ fundus was recapitulated using conventional (semiquantitative) RT-PCR, with HPRT as a reference gene (n=4 mice/genotype; P<0.01; Fig. 2B, C). Notably, fundic Kcne3 protein expression was found to be increased 5-fold by *Kcne2* deletion (n=7 independent preps, 21–35 mice/genotype, $P<1\times10^{-4}$; Fig. 2D, E).

Kcne3 forms PC basolateral complexes with Kcnq1 in the absence of Kcne2

The fundic remodeling data (Fig. 2) suggested Kcne3 as the most likely Kcne candidate for diversion of Kcnq1 to the basolateral membrane in *Kcne2*$^{-/-}$ PCs. We adopted several biochemical and genetic approaches to test this hypothesis. First, we performed native co-IP studies using fundic tissue, and found greatly increased

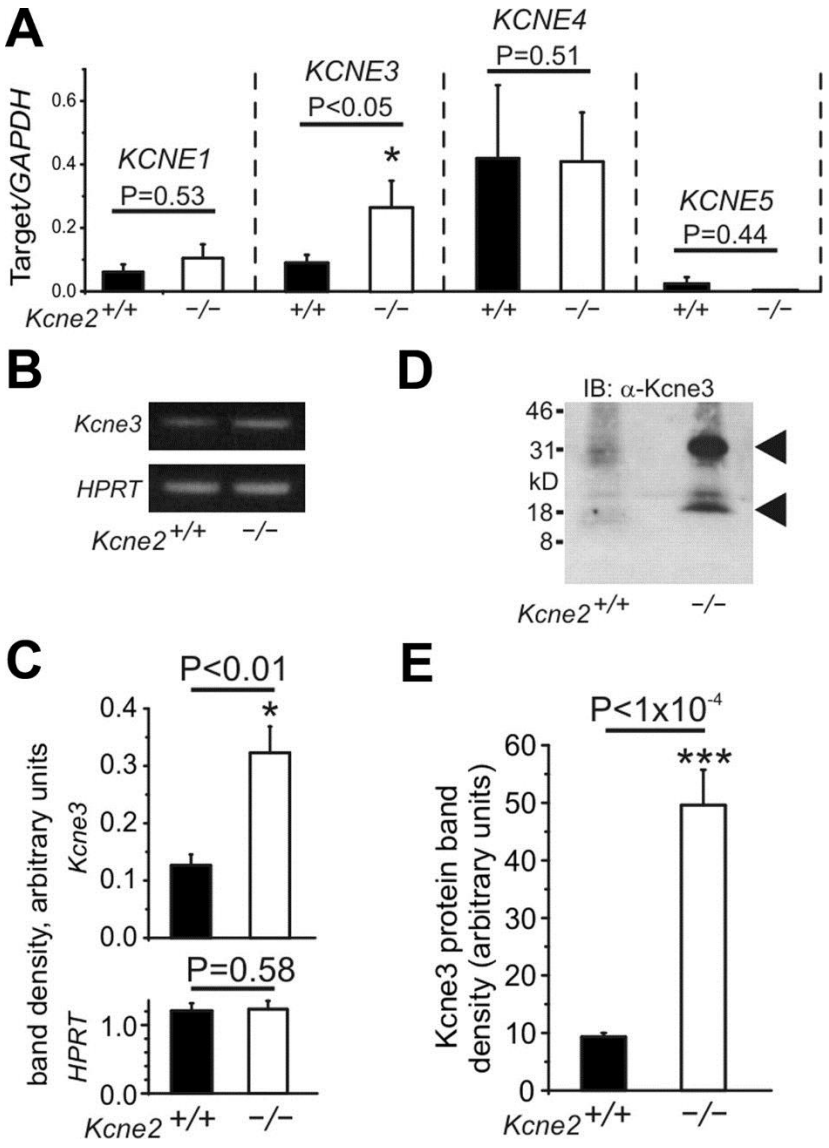

Figure 2. PC *Kcne3* is selectively up-regulated in remodeling arising from targeted deletion of *Kcne2*. A) qRT-PCR analysis of mRNA expression level of Kcne genes expressed as a ratio to GAPDH; *n*=10 mice/genotype/gene. B) Representative semiquantitative RT-PCR of gastric mucosal lysates from *Kcne2*$^{+/+}$ and *Kcne2*$^{-/-}$ mice for *Kcne3* and the reference gene HPRT. C) Mean band optical densities from samples as in panel *B*; *n*=4 independent preps/genotype. D) Representative Western blot of Kcne3 protein in membrane fractions from *Kcne2*$^{+/+}$ and *Kcne2*$^{-/-}$ mouse fundus preparations as indicated. Arrows indicate expected sizes of nonglycosylated and fully glycosylated (mature) Kcne3. E) Band optical density from Kcne3 (mature form) Western blots of *Kcne2*$^{+/+}$ and *Kcne2*$^{-/-}$ gastric mucosal membrane fractions, as in panel *D*; *n*=7 independent preps from 3–5 stomachs each; total of 21–35 stomachs/genotype. Error bars = sem.

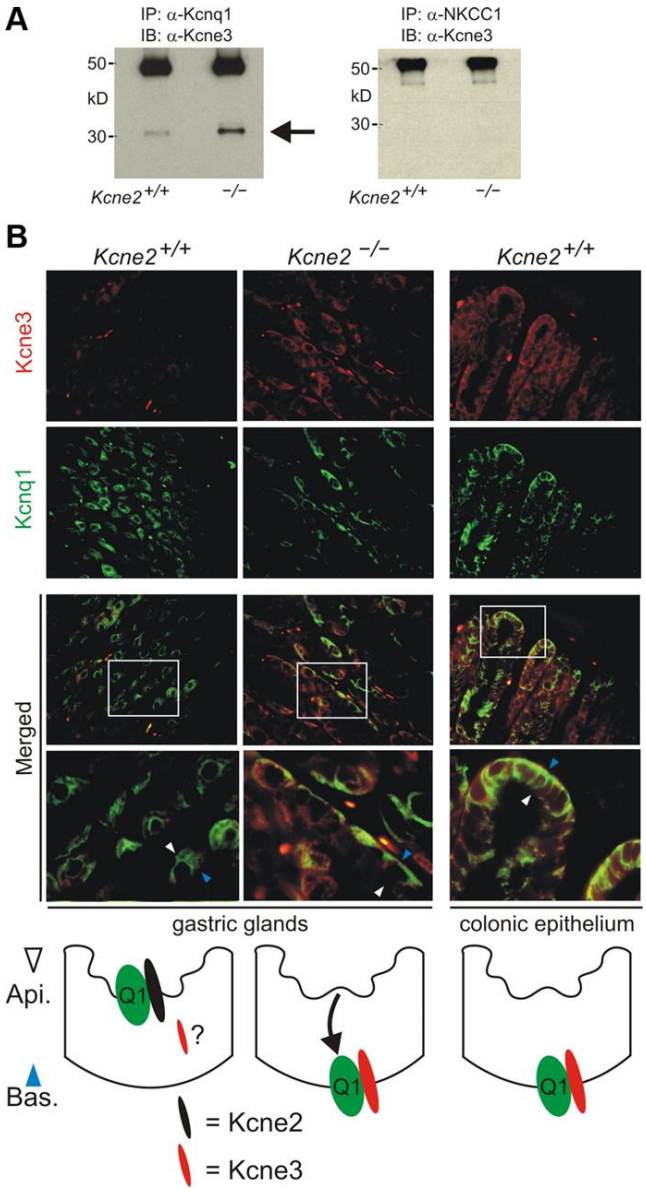

Figure 3: Remodeled *Kcne3* forms basolateral complexes with Kcnq1 in *Kcne2*$^{-/-}$ PCs. A) Co-IPs showing complex formation of Kcne3 with Kcnq1 (*left*) but not with NKCC1 (*right*) from mouse fundic membrane fractions. IPs from *Kcne2*$^{+/+}$ and *Kcne2*$^{-/-}$ mice using antibodies against Kcnq1 or NKCC1, and probed with anti-Kcne3 antibody. Arrow indicates expected mature Kcne3 migration distance. *n*=2 experiments/antibody, with each prep pooled from 3–5 mouse stomachs/genotype. B) *Top:* exemplar IF labeling of Kcne3 (red) and Kcnq1 (green) in *Kcne2*$^{+/+}$ or *Kcne2*$^{-/-}$ gastric glands, or *Kcne2*$^{+/+}$ colonic crypts, as indicated. Bottom merged panel shows expanded view of the boxed region. Width of view (except bottom merge): 100 μm. Representative of results from at least two mice, 3–5 sections/mouse/genotype. *Bottom:* cartoons summarizing IF data.

formation of Kcnq1–Kcne3 complexes in *Kcne2*$^{-/-}$ tissue compared to *Kcne2*$^{+/+}$ tissue, with NKCC1 providing a negative control for Kcne3 co-IP (Fig. 3A). These data were supported by IF analyses, which indicated increased *Kcne3* expression compared to *Kcne2*$^{+/+}$ PCs, and basolateral colocalization of Kcne3 with Kcnq1, in *Kcne2*$^{-/-}$ PCs— similar to that observed in wild-type colonic epithelium (Fig. 3B).

Kcne3 is necessary and sufficient for trafficking of Kcnq1 to the PC basolateral membrane

These observations were suggestive of an active role for Kcne3 in rerouting Kcnq1 to the PC basolateral membrane, but it was still possible that Kcnq1 could target to the PC basolateral side regardless of Kcne3, in the absence of Kcne2. To resolve this, we generated *Kcne3*$^{-/-}$ mice by targeted deletion of the Kcne3 gene (Fig. 4A), and then crossed them with *Kcne2*$^{-/-}$ mice to generate heterozygous, and ultimately double-knockout, *Kcne2*$^{-/-}$*Kcne3*$^{-/-}$ mice. We confirmed their genotypes with PCR (Fig. 4B) and with Western blots from colon tissue, in which Kcne3 is known to be expressed (10) (Fig. 4C). Next, we determined whether there was remodeling of *Kcne1*, *Kcne4*, or *Kcne5* due to concomitant *Kcne2* and *Kcne3* deletion, again using qRT-PCR. These experiments did not identify statistically significant changes in mRNA expression of these 3 genes; there was a general trend toward reduced expression, but considerable variability in expression within each genotype (Fig. 4D). Strikingly, IF studies showed that Kcnq1 colocalized in the apical compartment with HKA β, and not basolaterally with NKCC1, in *Kcne2*$^{-/-}$*Kcne3*$^{-/-}$ mouse PCs (Fig. 4E, F). As we might have expected, Kcnq1 was also apically expressed in *Kcne2*$^{+/+}$*Kcne3*$^{-/-}$ mouse PCs (Fig.

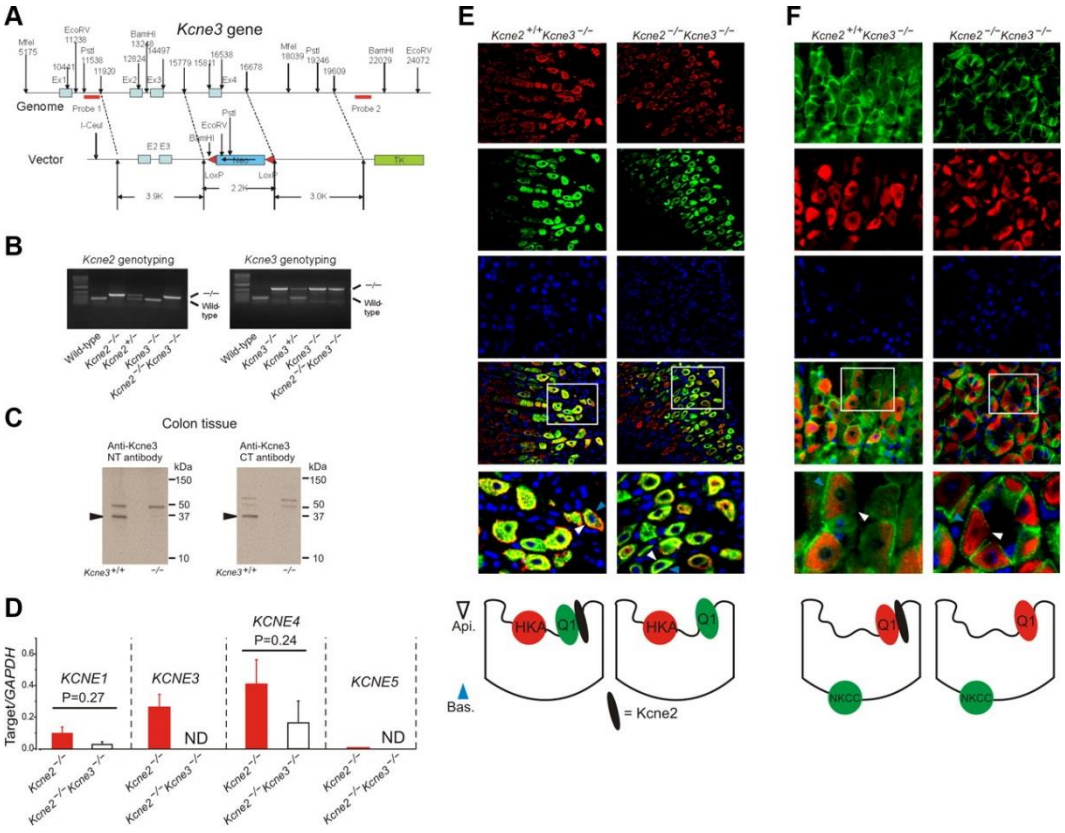

Figure 4: Kcne3 deletion restores apical trafficking of Kcnq1 in Kc*ne2*$^{-/-}$ mice. A) Targeting strategy for genomic deletion of *Kcne3*. B) PCR genotyping of wild-type, heterozygous, and homozygous single-knockout and double-knockout *Kcne2*$^{-/-}$ and *Kcne3*$^{-/-}$ mice. C) Western blots of Kcne3 in membrane fractions from colonic crypts of *Kcne3*$^{+/+}$ and *Kcne3*$^{-/-}$ mice as indicated, using an in-house antibody raised against an N-terminal epitope (*left*), and a commercial antibody (Alomone) raised against a C-terminal epitope (*right*). Arrows indicate band at 37 kDa unique to wild-type tissue. D) qRT-PCR analysis of fundic Kcne expression profile expressed as a ratio to that of reference gene GAPDH amplified in parallel each time; *n*=10 mice/single gene deletion genotype; *n*=5 mice/double gene deletion genotype. ND, not determined (for Kcne3, not measured in *Kcne2*$^{-/-}$*Kcne3*$^{-/-}$ mice; for Kcne5, unable to detect signal conforming to quality controls as described in Materials and Methods). Error bars = sem. E, F) *Top:* exemplar IF colabeling of *Kcne2*$^{+/+}$*Kcne3*$^{-/-}$ and *Kcne2*$^{-/-}$*Kcne3*$^{-/-}$ gastric glands as indicated. Bottom two IF panels are merged views of the 3 panels above; bottom merged panel shows expanded view of the boxed region in the top merged panel. Blue arrowheads, PC basolateral side; white arrowheads, PC apical side. Counterstained with DAPI (blue). Representative results from ≥2 mice, 3–5 sections/mouse/genotype. Width of view (except bottom merge): 100 μm (E); 50 μm (F). *Bottom:* cartoons summarizing IF data.

4E, F). Thus, in PCs, Kcne2 is not required for apical localization of Kcnq1 in the absence of Kcne3. However, in the absence of Kcne2, Kcne3 is up-regulated and is necessary and sufficient to actively chaperone Kcnq1 to the PC basolateral membrane.

Kcne2 is required for Kcnq1 function at the PC apical membrane

Our findings suggested that in *Kcne2*$^{-/-}$*Kcne3*$^{+/+}$ mouse PCs, Kcnq1–Kcne3 channels could form an additional basolateral K^+ efflux route, but that there would be no apical K^+ recycling pathway. In contrast, in *Kcne2*$^{-/-}$*Kcne3*$^{-/-}$ mouse PCs, homomeric Kcnq1 could potentially provide an apical K^+ recycling pathway, but in the absence of *Kcne2* its functionality might be limited, due to an inability to function efficiently at low pH and/or negative membrane potentials. There are several hypothetical consequences of these mistrafficking and subunit rearrangement events. Basolateral Kcnq1–Kcne3 channels in *Kcne2*$^{-/-}$*Kcne3*$^{+/+}$ mice could potentially restore some gastric acid secretion by alleviating PC K^+ accumulation. In contrast, *Kcne2*$^{-/-}$*Kcne3*$^{-/-}$ mice would exhibit restored gastric acidification if Kcnq1 was able to function alone at the apical membrane, but if homomeric Kcnq1 did not have this capability, *Kcne2*$^{-/-}$*Kcne3*$^{-/-}$ mice would potentially have the most severe gastric pathology of all the genotypes. *Kcne2*$^{+/+}$*Kcne3*$^{-/-}$ mice would be predicted to have normal gastric acidification.

We tested these hypotheses by measuring stomach mass to quantify gastric hyperplasia (one consequence of achlorhydria), and by quantifying gastric luminal pH. These studies yielded the striking finding that Kcne3 indeed affected gastric function

and cell proliferation in *Kcne2*-depeleted mice, but not in mice with both *Kcne2* alleles. Thus, 3-mo-old *Kcne2*$^{-/-}$*Kcne3*$^{-/-}$ mice exhibited massive gastric hyperplasia, with twofold heavier stomachs than age-matched *Kcne2*$^{-/-}$*Kcne3*$^{+/+}$ mice, whereas *Kcne2*$^{+/+}$*Kcne3*$^{-/-}$ mice had normal stomach mass (Fig. 5A, B). Notably, Kcne3 also prevented gastric hyperplasia in *Kcne2*$^{+/-}$*Kcne3*$^{+/+}$ mice, which had significantly smaller stomachs than those of *Kcne2*$^{+/-}$*Kcne3*$^{-/-}$ mice (Fig. 5B). These data were supported by results from stomach lumen pH quantification, which indicated that *Kcne2*$^{+/-}$*Kcne3*$^{-/-}$ mice had significantly less gastric acidification upon histamine stimulation than *Kcne2*$^{+/-}$*Kcne3*$^{+/+}$ mice, although Kcne3 did not affect the stomach lumen pH or response to histamine of *Kcne2*$^{-/-}$ mice. As expected, *Kcne2*$^{+/+}$*Kcne3*$^{-/-}$ mice had normal stomach pH and response to histamine (Fig. 5C).

These findings are consistent with a novel model in which, in the absence of Kcne2, Kcne3 is upregulated and chaperones Kcnq1 to the PC basolateral side. When both *Kcne3* and *Kcne2* are deleted, homomeric Kcnq1 localizes to the apical membrane, but without restoration of gastric acidification. This indicates that Kcnq1 cannot function in the absence of both Kcne2 and Kcne3 in PCs, even if at the apical membrane, due either to inhibition by low extracellular pH, inability to constitutively activate, or both (Fig. 5D).

Implications of Kcne-directed polarized trafficking of Kcnq1

This study describes two main novel findings: discovery of the capacity of a KCNE subunit to act as a polar trafficking chaperone, and identification of KCNE subunit remodeling (and its functional consequences) *in vivo*. In native PCs, Kcnq1 probably localizes primarily in deeply invaginated sections of the apical membrane both at rest

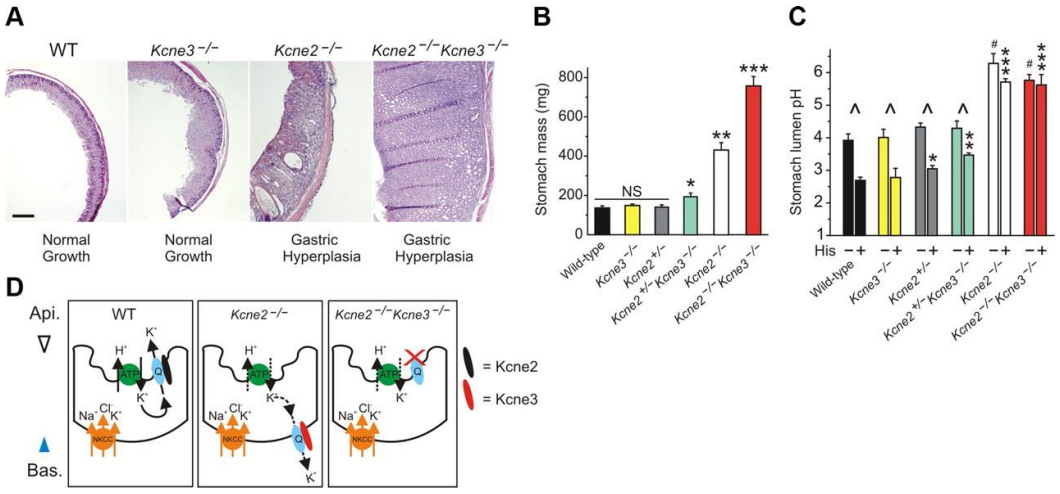

Figure 5: *Kcne3* deletion exacerbates gastric hyperplasia and achlorhydria in *Kcne2*-deficient mice. A) Exemplar H&E-stained sections of gastric mucosa from 3-mo-old wild-type, *Kcne3*$^{-/-}$, *Kcne2*$^{-/-}$ and double-knockout *Kcne2*$^{-/-}$*Kcne3*$^{-/-}$ mice. Scale bar = 250 µm. Representative of ≥2 sections each from ≥2 mice/genotype. B) Mean stomach mass measured *ex vivo* from 3-mo-old mice, genotypes as indicated, *n*=6–16. NS, nonsignificant. *P < 0.05; **P < 2×10^{-4}; ***P < 4×10^{-5}. C) Mean stomach lumen pH measured *ex vivo* from 3-mo-old mice, genotypes as indicated, with (+) or without (−) stimulation with 300 µM histamine (His); *n*=3–5. *P < 0.05, **P < 0.03, ***P < 0.002 vs. all other His groups; #P < 0.01 vs. all other control groups; ^P < 0.05 vs. corresponding control group. D) Summary illustrating Kcne control of Kcnq1 trafficking in mouse PCs. Error bars = sem.

and when stimulated, although a fraction of it may be located in intracellular vesicles and move to the apical surface on secretagogue stimulation; in contrast, HKA is primarily located in intracellular vesicles until stimulation triggers its trafficking to the apical membrane (16, 24). Here, we show that *Kcne2* deletion results in Kcnq1 residing basolaterally in PCs instead, and that Kcne3 is necessary and sufficient for this rerouting. In a previous study of MDCK cells, Kcnq1 was basolaterally located regardless of which Kcne subunit (subunits 1 through 5) it was heterologously coexpressed with (17), and we recently found that Kcnq1–Kcne2 channels are basolaterally located in thyrocytes (18). Furthermore, Kcne3 does not appear necessary for basolateral location of Kcnq1 in colonic epithelium, although potential remodeling of other Kcne subunits was not determined in that study (13). Clearly, the influence of Kcne subunits on Kcnq1 targeting in polarized cells is highly cell-type specific, perhaps due to differences in expression of proteins such as μ1B, an AP-1 clathrin adaptor complex that directs polarized trafficking (25,–,27).

The discovery of Kcne remodeling due to genetic disruption of another Kcne subunit has potentially profound implications for the etiology of Kcne-related disease states and for study of Kcne-knockout mice. In previous studies examining K^+ channel α subunit gene deletion, a concern has been that functional redundancy exists given the similarity of some α subunits, e.g., $K_v3.1$ and $K_v3.2$ (28). Here, studying β subunits, we have unearthed a novel remodeling phenomenon, wherein the location of the α subunit in the absence of its regular β subunit partner is the polar opposite of that observed in wild-type mice—due to hijacking by a remodeled (upregulated), related β

subunit. We suspect we have merely scratched the surface with respect to the prevalence of Kcne subunit remodeling in both model systems and in animal and human disease states in a variety of tissues, a hypothesis to be tested further in the future. The present findings highlight the importance not only of an apical localization per se for Kcnq1, but also the association with Kcne2 for full functionality at the apical side. Kcnq1–Kcne3 channels are acid-insensitive (29) and, like Kcnq1–Kcne2, are constitutively active, so one would assume they could provide an apical K^+ recycling conduit if located there, but they could not rescue gastric acid secretion in *Kcne2*$^{-/-}$ mice because they were basolaterally located in parietal cells, although they partially restored function in *Kcne2*$^{+/-}$ mice. By the same token, even when apically located, Kcnq1 could not serve as a K^+ recycling channel without Kcne2 in PCs—we speculate this is because homomeric Kcnq1 is voltage dependent and inhibited by acid. Our data suggest that Kcnq1 defaults to the apical side in the absence of Kcne2 or Kcne3, but further studies are required, perhaps adopting a proteomic approach together with the genetic models described here, to determine whether Kcnq1 requires an additional subunit to traffic apically in parietal cells, which is either upregulated on *Kcne2* and *Kcne3* double knockout, or simply permitted to associate with Kcnq1 only in the absence of these subunits. The mechanism underlying basolateral trafficking of Kcnq1– Kcne3 complexes in parietal cells is likely both Kcne3 and parietal cell dependent, and its elucidation will require use of chimeric Kcne subunits introduced either *in vivo* or into a suitable polarized parietal cell line; the former is more attractive because physiological consequences would be readily assayable. Our co-IP data

suggest some (albeit relatively low-level) formation of Kcnq1–Kcne3 complexes even in wild-type gastric epithelium, which could correspond to complexes in gastric surface cells, or in chief cells, two gastric mucosal cell types suggested to express basolateral Kcnq1 and Kcne3; these cells are not located midgastric gland and do not express Kcne2 or HKA, and thus are easily distinguishable from PCs in IF studies (13, 29). Alternatively, Kcnq1–Kcne3 complexes could be occurring even in wild-type PCs, again albeit at relatively low levels. Further studies will identify what if any function these putative channels perform in PCs, and whether or not these are actually mixed Kcnq1–Kcne2–Kcne3 complexes, perhaps with functional characteristics we do not yet understand. This type of tripartite complex has been reported for Kcne1, Kcne3, and Kcnh3 in mouse brain (30).

Future work will determine which Kcne subunits or other factors control polarized trafficking of Kcnq1 in, e.g., the thyroid, and of other α subunits in polarized cells in general, together with a search for the molecular signals that cause, e.g., *Kcne3* transcript up-regulation in *Kcne2*$^{-/-}$ mouse PCs. The extent to which perturbation of this polarized trafficking contributes directly to, or is reflective of compensatory remodeling in, the molecular etiology of human diseases of the epithelia and other related systems, will be explored—particularly in the light of our recent finding that *Kcne2*$^{-/-}$ mice develop gastritis cystica profunda and gastric neoplasia (31).

References

1. Lee, M. P., Ravenel, J. D., Hu, R. J., Lustig, L. R., Tomaselli, G., Berger, R. D., Brandenburg, S. A., Litzi, T. J., Bunton, T. E., Limb, C., Francis, H., Gorelikow, M., Gu, H., Washington, K., Argani, P., Goldenring, J. R., Coffey, R. J., and Feinberg, A. P. (2000) Targeted disruption of the Kvlqt1 gene causes deafness and gastric hyperplasia in mice. *J. Clin. Invest*. **106**, 1447–55

2. Roepke, T. K., Anantharam, A., Kirchhoff, P., Busque, S. M., Young, J. B., Geibel, J. P., Lerner, D. J., and Abbott, G. W. (2006) The KCNE2 potassium channel ancillary subunit is essential for gastric acid secretion. *J. Biol. Chem*. **281**, 23740–23747

3. Fujita, A., Horio, Y., Higashi, K., Mouri, T., Hata, F., Takeguchi, N., and Kurachi, Y. (2002) Specific localization of an inwardly rectifying K^+ channel, Kir4.1, at the apical membrane of rat gastric parietal cells; its possible involvement in K+ recycling for the H(+)-K(+)-pump. *J. Physiol*. **540**, 85–92

4. Malinowska, D. H., Sherry, A. M., Tewari, K. P., and Cuppoletti, J. (2004) Gastric parietal cell secretory membrane contains PKA and acid-activated Kir2.1 K+ channels. *Am. J. Physiol. Cell Physiol*. **286**, C495–C506

5. Barhanin, J., Lesage, F., Guillemare, E., Fink, M., Lazdunski, M., and Romey, G. (1996) K(V)LQT1 and lsK (minK) proteins associate to form the I(Ks) cardiac potassium current. *Nature* **384**, 78–80

6. Sanguinetti, M. C., Curran, M. E., Zou, A., Shen, J., Spector, P. S., Atkinson, D. L., and Keating, M. T. (1996) Coassembly of K(V)LQT1 and minK (IsK) proteins to form cardiac I(Ks) potassium channel. *Nature* **384**, 80–83

7. Abbott, G. W., Sesti, F., Splawski, I., Buck, M. E., Lehmann, M. H., Timothy, K. W., Keating, M. T., and Goldstein, S. A. (1999) MiRP1 forms I_{Kr} potassium channels with HERG and is associated with cardiac arrhythmia. *Cell* **97**, 175–187

8. McCrossan, Z. A., and Abbott, G. W. (2004) The MinK-related peptides. *Neuropharmacology* **47**, 787–821

9. Panaghie, G., and Abbott, G. W. (2007) The role of S4 charges in voltage-dependent and voltage-independent KCNQ1 potassium channel complexes. *J. Gen. Physiol.* **129**, 121–133

10. Schroeder, B. C., Waldegger, S., Fehr, S., Bleich, M., Warth, R., Greger, R., and Jentsch, T. J. (2000) A constitutively open potassium channel formed by KCNQ1 and KCNE3. *Nature* **403**, 196–199

11. Tinel, N., Diochot, S., Borsotto, M., Lazdunski, M., and Barhanin, J. (2000) KCNE2 confers background current characteristics to the cardiac KCNQ1 potassium channel. *EMBO J.* **19**, 6326–6330

12. Dedek, K., and Waldegger, S. (2001) Colocalization of KCNQ1/KCNE channel subunits in the mouse gastrointestinal tract. *Pflügers Arch.* **442**, 896–902

13. Preston, P., Wartosch, L., Gunzel, D., Fromm, M., Kongsuphol, P., Ousingsawat, J., Kunzelmann, K., Barhanin, J., Warth, R., and Jentsch, T. J. (2010) Disruption of the K+ channel beta-subunit KCNE3 reveals an important role in intestinal and tracheal Cltransport. *J. Biol. Chem.* **285**, 7165–7175

14. Vallon, V., Grahammer, F., Volkl, H., Sandu, C. D., Richter, K., Rexhepaj, R., Gerlach, U., Rong, Q., Pfeifer, K., and Lang, F. (2005) KCNQ1-dependent transport in renal and gastrointestinal epithelia. *Proc. Natl. Acad. Sci. U. S. A.* **102**, 17864–17869

15. Okada, Y., and Ueda, S. (1984) Electrical membrane responses to secretagogues in parietal cells of the rat gastric mucosa in culture. *J. Physiol.* **354**, 109–119

16. Heitzmann, D., Grahammer, F., von Hahn, T., Schmitt-Graff, A., Romeo, E., Nitschke, R., Gerlach, U., Lang, H. J., Verrey, F., Barhanin, J., and Warth, R. (2004) Heteromeric KCNE2/KCNQ1 potassium channels in the luminal membrane of gastric parietal cells. *J. Physiol.* **561**, 547–557

17. Jespersen, T., Rasmussen, H. B., Grunnet, M., Jensen, H. S., Angelo, K., Dupuis, D. S., Vogel, L. K., Jorgensen, N. K., Klaerke, D. A., and Olesen, S. P. (2004) Basolateral localisation of KCNQ1 potassium channels in MDCK cells: molecular identification of an N-terminal targeting motif. *J. Cell Sci.* **117**, 4517–4526

18. Roepke, T. K., King, E. C., Reyna-Neyra, A., Paroder, M., Purtell, K., Koba, W., Fine, E., Lerner, D. J., Carrasco, N., and Abbott, G. W. (2009) Kcne2 deletion uncovers its crucial role in thyroid hormone biosynthesis. *Nat. Med.* **15**, 1186–1194

19. Bustin, S. A., Benes, V., Garson, J. A., Hellemans, J., Huggett, J., Kubista, M., Mueller, R., Nolan, T., Pfaffl, M. W., Shipley, G. L., Vandesompele, J., and Wittwer, C. T. (2009) The MIQE guidelines: minimum information for publication of quantitative real-time PCR experiments. *Clin. Chem*. **55**, 611–622

20. Spandidos, A., Wang, X., Wang, H., Dragnev, S., Thurber, T., and Seed, B. (2008) A comprehensive collection of experimentally validated primers for polymerase chain reaction quantitation of murine transcript abundance. *BMC Genomics* **9**, 633

21. Roepke, T. K., Kontogeorgis, A., Ovanez, C., Xu, X., Young, J. B., Purtell, K., Goldstein, P. A., Christini, D. J., Peters, N. S., Akar, F. G., Gutstein, D. E., Lerner, D. J., and Abbott, G. W. (2008) Targeted deletion of kcne2 impairs ventricular repolarization via disruption of I(K,slow1) and I(to,f). *FASEB J*. **22**, 3648–3660

22. McDaniel, N., Pace, A. J., Spiegel, S., Engelhardt, R., Koller, B. H., Seidler, U., and Lytle, C. (2005) Role of Na-K-2Cl cotransporter-1 in gastric secretion of nonacidic fluid and pepsinogen. *Am. J. Physiol. Gastrointest. Liver Physiol*. **289**, G550– G560

23. Courtois-Coutry, N., Roush, D., Rajendran, V., McCarthy, J. B., Geibel, J., Kashgarian, M., and Caplan, M. J. (1997) A tyrosine based signal targets H/K-ATPase to a regulated compartment and is required for the cessation of gastric acid secretion. *Cell* **90**, 501–510

24. Kaufhold, M.-A., Krabbenhoft, A., Song, P., Engelhardt, R., Riederer, B., Fahrmann, M., Klocker, N., Biel, W., Manns, M., Hagen, S. J., and Seidler, U. (2008) Localization, trafficking, and significance for acid secretion of parietal cell Kir4.1 and KCNQ1 K channels. *Gastroenterology* **134**, 1058–1069

25. Matter, K., Hunziker, W., and Mellman, I. (1992) Basolateral sorting of LDL receptor in MDCK cells: the cytoplasmic domain contains two tyrosine-dependent targeting determinants. *Cell* **71**, 741–753

26. Odorizzi, G., Pearse, A., Domingo, D., Trowbridge, I. S., and Hopkins, C. R. (1996) Apical and basolateral endosomes of MDCK cells are interconnected and contain a polarized sorting mechanism. *J. Cell Biol.* **135**, 139–152

27. Duffield, A., Folsch, H., Mellman, I., and Caplan, M. J. (2004) Sorting of H,K-ATPase beta-subunit in MDCK and LLC-PK cells is independent of mu 1B adaptin expression. *Traffic* **5**, 449–461

28. Porcello, D. M., Ho, C. S., Joho, R. H., and Huguenard, J. R. (2002) Resilient RTN fast spiking in Kv3.1 null mice suggests redundancy in the action potential repolarization mechanism. *J. Neurophysiol*. **87**, 1303–1310

29. Heitzmann, D., and Warth, R. (2008) Physiology and pathophysiology of potassium channels in gastrointestinal epithelia. *Physiol. Rev*. **88**, 1119–1182

30. Clancy, S. M., Chen, B., Bertaso, F., Mamet, J., and Jegla, T. (2009) KCNE1 and KCNE3 beta-subunits regulate membrane surface expression of Kv12.2 K(+) channels in vitro and form a tripartite complex in vivo. *PLoS ONE* **4**, e6330

31. Roepke, T. K., Purtell, K., King, E. C., La Perle, K. M., Lerner, D. J., and Abbott, G. W. (2010) Targeted deletion of Kcne2 causes gastritis cystica profunda and gastric neoplasia. *PLoS ONE* **5**, e11451